

STATUS OF THESIS

Title of thesis Fly Ash Nanoparticles Assisted Foam Injection Water Alternating Gas for Enhanced Oil Recovery

I PHONG GUAN MING

hereby allow my thesis to be placed at the Information Resource Center (IRC) of Universiti Teknologi PETRONAS (UTP) with the following conditions:

1. The thesis becomes the property of UTP
2. The IRC of UTP may make copies of the thesis for academic purposes only.
3. This thesis is classified as

Confidential

Non-confidential

If this thesis is confidential, please state the reason:

The contents of the thesis will remain confidential for _____ years.

Remarks on disclosure:

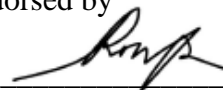


Signature of Author

Permanent address: 97, Jalan
Dato Lau Pak Khuan, 31400,
Taman Ipoh, Perak, Malaysia

Date: 15/04/2020

Endorsed by



Signature of Supervisor

Name of Supervisor
Dr Rashidah Binti Mohd Pilus

Date : 15/08/2020

UNIVERSITI TEKNOLOGI PETRONAS

FLY ASH NANOPARTICLES ASSISTED FOAM INJECTION WATER
ALTERNATING GAS FOR ENHANCED OIL RECOVERY

By

PHONG GUAN MING

The undersigned certify that they have read, and recommend to the Postgraduate Studies Programme for acceptance of this thesis for the fulfillment of the requirements for the degree stated.

Signature:



Main Supervisor:

Dr Rashidah Binti Mohd Pilus

Signature:



Co-Supervisor:

Prof. Dr Noraini Muti Binti Mohamed

Signature:

Head of Department:

Assoc. Prof. Dr Khaled Abdalla Elraies

Date:

15/08/2020

FLY ASH NANOPARTICLES ASSISTED FOAM INJECTION WATER
ALTERNATING GAS FOR ENHANCED OIL RECOVERY

by

PHONG GUAN MING

A Thesis

Submitted to the Postgraduate Studies Programme

as a Requirement for the Degree of

MASTER OF SCIENCE

PETROLEUM ENGINEERING

UNIVERSITI TEKNOLOGI PETRONAS

BANDAR SERI ISKANDAR,

PERAK

MARCH 2021

DECLARATION OF THESIS

Title of thesis

Fly Ash Nanoparticles Assisted Foam Injection Water Alternating Gas for Enhanced Oil Recovery

I PHONG GUAN MING

hereby declare that the thesis is based on my original work except for quotations and citations which have been duly acknowledged. I also declare that it has not been previously or concurrently submitted for any other degree at UTP or other institutions.

Witnessed by



Signature of Author



Signature of Supervisor

Permanent address: 97, Jalan
Dato Lau Pak Khuan, 31400,
Taman Ipoh, Perak, Malaysia

Name of Supervisor
Dr Rashidah Binti Mohd Pilus

Date: 15/04/2020

Date : 15/08/2020

DEDICATION

To my beloved parents and family members

ACKNOWLEDGEMENTS

I would like to give thanks to my supervisor Dr Rashidah binti Mohd Pilus for her continuous dedication, support, and knowledge for me to be able to overcome any obstacles throughout my postgraduate study in Master of Petroleum Engineering in Universiti Teknologi Petronas (UTP). I would like to express my gratitude to my co-supervisor Prof Dr Norani Muti binti Mohamed for her contribution and immense knowledge on nanoparticles studies. My heartfelt regards to Dr Lakshmi Priya Thangavel for her technical guidance in nanoparticles characterization and nanoparticles synthesising process.

My sincere thanks to my project colleagues Mr Mohd Afiq bin Mustaffa, Ms Maisarah binti Musa and Ms Nur Asyimah binti Md Asri for their continuous guidance and knowledge sharing in foam injection studies with me throughout my research program. My heartfelt regards to all of my COREOR (Center of Research in Enhanced Oil Recovery) colleagues mainly Dr Suleiman Akilu, Mr Davood Zivar, Mr Mohamed Gamal Rezk and Mr Krishna Shwetank for their valuable insights and constructive suggestion for me to enhance my research findings in FAWAG injection.

A special thanks to the UTP-TU DELF- SHELL- Petronas (0153 AB-DA8) project for the opportunity and funding for me to continue my studies in Universiti Teknologi Petronas (UTP)

ABSTRACT

The success of foam injection as a displacing fluid in the porous media mainly depends on the stability of the foam. However, foam stability tends to decrease once exposed to crude oil and reservoir conditions. In the last few decades, research on nanoparticles as a foam stabilizer has shown favourable results, however, for field-scale application the nanoparticles for foam stabilization would have to be commercially feasible thus require an inexpensive alternative source that can be produced in large quantity. Coal fly ash is a by-product of burning coal for electricity in Malaysia, thus can serve as a source for low-cost large-scale production of nanoparticles. A chemical synthesis technique is used to synthesize nanoparticles from the coal fly ash as the technique is proven successful in producing much smaller nanoparticles capable of effective movement in the narrow lamellae space of the gas-liquid interface as compared to the larger-sized particles. The diameter size of FANP1 (Synthesized Fly Ash Nanoparticles) was between 10 nm to 20 nm whereas, the diameter size of FANP2 (Synthesized Fly Ash Nanoparticles coated with MFOMAX) was 40 nm to 60 nm. The main composition of both nanoparticles was SiO_2 , Al_2O_3 and Na_2SO_4 . Static foam stability and lamella number calculation were done as a screening process for core flooding experiment. In both experiment, foam with FANP1 nanoparticles has the highest foam stability compared to coated FANP2 nanoparticles and commercial nanoparticles, R1 (50% of SiO_2 & 50% of Al_2O_3) and R2 (33.3% SiO_2 & 66.7% of Al_2O_3). The core flooding experiment, the foam with FANP1 nanoparticles produced the highest mobility reduction factor compared to other nanoparticles. However, foam with R1 nanoparticles produced higher oil recovery than FANP1 and FANP2 nanoparticles and between the two synthesized nanoparticles, FANP2 produced higher oil recovery than FANP1 nanoparticles even though FANP1 gives better MRF value. The sensitivity analysis is done to determine the factor governing oil recovery and it indicates that surfactant adsorption with an optimum foam stability has a major influence on increasing oil recovery compared to stability of the foam.

ABSTRAK

Kejayaan menggunakan suntikan busa sebagai cecair yang mengalir ke dalam media berpori bergantung pada kestabilan busa. Namun begitu, kestabilan busa akan merosot masa busa didedah dengan minyak mentah dan keadaan takungan. Dalam beberapa dekad terakhir, penyelidikan tentang menggunakan nanopartikel sebagai penstabil busa menunjukkan keputusan yang memberangsangkan, namun begitu, kegunaan nanopartikel sebagai penstabilan busa secara skala padang akan memerlukan sumber alternatif yang murah dan senang dihasilkan dalam jumlah yang besar. Abu arang batu merupakan produk sampingan daripada pembakaran arang batu untuk penjanaan elektrik dalam negara Malaysia, boleh dijadikan sebagai sumber pengeluaran nanopartikel secara berskala besar disebabkan kos rendah. Nanopartikel boleh disintesis dari abu arang batu menggunakan prosedur sintesis kimia dan prosedur berjaya menghasilkan nanopartikel yang mempunyai saiz yang lebih kecil serta mampu lebih berkesan bergerak dalam ruang lamellae yang sempit antara muka gas-cecair berbanding dengan nanopartikel yang bersaiz lebih besar. Saiz diameter FANP1 (Abu arang batu yang disintesis) adalah antara 10nm hingga 20nm, manakal saiz diameter FANP2 (Abu arang batu yang disintesis dengan campuran MFOMAX surfactant) adalah antara 40nm hingga 60nm. FANP1 dan FANP2 yang disintesis hanya mengandungi SiO_2 , Al_2O_3 dan Na_2SO_4 . Eksperimen kestabilan buih dan pengiraan lamela dilakukan untuk proses penyaringan nanopartikel untuk eksperimen suntikan buih. Dalam kedua-dua eksperimen tersebut, nanopartikel FANP1 mempunyai kestabilan busa tertinggi berbanding dengan nanopartikel FANP2 bersalut dan nanopartikel komersial, R1 (50% of SiO_2 & 50% of Al_2O_3) atau R2 (33.3% SiO_2 & 66.7% of Al_2O_3). Dalam eksperimen suntikan buih, buih yang mengandungi nanopartikel FANP1 menghasilkan faktor pengurangan mobiliti tertinggi berbanding dengan nanopartikel lain. Namun begitu, busa yang mengandungi nanopartikel R1 menghasilkan minyak yang tertinggi berbanding dengan busa yang mengandungi

nanopartikel FANP1 atau FANP2. Tambahan pula, antara dua nanopartikel yang disintesis daripada abu arang batu, FANP2 menghasilkan lebih banyak minyak daripada busa yang mengandungi nanopartikel FANP1 walaupun busa yang mengandungi FANP1 mempunyai kestabilan busa yang tertinggi. Analisis kepekaan dilakukan untuk menentukan faktor utama suntikan buih untuk penghasilan minyak dan simulasi tersebut telah menunjukkan bahawa penjerapan surfaktan oleh batu takungan mempunyai pengaruh besar terhadap faktor penghasilan minyak utama berbanding dengan kestabilan busa.

In compliance with the terms of the Copyright Act 1987 and the IP Policy of the university, the copyright of this thesis has been reassigned by the author to the legal entity of the university,

Institute of Technology PETRONAS Sdn Bhd.

Due acknowledgement shall always be made of the use of any material contained in, or derived from, this thesis.

© Phong Guan Ming, 2021

Institute of Technology PETRONAS Sdn Bhd

All rights reserved.

TABLE OF CONTENT

ABSTRACT.....	vii
ABSTRAK.....	viii
LIST OF FIGURES	xiv
LIST OF TABLES	xv
LIST OF ABBREVIATIONS.....	xvi
LIST OF SYMBOLS	xvii
CHAPTER 1 INTRODUCTION	1
1.1 Background Study	1
1.2 Problem Statement.....	3
1.3 Research Objectives.....	4
1.4 Significance of the Research	4
1.5 Scope of Study	5
1.6 Organization of the Thesis.....	5
CHAPTER 2 LITERATURE REVIEW	7
2.1 Chapter Overview	7
2.2 Foam Fundamental	7
2.2.1 Foam Definition	8
2.2.2 How is Foam Formed?	8
2.2.3 Foam Parameters	9
2.3 Foam in Porous Media for Enhanced Oil Recovery (EOR)	11
2.3.1 Effect of Foam Parameters on Foam Stability	12
2.3.1.1 Capillary Suction Effect.....	12
2.3.1.2 Gibbs Surface Elasticity and Marangoni Theory.....	14
2.3.1.3 Disjoining Pressure	16
2.3.1.4 Gravity Drainage.....	17
2.3.2 Effect of External Parameters on Foam Stability	18
2.3.3 Foam Generation Mechanism in the Porous Media	26
2.3.3.1 Leave Behind	26
2.3.3.2 Lamella-division	27

2.3.3.3 Snap-off.....	28
2.3.3.4 Neighbour-induced bubble pinch-off.....	29
2.3.4 Mechanism of Foam Destruction in Porous Media.....	30
2.4 Nanoparticles as a Foam Stabilizer in FAWAG Injection	32
2.4.1 Mechanism of Nanoparticles as a Foam Stabilizer in FAWAG Injection	33
2.4.1.1 High Particle Detachment Energy	33
2.4.1.2 Particle Arrangement During Film Drainage.....	34
2.4.1.3 Reduced Capillary Pressure	35
2.4.1.4 Maximum Capillary Pressure of Foam Coalescence	38
2.4.2 Effect of Nanoparticles on Foam Stability Against External Parameters.....	39
2.4.3 Influence of Nanoparticle’s Parameters on Stability of the foam	42
2.5 Nanoparticles Assisted Foam Injection Using Fly Ash Nanoparticles.....	47
2.6 Chapter Summary	50
CHAPTER 3 MATERIALS METHODOLOGY	51
3.1 Chapter Overview	51
3.2 Chemicals and Materials.....	53
3.3 Synthesis of Nanoparticles from Coal Fly Ash using Chemical Treatment....	56
3.3.1 Synthesis of FANP1 Nanoparticles using Chemical Treatment	57
3.3.2 Synthesis of FANP2 Nanoparticles using Chemical Treatment	58
3.4 Preparation of Foaming Solution.....	60
3.5 Characterization of Nanoparticles and Coal Fly Ash	62
3.5.1 Nanoparticle’s Size Measurement.....	63
3.5.2 Nanoparticle’s Composition Analysis.....	64
3.5.3 Sedimentation of Synthesized Nanoparticles Experiment	65
3.6 Interfacial Tension (IFT) Measurement.....	66
3.7 Static Foam Stability Measurement.....	68
3.8 Core Flooding Experiment	69
3.8.1 Core Cleaning Methodology	69
3.8.2 Porosity and Permeability of Berea Core Measurement	70
3.8.3 Foam Injection Experiment	71

3.9 History Matching and Sensitivity Analysis	72
3.10 Chapter Summary	74
CHAPTER 4 RESULT AND DISCUSSION	75
4.1 Chapter Overview	75
4.2 Nanoparticle's Size Measurement	76
4.3 Nanoparticle's Composition Analysis Study.....	79
4.4 Sedimentation Experiment of Synthesized Nanoparticles and Coal Fly Ash..	84
4.5 Interfacial Tension (IFT) Measurement.....	86
4.6 Static Foam Stability Measurement.....	89
4.7 Study of Foam and Oil Interaction	93
4.8 Foamability of Nanoparticle Assisted Foam Injection Measurement	95
4.9 Core Flooding Experiment	96
4.9.1 Mobility Reduction Factor (MRF)	97
4.9.2 Oil Produced by SAG Injection Measurement.....	101
4.10 History Matching	103
4.11 Sensitivity Analysis	104
4.11.1 Forecasting of Oil Recovery Study using Surfactant Adsorption by Reservoir Rock	105
4.11.2 Forecasting of Oil Recovery Study using Half-life of Foam Study	106
4.12 Chapter Summary	107
CHAPTER 5 CONCLUSION AND RECOMMENDATION	108
5.1 Conclusion	108
5.2 Recommendation	110
APPENDIX A.....	112

LIST OF FIGURES

Figure 2.1: Schematic illustration of the liquid structure in the foam [42].....	8
Figure 3.1: Research methodology of the research.....	52
Figure 3.2: Procedure of how nanoparticles are synthesized from coal fly ash	57
Figure 3.3: Methodology of Synthesized Nanoparticles FANP1	58
Figure 3.4: Methodology of Synthesized Nanoparticles FANP2	59
Figure 4.1: FESEM Image of CFA nanoparticles [176].....	76
Figure 4.2: FESEM Image of FANP1 nanoparticles	77
Figure 4.3: FESEM Image of FANP2 nanoparticles	77
Figure 4.4: FESEM Image of SiO ₂ nanoparticles	78
Figure 4.5: FESEM Image of Al ₂ O ₃ nanoparticles.....	79
Figure 4.6: XPS analysis of CFA, FANP1 and FANP2 nanoparticles	82
Figure 4.7: Turbidity experiment for CFA, PFA and SFA nanoparticles.....	85
Figure 4.8: Interfacial tension of foam solution with different type of nanoparticles .	87
Figure 4.9: ANOVA of the IFT measurement with different types and concentration of nanoparticles.....	88
Figure 4.10: Foam stability experiment with different type and concentration of nanoparticles	90
Figure 4.11: Nanoparticles and nanoparticles interaction energy profile generated by DLVO theory [223].....	91
Figure 4.12: Nanoparticles adsorption at the gas-liquid interface in form of (a) Monolayer (b) Close-packed monolayer or a bilayer (c) Network of particles aggregate at the gas-liquid interface [132].....	93
Figure 4.13: Foamability of foam with different concentration and type of nanoparticles	96
Figure 4.14: Pressure drops of foam injection and gas injection for different type of nanoparticles	98
Figure 4.15: MRF of SAG with different type of nanoparticles.....	100
Figure 4.16: Oil recovery for different levels of surfactant adsorption rate	105
Figure 4.17: Oil recovery comparison with different stability of foam half-life	106

LIST OF TABLES

Table 3.1: Chemicals and Materials.....	53
Table 3.2: Composition of Baronia Composition of Baronia Crude Oil in term of Hydrocarbon Chain.....	54
Table 3.3: Composition of Berea sandstone	55
Table 3.4: Properties of Nitrogen Gas	55
Table 4.1: Composition of nanoparticles using EDX analysis	81
Table 4.2: XPS energy peak analysis on CFA nanoparticles.....	83
Table 4.3: XPS energy peak analysis on FANP1 nanoparticles	83
Table 4.4: XPS energy peak analysis on FANP2 nanoparticles	84
Table 4.5: Nanoparticles stabilized foam interaction between oil and foam at concentration ratio of 80:20	95
Table 4.6: Properties of the Berea sandstone core	97
Table 4.7: Oil recovery of foam injection with different types of nanoparticles.....	102
Table 4.8: Oil recovery comparison between experimental and simulation run	104

LIST OF ABBREVIATIONS

EOR	Enhanced oil recovery
FAWAG	Foam assisted water alternating gas
IFT	Interfacial tension (N/m)
CMC	Critical micelle concentration
MRF	Mobility reduction factor
SAG	Surfactant alternating gas
PV	Pore volume
API	American Petroleum Institute
FESEM	Emission Scanning Electron Microscope
EDX	Energy-Dispersive X-ray Spectroscopy
XPS	X-ray Photoelectron Spectrometer
NTU	Nephelometric Turbidity Unit
MMP	Minimum Miscibility Pressure
PSD	Particle Size Distribution

LIST OF SYMBOLS

A_s	Total surface area in liquid-gas interfaces in the foam
A	Area
β	Theoretical packing parameter
ε_F	Specific foam surface of foam
ε_G	Specific foam surface of gas
ε_L	Specific foam surface of liquid
E_G	Gibbs surface of elasticity
FM	Non-dimensional of mobility reduction factor
f_{mmob}	Reference mobility factor
F_{surf}	Mobility reduction factor due to surfactant concentration
F_{dry}	Mobility reduction factor due to water saturation
F_{oil}	Mobility reduction factor due to oil saturation
F_{cap}	Mobility reduction factor due to capillary number
F_q	Foam quality
g	Gravitational force
H	Foam height or foam volume
h_f	Thin film (lamellae) thickness
k	Permeability of the reservoir rock
k_{rw}^0	End point of relative permeability of water
k_{rf}	Foam relative permeability
L	Length of the core
N_c	Capillary number
π_t	Total force
π_{st}	Steric force

π_{dis}	Dispersion force
π_{el}	Electrostatic force
\emptyset	Porosity
σ	Interfacial tension between gas and liquid
θ	Contact angle
σ_{ow}	Interfacial tension between oil and water
P_c	Capillary pressure
p_c^*	Critical capillary pressure
p_o	Reference pressure
p_e	Entry pressure
P_c^{max}	Maximum capillary pressure
P_{film}	Film pressure
P_o	Reference Pressure
p^{min}	Minimum pressure drops required to mobilize one lamella
P_{foam}	Pressure drop across the core during SAG injection
$P_{without\ foam}$	Pressure drop across the core during gas injection
ρ_{brine}	Density of the brine solution
q	Injection flow rate
R	Radius
S_{oi}	Oil saturation
S_{wirr}	Irreducible water saturation
S_{or}	Residual oil saturation
u_w	Velocity of water
μ_w	Viscosity of water
u_e	Viscosity of the aqueous phase
u_g^f	Gas viscosity with foam

u_g	Viscosity of gas
V_F	Foam volume
V_L	Volume of liquid content
V_G	Gas volume in the foam
v	Velocity
W	Work energy
W_r	Energy required to remove the particle from the interface of the foam
W_{after}	Weight of the core after submerging into the brine
W_{before}	Weight of the core before submerging into the brine
γ	Interfacial tension
γ_{GL}	Interfacial tension between gas and liquid
γ_{gw}	Interfacial tension of oil and water phase
γ_{og}	Interfacial tension of oil and gas phase
$\gamma_{\alpha\beta}$	Interfacial tension of two fluids
γ_{aw}	Interfacial tension of air and water
z	Height

CHAPTER 1

INTRODUCTION

1.1 Background Study

The production life cycle of a hydrocarbon reservoir consists of three stages which are primary recovery, secondary recovery, and enhanced oil recovery. In the primary recovery stage, the hydrocarbons are produced without any external stimulus due to sufficient reservoir pressure pushing the hydrocarbons upwards towards the surface. As a result of continuous production, the reservoir pressure will decline and consequently, reduce the hydrocarbons production. Therefore, to overcome this declining trend, a secondary injection technique is used to maintain the pressure. In enhanced oil recovery, some techniques are used to change the properties of the hydrocarbons such as gas injection, steam injection, surfactant injection, polymer injection and alkaline injection. Gas injection is one of the most widely used EOR method [1]–[4] due to its higher sweep efficiency than other EOR methods [5]. However, due to the characteristics of gas injection having lower density and viscosity than the crude oil, the process usually leads to viscous fingering, gravity segregation and early breakthrough [6]. Additionally, the heterogeneity of the reservoir will also contribute to poor volumetric sweep efficiency of oil production [7]. Therefore, to alleviate the drawbacks of gas injection, a combination of gas and chemical injection better known as foam assisted water alternating gas (FAWAG) injection or foam injection was proposed to reduce the effect of viscous fingering, gravity segregation and early breakthrough by increasing the displacing fluid viscosity and density [8], [9]. In other words, the foam injection will serve as a mobility control agent during gas injection [10], [11] by trapping the gas into the foaming solution. When the foam is formed, the gases are trapped in the foam and therefore, reduces the high mobility of the gas phase in the porous media [12], [13].

The concept of foam injection was first introduced in 1958 by Boud and Holbrook [14]. The foam is formed when the gas enters the layers of the foaming solutions that expands to trap the gas with a film of liquid membrane [15]. Normally, the shape of the foam is hexagonal which structure consists of a gas cells and the cell walls consist of lamellae that contains chemical solutions [16]. Maintaining the foam stability in the porous media under the condition of high temperature and high salinity conditions, however, is proven to be quite a challenging task. This is because the viscosity of the foaming solution tends to decrease with high temperature and enhances liquid drainage and increases gas diffusion in the foam lamellae [17], [18]. Secondly, liquid drainage leads to surfactants in the foaming solutions to start precipitate in the porous media when there is a high salinity condition. Precipitation is due to surfactants' reaction with the multivalent ions from the brine solutions [19], [20]. In addition, surfactants also tend to undergo a higher rate of thermal degradation process with the rise in temperature owing to the fact that they mostly have low thermal stability [21]. Lastly, and most observed phenomena is, the foam stability decreases with the presence of oil in the porous media [22].

The usage of nanoparticles in oil and gas industries is widely studied in EOR, drilling fluids, fracturing fluids and production application [23]–[26]. In EOR, nanoparticles are particularly useful for improving the foam stability. The adsorbed nanoparticles tend to reduce the direct contact between the fluids, therefore reducing the effect of liquid drainage, gas diffusion, and bubbles coarsening, which are the causes of foam instability [27]. Moreover, previous studies have shown that nanoparticles are less likely to suffer from the adsorption by reservoir rocks compared to surfactants [28]. Despite the advantages of nanoparticles, the application of nanoparticles for foam stabilization is deferred because a large amount of nanoparticles required to allow for field application on a commercial scale. [29]. Therefore, this study is focused on the: 1) economical production of nanomaterials from an abundant local waste material of coal fly ash, and 2) the effective use of the nanoparticles to stabilize foam in FAWAG injection for Malaysian field at the given reservoir conditions, and 3) the comparison between the produced and commercially available nanoparticles efficiency in stabilizing foam and increasing oil recovery. Coal fly ash is a waste

produced from the burning of coal and it can serve as a source of a large scale production of nanoparticles [30]–[32].

1.2 Problem Statement

Foam assisted water alternating gas (FAWAG) injection is used to control gas mobility and to overcome the drawback of gas injection. However, a major concern about foam injection is the foam stability in the porous media. Therefore, the foam stability is considered the most crucial parameter of the foam injection in porous media. This is because if the foam stability is low, the control of gas mobility will be low and results in early gas breakthrough. The foam stability is affected by many external parameters such as reservoir temperature, salinity of the brine and the presence of crude oil in the reservoir.

In recent years, the application of nanoparticles as an additive to increase the foam stability has proven to be a success. This is because the adsorbed nanoparticles into the foam interface will reduce the direct contact between the fluids (gas and surfactant), therefore reducing the effect of liquid drainage, gas diffusion, and bubbles coarsening. In addition, nanoparticles tend to provide a higher tolerance against the presence of oil when added into the foaming solution. This is because the adsorbed nanoparticles at the interface of the gas-liquid will strengthen the interface of the gas-liquid film and thus, reduces the liquid drainage rate, in which will lead to a stronger and stable foam production [33]. Although, foam stability increases with the addition of nanoparticles in the foaming solution, the availability of the nanoparticles such as silicon oxide and aluminium oxide for a large and economical scale applications may be hard to achieve. This is because 95% of silicon oxide produced in the world are used for construction and 90% of aluminium oxide produced are used for production of aluminium metal [34], [35]. Therefore, an alternative source is needed to replace the commercial source. In this research, an alternative source called coal fly ash is introduced as a replacement for silicon oxide and aluminium oxide. The minerology of coal fly ash contains mainly glassy aluminosilicates with some magnetic fractions such as hematite, magnetite iron, copper, and some non-magnetic fractions such as calcite, lime and quartz [29]. However, recent investigations describe the size of coal fly ash is bigger than 1 μ m in

size and cannot be classified as nanoparticles. Furthermore, the effectiveness of coal fly ash as a foam stabilizer is much lower compared to silicon oxide and aluminium oxide nanoparticles. However, in recent research such as wet grinding and chemical synthesis technique have manage to synthesis nanoparticles size [36]. According to Priya et al, the composition of the synthesized nanoparticles are mainly silicon oxides, aluminium oxide, and sodium sulphate [37]. Therefore, in this research, we will be focus on using chemical synthesis technique to synthesis nanoparticles from raw coal fly ash and investigate the effectiveness of synthesis nanoparticles compare to the commercial nanoparticles. Lastly, a simulation run is performed to determine the main governing factor of foam application in oil recovery for future research work in foam injection.

1.3 Research Objectives

- To evaluate the size and composition of nanoparticles synthesized from the coal fly ash through the chemical synthesis process in comparison to commercial nanoparticles.
- To determine the capability of synthesized nanoparticles to enhance foam stability and affect oil recovery under reservoir conditions in comparison with commercial nanoparticles.
- To determine the main governing factor of foam injection in increasing oil recovery using reservoir simulation

1.4 Significance of the Research

The research about using nanoparticles in the oil and gas industry has been increasing lately specially in the last few years and one of them is using nanoparticles as a foam stabilizer in FAWAG injection. Unfortunately, the usage of coal fly ash as a potential nanoparticle for foam stabilizer is limited. There was no reported synthesis technique to convert them to nanoparticle size required nor the study on its content for commercial application to date.

In this research, a two-step chemical synthesis technique is used to synthesize size nanoparticles that are to less than 100nm size and to investigate the capability of synthesized nanoparticles in increasing the half-life of the foam in comparison with other potential nanoparticles. The success of this study will enable the industry to mass produce the synthesized coal fly ash nanoparticles as a foam stabilizer for FAWAG injection. In addition, a simulation study is done to determine the main governing factor in improving oil recovery when using FAWAG injection.

1.5 Scope of Study

The scope of study is divided into three parts. The first part is the characterization study of coal fly ash nanoparticles after using the two-step chemical synthesis method. The purpose is to determine whether the two-step chemical synthesis process can successfully extract nano-size particles from the large and abundant sources: coal fly ash using FESEM (Field Emission Scanning Electron Microscope) analysis. In addition, the composition of extracted synthesized nanoparticles are also studied to determine the main component in the produced nanoparticles EDX (Energy-dispersive X-ray) and XPS (X-ray photoelectron spectroscopy) analysis. Meanwhile, the second part is to study the effectiveness of the synthesized nanoparticles in the porous media by comparing with the commercial nanoparticles; silicon oxide and aluminium oxide in terms of foam stability and oil recovery. The oil recovery experiment is also conducted to determine the relationship of foam stability and oil recovery using IFT experiment and core flooding experiment. The third part of the research is to determine the main governing factor of oil recovery using FAWAG injection using reservoir simulator.

1.6 Organization of the Thesis

This thesis is divided into five chapters and are describe as follows:

Chapter 1 includes the background study, problem statement, objective, significant of this research and scope of study of this research.

Chapter 2 includes explanation of foam concepts, definitions, and foam application in enhanced oil recovery such as foam generation methods, foam mechanism in porous media, foam destruction mechanism, and parameters affecting foam stability. The study of nanoparticles as a foam stabilizer is also included in this chapter which includes mechanism of nanoparticles as a foam stabilizer and parameters affecting nanoparticles stabilized foam.

Chapter 3 is discussion about research methodology and workflow of this research including chemicals, materials, equipment used and procedure for experimental works.

Chapter 4 comprises the experimental result and discussion of nanoparticles characterization process, characterization of nanoparticles, foam stability studies, oil recovery studies and sensitivity analysis the governing factor in foam for oil recovery.

Chapter 5 concludes the overall experimental and research work including the proposed recommendation for future experimental works.

CHAPTER 2

LITERATURE REVIEW

2.1 Chapter Overview

In this chapter, the explanation of the foam fundamentals, formation of foam in the porous media, effect of nanoparticles as foam stabilizer and coal fly ash as foam injected were discussed. The chapter is divided into four sections. The first section is the explanation of foam fundamentals such as definition, foam parameters, how foam is generated and method of foam generation. The second section described the foam stability in the porous media including its destruction mechanism and external parameters affecting foam stability. The third section is the discussion of nanoparticles usage in foam, its mechanism of affecting foam stability and effect of nanoparticles against external parameters such as reservoir temperature, salinity, surfactant adsorption by the reservoir rock and presence of crude oil in the porous media. The last section is the discussion on previous study on coal fly ash performance as a foam stabilizer for FAWAG injection.

2.2 Foam Fundamental

The foams played a major part in almost every industrial sector from food technology, medicine, cosmetics, and from environmental technology to oceanography. Foams were actually formed by the thousands of tiny bubbles from a solution by an external energy either from a mechanical origin or chemical origin [38]. In this section, the fundamentals of foam were described thoroughly to enhance the understanding on foam.

2.2.1 Foam Definition

The foam can be defined as the non-continuous dispersion system that consist of gas bubbles separated by the foaming liquid layers [39]–[41]. Figure 2.1 illustrated the gas bubbles trapped in the liquid structure in the foam [42]. The region that encompassed the two gas-liquid interfaces which was separated by a layer of thin film of liquid called lamella, and each gas-liquid interface has a surface tension. In Figure 2.1, the blue circle indicated the plateau border and plateau border was defined as the connection of three lamellae connected to each other and the connection of the lamellae is at 120° each [43].

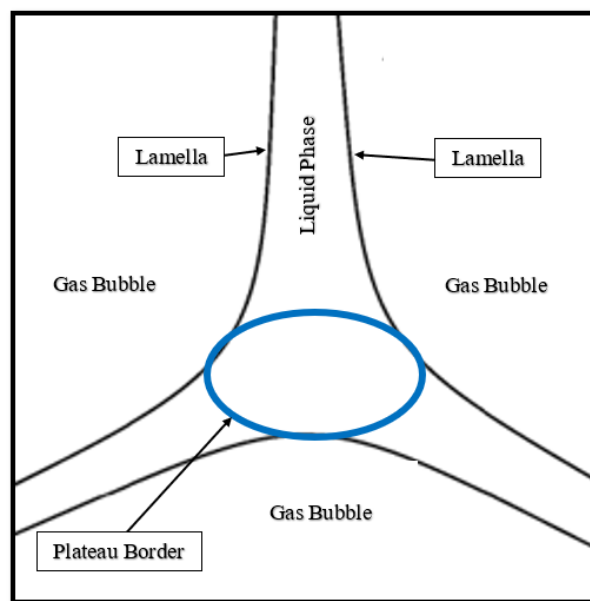


Figure 2.1: Schematic illustration of the liquid structure in the foam [42]

2.2.2 How is Foam Formed?

The foam was formed through the transformation of gas emulsion into polyhedral foam when the gas content in the foam reaches between 50% to 70%. The formation of foam can be observed through the behaviour of the rising bubbles. Each bubble will form a hemispherical liquid film when reaching the liquid surface. The foam can be explained as followed [44]:

1. Smaller bubbles were dissolved, while bigger bubbles grew bigger due to the diffusion of small bubbles in the continuous phase.
2. Gas bubbles rapidly cream, thereby causing a segregation into a foam layer on top of the surface of the liquid.
3. As the number of gas bubbles increases at the surface, the distance between each gas bubbles will become closer. The capillary attraction between gas bubbles will helped the process of bubble contact and deformation in which resulting in the formation of polyhedral foam.

The presence of surfactant will ensure the liquid films to have a longer lifetime. As the number of gas bubbles increases at the interface, the distance between each gas bubble will become closer. The capillary attraction between gas bubbles will helped the process of bubble contact and deformation, resulting in thin liquid film formation between neighbouring bubbles [45].

2.2.3 Foam Parameters

The foam quality and foam stability are the two important parameters in characterising the foam, to determine whether the foam is stable or unstable condition [45]. The foam quality can be defined as ratio between the foam volume and the volume of liquid content and can be expressed mathematically by the following equation (2.1):

$$F_q = \frac{V_G}{V_F} = \frac{V_G}{(V_G + V_L)} \quad (2.1)$$

Where:

V_F = Foam volume

V_L = Volume of liquid content

V_G = Gas volume in the foam

F_q = Foam quality

The foam stability can be defined as the ability of a foam to maintain its foam shape and parameter at a constant with time such as the total foam volume, liquid content, and foam bubble size. The half-life of foam is the most common usage to measure foam stability [46] and can be defined as the time taken for the foam volume to decrease down to half-of its original foam volume [47]. Bikerman test is the most common method to measure foam stability as shown in Figure 2.2 [48]. The gas was injected from the bottom through a porous plug into the liquid and the Bikerman coefficient can be measured at this stage. The Bikerman coefficient or foam half-life can be calculated by measuring the average bubble lifetime in foam before it collapses, and it can be expressed as in equation (2.2) and foam height is the maximum height of the foam generated.

$$\Sigma = \frac{H}{v} \quad (2.2)$$

Where:

Σ = Bikerman coefficient

H = Foam height or foam volume

v = linear gas velocity

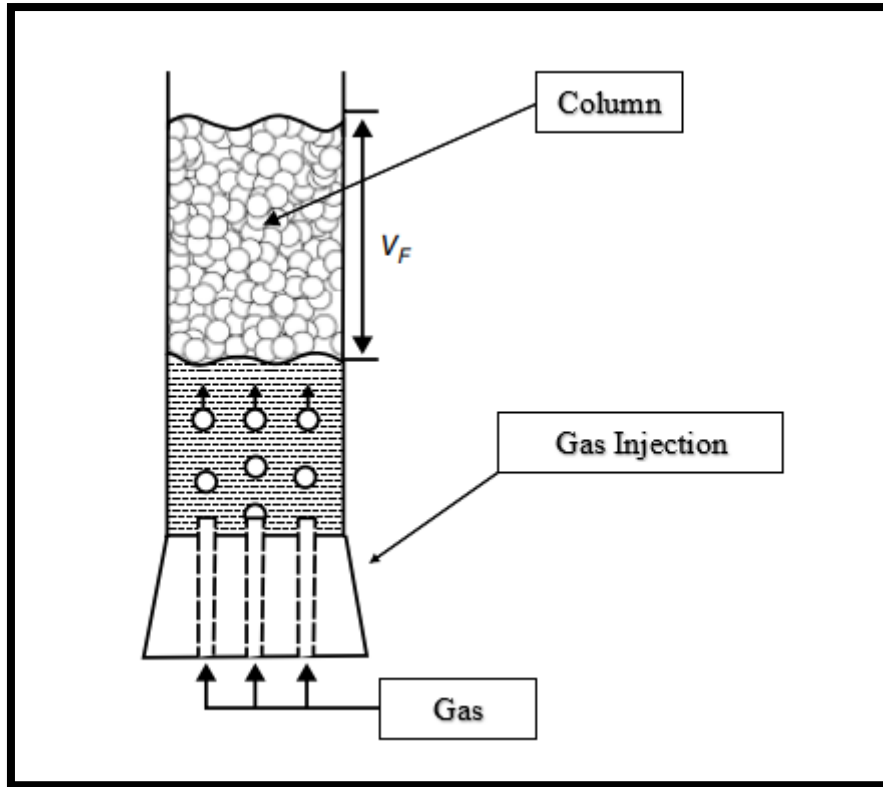


Figure 2.2: Foam Stability Experiment using the Bikerman approach, where the gas is injected through a porous plug and the height of the foam volume is measured over time [48]

2.3 Foam in Porous Media for Enhanced Oil Recovery (EOR)

Foam injection can be defined as a dispersion of gas molecules into the liquid phase while the liquid phase remains as a continuous phase with the lamella creating a discontinuity of the gas phase [49] to control gas mobility and overcoming the deficiency of gas injection [50]. In this section, we will be discussing about the foam parameters, external influence on the foam stability and foam generation of foam injection in the porous media.

2.3.1 Effect of Foam Parameters on Foam Stability

Foam stability is considered the most critical parameter to control gas mobility because the weak foam stability will be no difference than a normal gas injection. The parameters that affect the foam stability are the surface tension of two fluids, capillary pressure, Gibbs-Marangoni effect, and disjoining pressure. During the foam formation, the big unstable bubbles will reduced into smaller stable bubbles and five phenomena occurred which were [51]:

1. The liquid flowed over from the interfacial films (Capillary suction)
2. Diffusion of gas from smaller bubbles into larger ones (Bubble coalescence)
3. Redistribution of the bubbles along the height of the foam volume (Gibbs-Marangoni Effect)
4. Natural escape of liquid from the foam (Gravity drainage)
5. Destruction of inter-bubble films (Film rupture)

Therefore, in this section, we will be discussing the mechanism of destabilization foams such as capillary suction effect, Gibbs-Marangoni effect, disjoining pressure, disjoining pressure and gravity drainage.

2.3.1.1 Capillary Suction Effect

Capillary pressure can be defined as the pressure difference across the interface between two immiscible fluids [43]. According to the Young-Laplace equation, the surface tension played a major role in controlling capillary pressure. When the surface tension between gas and liquid reduces, the capillary pressure will be increased, and it be expressed in equation (2.3):

$$P_c = P_g - P_w = \frac{2 \sigma \cos \theta}{R} \quad (2.3)$$

Where:

P_c = Capillary pressure

σ = Interfacial tension between gas and liquid

θ = Contact angle

R = Radius of curvature

When the pressure of the liquid in the lamella is higher than the pressure of liquid at the plateau border, the pressure difference between them will cause the liquid to flow towards the plateau border. The pressure difference of liquid in the lamella and plateau border is called capillary suction effect and this will result to the reduction in lamella thickness and film thinning of the foam [52]. Figure 2.3 showed the illustration of capillary suction effect.

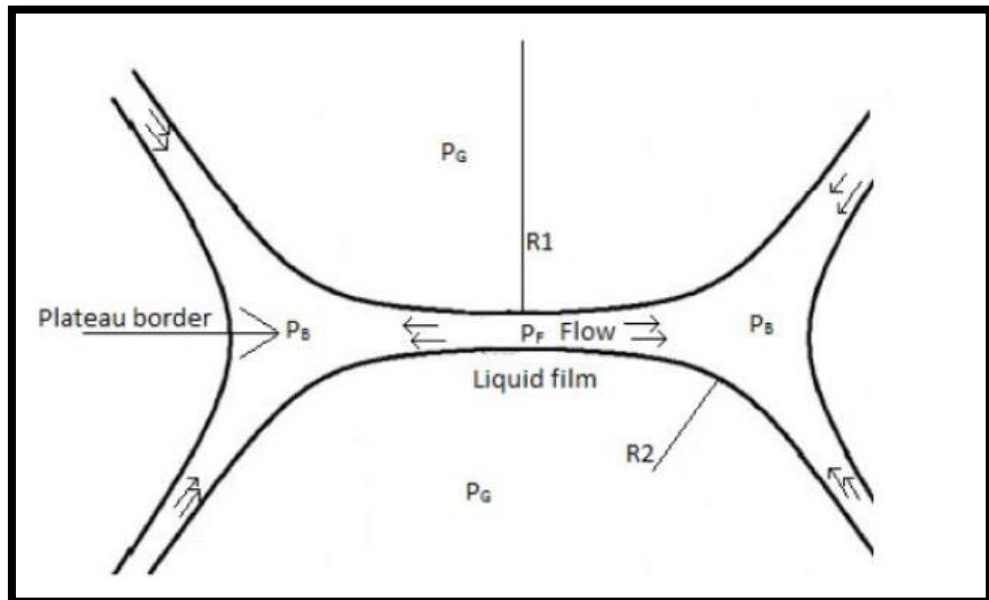


Figure 2.3: Illustration of capillary suction effect [52]

2.3.1.2 Gibbs Surface Elasticity and Marangoni Theory

When the expansion of the thin film occurred, some of the expanded area of the thin film will have a higher surface tension due to lack of surfactant molecules presence in these areas. When there is a higher surface tension at a certain area, the surfactant molecules will move from a lower surface tension area to a higher surface tension area, in order to reduce the surface tension of the area until an equilibrium of the foam is achieved. The movement of surfactant molecules from a lower surface tension area to a higher surface tension area in order to repair the foam films and prevent the whole film area from rupture is called Marangoni theory [53], [54].

The foam elasticity is defined as the energy exerted to the lamella due to external stress on the surface layer and it is an important parameter to reduce film thinning because it promote the self-heal effect during deformation in order to avoid rupture [43]. When the surfactant molecules moved along the interface in order to relieve the surface tension gradient of the other area, the movement along the interface will induced an elasticity in the film surface and the elasticity effect is called Gibbs surface elasticity [55]. The surface elasticity can be increased by increasing the surfactant concentration and if the surface elasticity is higher, the foam stability will be higher. However, when the concentration of surfactant reaches the critical micelle concentration (CMC), the surface elasticity will decreased gradually [56]. The Gibbs surface of elasticity can be mathematically explained in equation (2.4):

$$E_G = \frac{d\gamma}{d \ln A} \quad (2.4)$$

Where:

E_G = Gibb's surface of elasticity

A = Area of the surface.

γ = Surface tension of liquid and gas

Therefore, to increase the surface elasticity of the foam, a lower surface tension will be needed. Figure 2.4 explained the illustration of Gibbs-Marangoni effect [57].

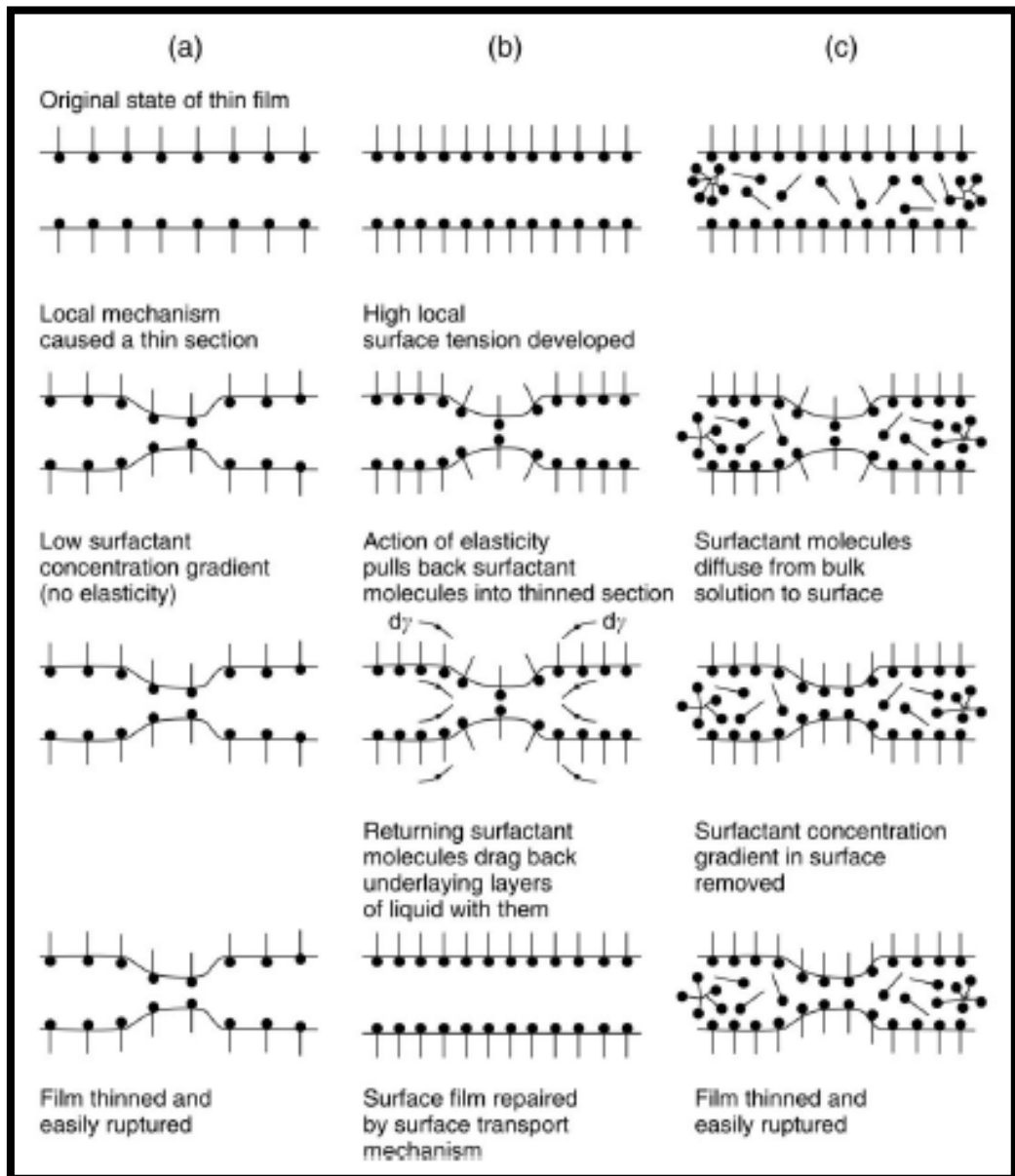


Figure 2.4: Gibbs–Marangoni effect: (a) surfactant concentration $< CMC$; (b) surfactant concentration = CMC ; (c) surfactant concentration $> CMC$

2.3.1.3 Disjoining Pressure

The disjoining pressure can be defined as the summation of the dispersion force (per unit area), the electrostatic forces and the steric forces, as defined in equation (2.5) [58]

$$\pi_t = \pi_{st} + \pi_{dis} + \pi_{el} \quad (2.5)$$

Where:

π_t = Total force

π_{st} = Steric force

π_{dis} = Dispersion force

π_{el} = Electrostatic force

During the formation of two monolayers at the gas-liquid interface by the surfactant molecules, the pressure between the two gas-liquid interfaces in the lamellae will cause lamella to be thinner [59]. However, this process can be stopped by the interaction between the two surfaces of the lamellae which is called disjoining pressure as shown in Figure 2.5. The disjoining pressure was contributed by the following three forces which were [60]:

1. The Steric repulsion force can only be generated at a very small distance where electron clouds of the molecules start to overlap to stabilize the film.
2. The London attractive dispersion force is a weak force that has a negative effect on destabilizing the film by exerting forces between the two non-permanent dipoles.
3. The force exerted between two opposite charges molecules is called electrostatic repulsive force. This force helps to separate the two charged molecules in the interfaces apart. Thus, the force will have a stabilizing effect on stabilizing the film.

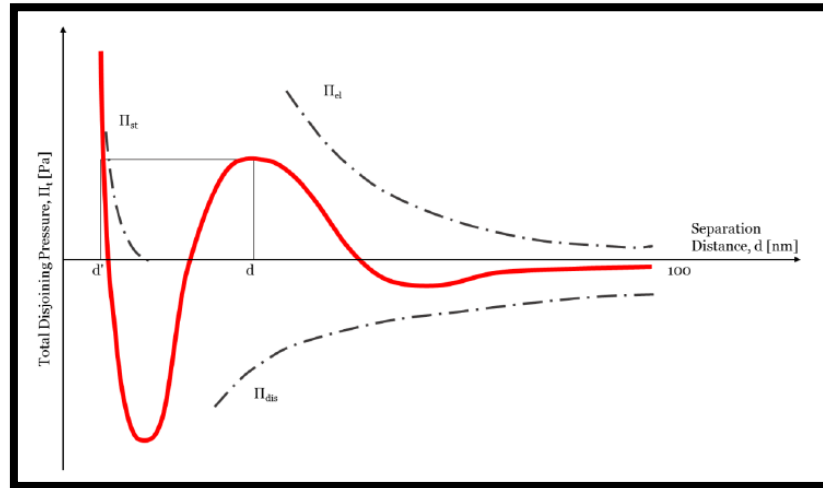


Figure 2.5: Graph of total disjoining pressure vs the separation distance between two interfaces. The dotted lines represent the three forces contributing to the total disjoining pressure [60]

2.3.1.4 Gravity Drainage

Gravity drainage is defined as a phenomenon where a denser fluid (liquid) will start to flow downwards and out from the foam interface due to the gravitational force effect [61]. The drainage will eventually convert the wet foam into a dry foam after a certain period. When the foam changed from a wet foam to a dry foam, the structure of the foam will also change from a spherical shape into a polyhedral shape. Furthermore, based on the Young-Laplace law, the capillary pressure of liquid in the dry foam will be lower than the capillary pressure of liquid in the wet foam [62]. Hence, the gravity drainage in the dry foam will decreased.

2.3.2 Effect of External Parameters on Foam Stability

In the last few years, there have been some significant studies on the external parameters that will affect the foam stability such as types of surfactant, concentration of surfactant, reservoir temperature, reservoir pressure, salinity of the brine, type of gas used, injection foam rate, surfactant adsorption by the reservoir rock, and the presence of crude oil.

The surfactant played a major role in the foam generation and maintaining the foam stability in the porous media. This is because the interfacial forces between the gas and liquid will be affected by the surfactant and in turn, the capillary pressure values will be affected [63]. Therefore, it is appropriate to select the suitable surfactant in generating a strong and stable foam against the high temperature and salinity conditions. Moreover, the surfactant should be capable of improving sweep efficiency while remains economical for implementation [63]. Surfactants are naturally amphiphilic which consist of a hydrophobic group (tail) and a hydrophilic group (head) [43] and can be classified into four types which are non-ionic, anionic, cationic, and amphoteric. A non-ionic surfactant does not contain any charges on its head group. Meanwhile, an anionic surfactant will contain a negative charge on the head and a cationic will contain a positive charge on its head group, respectively. Lastly, an amphoteric surfactant (zwitterionic) will contain both a positive and a negative charge in its head group.

Although, there were many different type of surfactants, all the surfactants have their own optimum concentration called “Critical Micelle Concentration (CMC)” [15]. When the surfactant concentration went beyond the CMC value, the number of micelles increases, and no other changes will occur. Figure 2.6 illustrated the surfactant molecules in gas-liquid interface when the concentration of surface is below the CMC value, equal to the CMC value, and above the CMC value. [64]. When the surfactant concentration is above the CMC value, the surfactant molecules will start formed a micelle arrangement when the hydrophobic tails will shield away from the liquid phase because the hydrophobic tails are afraid of water. Meanwhile, the hydrophilic head will be floating in the liquid phase. This is because the arrangement of this phenomenon helped to minimizes the surface free energy [65]. Although, the increasing of the

concentration of surfactant above CMC value does not change anything, the increasing of the surfactant concentration up to the CMC value will result in achieving a higher disjoining pressure and a more stable foam.

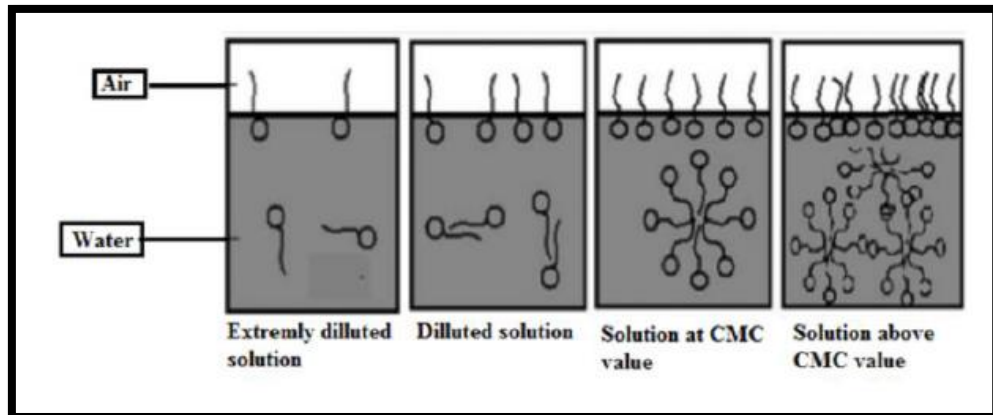


Figure 2.6: Illustration of surfactant in gas-liquid interface when the concentration of surface is below the CMC value, equal to the CMC value, and above the CMC value

The effect of high temperature of the reservoir is one of the parameters that will affect the foam stability. This is because the solubility of the surfactant in the brine will decrease due to the thermal degradation of the surfactant in high temperature conditions [66]. Furthermore, non-ionic surfactants or anionic surfactants are not suitable for foam generation in high temperature conditions due to the low cloud point of the surfactant. Cloud point is defined as the temperature at which cloudiness of the surfactant solution starts to appear due to the phase separation of the surfactant solution mixture [67]. For example, when the temperature is above the cloud point for non-ionic surfactants that consist of ethylene oxide groups, the hydrogen bonding between the ethylene oxide groups and water weakens with increasing temperature [68].

Reservoir pressure is one of the parameters that will affect foam stability of the foam that uses miscible gas such as carbon dioxide. This is because when the reservoir pressure increases, the miscible gas becomes denser and the intermolecular associations between the gas and the hydrophobic tails of the surfactant molecules will increase. In Chang et al. experiment, it was found that carbon dioxide foam injection has a higher sweep efficiency with increasing reservoir pressure regardless whether the reservoir

pressure is above or below the minimum miscibility pressure (MMP) [69]. The minimum miscibility pressure (MMP) is defined as the lowest pressure for carbon dioxide gas to develop the miscibility through a multi contact process with the crude oil in the reservoir at the certain reservoir pressure [70]. Furthermore, when the reservoir pressure is high, the London attractive force is weakened due to higher density of neighbouring gas molecules interacting with the surface water molecules [71]. When the London attractive force decrease, the disjoining pressure will increase. The surface tension of the gas-liquid interface was expected to decrease with the increasing of reservoir pressure [72]. This was partly due to the reduction of the density difference between the gas and liquid and the increase of surfactant adsorption at the gas-liquid interface. Equation (2.6) showed that the pressure gradient is inversely proportional to the surface tension of the gas-liquid interface [69]. When the pressure gradient increases, the surface tension of the gas-liquid interface decreases and hence, the stability of the foam increases.

$$\nabla p (p) = \frac{u_w \mu_w}{k k_{rw}^0} \left(\frac{p_c^*(p)}{p_e(p_o)} \right)^{2+3\lambda} \left(\frac{\gamma(p)}{\gamma(p_o)} \right)^{-(2+3\lambda)} \quad (2.6)$$

Where:

$\nabla p (p)$ = The changes of the pressure gradient

p_c^* = Critical capillary pressure

p_o = Reference pressure

$\gamma(p)$ = Surface tension of the solution at the limiting capillary pressure

$\gamma(p_o)$ = Surface tension of the solution at the reference pressure

p_e = Entry pressure

k = Permeability

k_{rw}^0 = End point of relative permeability of water

u_w = Velocity of water

μ_w = Viscosity of water

The salinity of the brine in the reservoir is another factor that will affect the foam stability. When the salinity of the brine is low, the presence of monovalent and divalent ions helped to reduce the electrostatic repulsion force between the surfactant molecules at the gas-liquid interface of the foam [43]. Therefore, it helped to promote more surfactant adsorption at the gas-liquid interface and resulted in the increase of the foam stability. However, when the salinity of the brine is high, the foam stability decreases. The foam stability decreases due to the decrease in electrostatic double layer (EDL) forces between the surfactant molecules at the gas-liquid interface. When the electrostatic forces decrease, the liquid drainage will increase thus the foam stability decreased [73]. Furthermore, with high salinity, the solubility of the surfactant into the brine decreases and the salt content in the brine will cause the precipitation of the surfactants. The precipitation was due to the reaction between the divalent ions and the surfactant molecules in the porous media and it will completely or partially block the pore of the porous media [74]. However, different brine solutions will have different reactions with different types of surfactants hence it will produce a different effect accordingly. Similarly, different types of surfactant will have different temperature tolerance, and salt tolerance [75]. In Liu et al. experiment, the anionic surfactants such as Chaser CD 1045 have a higher foam stability in the presence of high salinity solution [76] and in Torino et al. experiment, the presence of the high salinity solution also has a positive effect on the foam stability [77].

In foam injection, there are two types of foam injection which were immiscible and miscible foam injection. The main difference between the two injections was the type of gas used to generate foam. In immiscible foam injection, the inert gas such as nitrogen was used to generate foam whereas, for miscible foam injection, soluble gas such as carbon dioxide gas was used for foam injection. In the work of Frajzadeh et al., a comparison study between the miscible and the immiscible gas injection was done to determine the most suitable type of gas to generate foam and oil recovery improvement

in the porous media [78]. In the experiment, Alpha Olefin Sulfonate (AOS) surfactant was used as the surfactant and carbon dioxide or nitrogen gas were used as the comparison between miscible and immiscible gas to generate a higher foam stability and a higher oil recovery. The conclusion of the experiment was that immiscible foam injection produced a higher oil recovery than carbon dioxide foam injection. This is because the carbon dioxide foam produced a lower pressure build up than nitrogen foam, and a lower gas velocity than nitrogen gas. This is due to carbon dioxide gas being more soluble in water than to remain in gas phase itself thus consequently, most of the carbon dioxide molecules would preferred to be soluble in water resulting in a weaker foam [79]. In immiscible foam, different type of chemicals and additives can be added into the foam to improve the foam stability or the reduction of surfactant adsorption by the reservoir rock. [80]. However, carbon dioxide foam has a more favourable interactions with the crude oil due to the oil swelling effect will occur when the carbon dioxide gas is mixed with crude oil. Swelling effect occur when the carbon dioxide dissolved and mix into the crude oil droplets. Therefore, this phenomenon will leads to the reduction of oil viscosity and the carbon dioxide foam will have a higher tolerance in the presence of the crude oil than nitrogen foam [79].

The injection rate of the foam also played a vital role of affecting the foam stability [81]. When the injection rate is high, the fluid segregation between gas and surfactant increases greatly whereas, when the injection rate is low, fluid segregation is low and a higher oil recovery was observed [82]. This is because a higher injection rate will reduce the interaction between the gas and surfactant solution. The injection rate of gas and surfactant also determined the foam quality and the foam quality played a major role in determining the characteristics of foam propagation and mobility [83]. This is because the foam stability will decreased when the foam quality is too low (wet foam) or too high (dry foam) [84]. According to Chang et al., the optimum foam quality is between 45% to 95% to exhibit the longest foam stability and the highest gas mobility reduction [85]. When the foam quality is below 45%, the foam is classified as the wet foam and the foam normally loses its foam properties and only reflects on the flow behaviour of liquid phase whereas, when the foam quality is above 95%, %, the foam is classified as dry foam and is too dry to be stable.

Surfactant adsorption by the reservoir rocks is one of the unwanted problems in foam injection application. This is because when the surfactant is adsorbed by the reservoir rocks, the concentration of surfactant in the solution will be reduced greatly and resulted in the decrease of foam stability. Therefore, to improve the stability of foam, a higher concentration of the surfactant is needed to overcome the surfactant loss to adsorption effect and continuing to produce a stable foam. In addition, different types of surfactant have different surfactant adsorption rates [86]. For example, in a sandstone reservoir, the anionic, non-ionic, or amphoteric surfactants were used. This is because the cationic surfactant has a positive charge while, sandstone rock has a negative charge. Due to the magnetic attraction between a positive charge and a negative charge, the adsorption of cationic surfactant increased. In the carbonate reservoirs where the rocks are positive charge, the cationic surfactants were preferred [80]. The adsorption of surfactant by the reservoir can be affected by various parameters such as surfactant formulation, crude oil composition, brine composition, rock mineralogy, and reservoir condition (temperature and pressure) [63]. According to the Novosad et al showed that surfactant adsorption decreased with increasing temperature [87].

The presence of the crude oil is the single most important fact to be considered for foam injection. This is because the purpose of implementing foam injection is to produce a higher oil recovery. However, the presence of crude oil droplets in the foam affects the foam stability [88]. The foam tends to collapse in the presence of the crude oil which allowed the oil droplets to flow into the foam structure and therefore destabilized the foam. The foam destabilization mechanisms occur in the presence of the crude oil were described as follows [89]:

- Surfactants may be adsorbed by the oil, during the oil emulsification, and cause the surfactants to deplete in the foaming solution and therefore from the gas-liquid interface of the foam.
- Surfactants adsorbed by the oil may be re-adsorbed by the foam lamellae and form a mixed surfactant-oil layer and produced a less favourable weak foam.

- The oil may spread spontaneously onto the foam lamellae and destabilized the foam interface.
- Oil emulsification may occur and allowed the oil droplets to enter and rupture the foam stabilizing interface.

Therefore, to further study the interaction between foam and oil, two models have been proposed to predict the foam stability by using the entering, spreading and bridging coefficients model or lamella number model [90], [91]. The entering, spreading and bridging model is calculated using the interfacial tension between the gas, surfactant and oil which can be shown in Figure 2.7 [92].

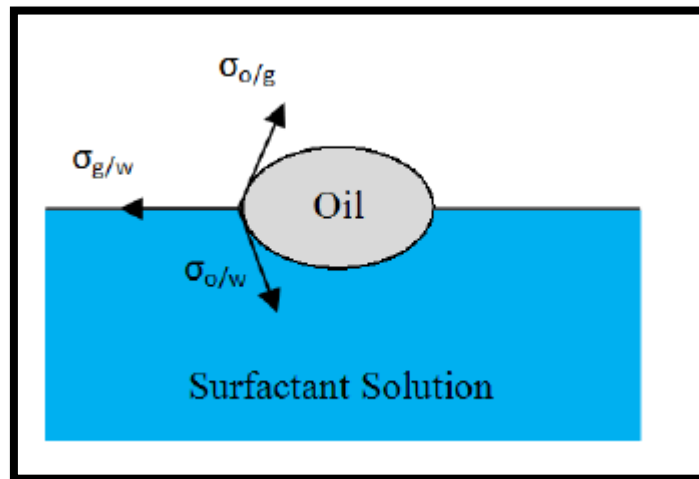


Figure 2.7: The interfacial tension of an oil droplet [92]

Equation (2.7) showed the entering coefficient equation. If the calculated entering coefficient of less than zero, it indicates the oil droplets were unable to enter the foam interface. Meanwhile if the entering coefficient is higher than zero, the oil droplets will entered the foam interface and thus, the foam become unstable [93]. Equation (2.8) indicated the spreading coefficient equation [94]. If the calculated value of spreading coefficient is less than zero, the spreading of oil into the liquid interface will not occur. However, if the value is higher than zero, the spreading of oil will flow into to the gas-water interface and results in the decreased of the foam stability. Then the oil droplets will formed a bridge when the oil droplets fully spread across the foam and the bridge is called the bridging coefficient as explained in equation (2.9) [95]. If the calculated bridging coefficient is less than zero, it indicates the foam is stable whereas, if the

bridging coefficient is higher than zero, the foam is unstable. This is because when the bridging coefficient is higher than zero, the capillary pressure pushes the water molecules away from the interface instead of the oil droplets [96].

$$\text{Entering coefficient, } E = \gamma_{gw} + \gamma_{ow} - \gamma_{og} \quad (2.7)$$

$$\text{Spreading coefficient, } S = \gamma_{gw} - \gamma_{ow} - \gamma_{og} \quad (2.8)$$

$$\text{Bridging coefficient, } B = \gamma_{gw}^2 + \gamma_{ow}^2 - \gamma_{og}^2 \quad (2.9)$$

$$\text{Lamella No., } L = 0.15 \frac{\gamma_{gw}}{\gamma_{ow}} \quad (2.10)$$

Where:

γ_{gw} = interfacial tension of gas and water phase

γ_{ow} = interfacial tension of oil and water phase

γ_{og} = interfacial tension of oil and gas phase

The second model is the lamella number model. The model was first proposed by Schramm et al., where the emulsification of the oil droplets in the foam will cause the lamella to rupture [97]. This model is introduced to study the interaction between the foam and oil in the porous media and the model can be described in equation (2.10) [96]. Based on the equation (2.10), if the lamella number is less than one, the foam generated will be stable in the presence of the oil droplets. If the lamella number between one and seven, the foam will be moderate stable. However, if the lamella number is higher than seven, the foam will be unstable [96].

2.3.3 Foam Generation Mechanism in the Porous Media

The foam was produced when the gas entered the layers of liquid and the gas is trapped in the gas with a film of the liquid membrane [15]. The foam then formed a hexagonal structure of gas cells whose cell walls consist of lamellae with approximately plane parallel sides [16]. In Rossen et al. study, the foam can be formed in three different section of the porous media [98].

1. The inertial flow may create foam generation at the well itself with the surface facilities.
2. Foam can be generated at the near-wellbore region where the pressure gradient and flow rate are still high.
3. In the formation far from the injection well where the pressure gradient and flow rate are much lower.

Each flow regime will be resulted in the entirely different foam generations and flow behaviours. There are three type of generation mechanisms that will lead to foam generation in the porous media which were leave behind, lamella-division, and snap-off foam generation mechanism [99]. In recent studies, there is another new concept of foam generation called neighbour-induced bubble pinch-off [100].

2.3.3.1 Leave Behind

The leave-behind foam generation mechanism only occurs when there are two or more gas fronts approaching the same pore body [101]. The two fronts will then converge together and formed a large parallel number of lamellae. Normally the foam generated using this mechanism will be a weak foam [101]. Furthermore, depending on the pore neck geometry, the foam may collapse when the gas exits the pore body due to the absent of the surfactant. However, this mechanism is the only mechanism that allowed the gas to have a continuous flow without any blockage [102]. Figure 2.8 illustrated the leave-behind foam generation mechanism [103].

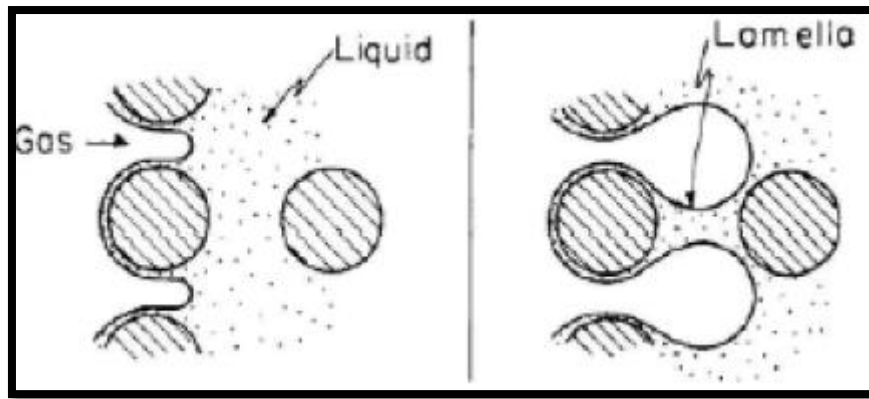


Figure 2.8: Leave-behind foam generation mechanism [103]

2.3.3.2 Lamella-division

Lamella-division is the second type of mechanism for foam generation. This mechanism happens when two or more lamellae are formed from a single lamella. However, this mechanism only occurred when using the pre-generated foam. The pre-generated foam starts to accumulate the gas in the foam and forms a larger bubble size than the pore body [104] and it only occurred if the large bubble encounters a branched point and with enough capillary pressure, a division of lamellae will occurred [105]. Figure 2.9 illustrated how the lamella-division mechanism occurred [103]. Initially, when the lamella entered the two pore throats, the lamella will stretch around the pore body so that it can break away and form another new lamella at each pore throat [106]. The lamella created by this method will have a lower gas mobility because the flow direction of lamella-division is perpendicular to the flow direction of snap-off mechanism [107].

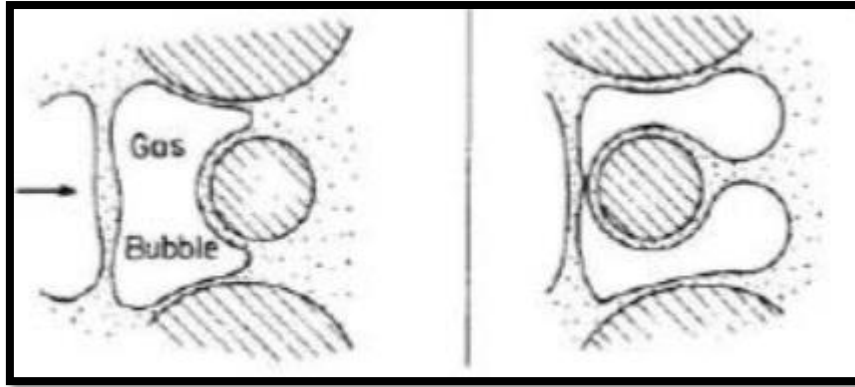


Figure 2.9: Lamella-division foam generation mechanism [103]

2.3.3.3 Snap-off

The third type of mechanism is the snap-off mechanism. This mechanism is the most dominant mechanism for foam generation in the porous media [108]. Figure 2.10 illustrated the snap-off mechanism in the porous media [103]. The snap-off mechanism occurred when the gas front is flowing through the pore throat to another pore body that is filled with the liquid. The gas then expands and formed a gradient of interfacial curvature between the gas at the pore throat and the gas outside the pore throat as the gas exits the pore throat. This gradient will create a pressure difference between the front and at the throat [109]. If the capillary pressure at the front is lower than the capillary pressure at the throat, the difference in capillary pressure will allowed the gas bubbles to snap off [110]. In order for the snap off mechanism to work, the ratio of pore throat to the pore body must be 1 to 2.67 ratio [111]. The foam generated using this mechanism can provide several hundred-fold of reduction in gas permeability meanwhile, leave-behind mechanism can only generated a maximum five-fold of reduction in gas permeability [112], [113]. Therefore, this mechanism is considered the most dominant mechanism due to its ability to produce a more stable foam than other two mechanisms.

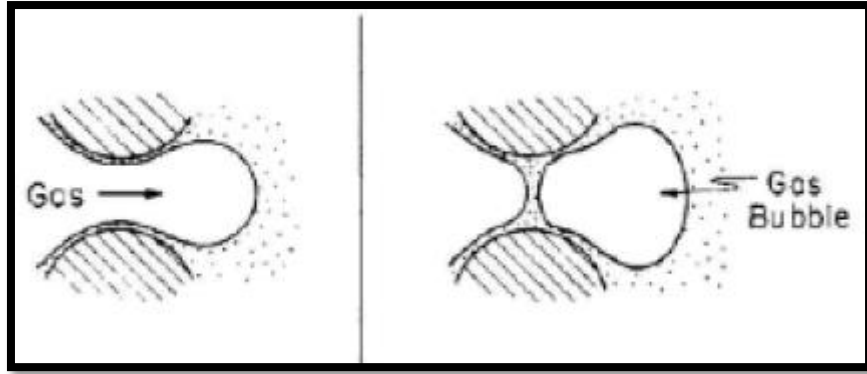


Figure 2.10: Snap-off foam generation [103]

2.3.3.4 Neighbour-induced bubble pinch-off

According to the Liontas et al. experiment, a new foam generation mechanism was discovered, and it was called the neighbour-induced bubble pinch-off. Foam generation using this method can be divided into two groups which were the neighbour-wall pinch off method and neighbour-neighbour pinch off method. In Figure 2.11(a) illustrated the neighbour-wall pinch off method, when the two bubbles were trying to squeeze into the same pore throat. One of the bubbles will try push the other bubble while trying to enter the pore throat, the slower bubble will then break the bubble that is flowing faster into two bubbles. The red arrow and the white arrow in Figure 2.11(a) indicate the flow direction of the two bubbles. In Figure 2.11(b) illustrated that three bubbles were trying to flow through the same pore throat, when the middle of the three bubbles is flowing faster than the other two, the middle bubble will break into two by the other two bubbles. The red arrows in Figure 2.11(b) indicate the flow of bubbles try to break the blue colour bubble into two [100].

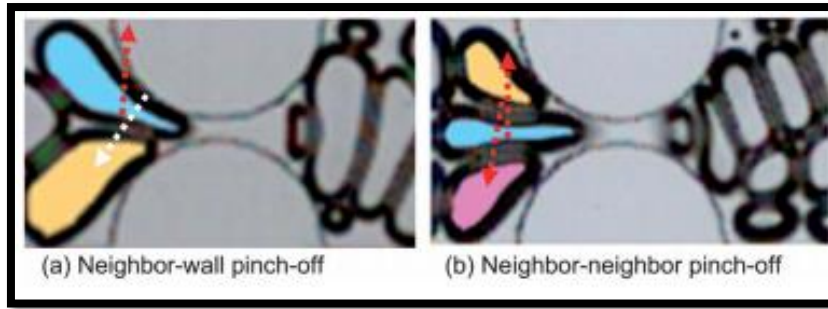


Figure 2.11: Neighbour-induced bubble pinch-off mechanism: (a) neighbour-wall pinch off and (b) neighbour-neighbour pinch off, the red and white arrows indicates the flow of the bubbles [100]

2.3.4 Mechanism of Foam Destruction in Porous Media

Foam destruction is one of the critical mechanisms for generating a stronger foam [114]. Therefore, in this section, the foam destruction was discussed in this section and the three mechanisms were bubble coalescence, bubble coarsening and liquid drainage [115]. Bubble coalescence is the result of two smaller bubbles merging into one larger bubble due to the rupture of liquid films between bubbles [116]. Figure 2.12 will be explaining the overall process of bubbles coalescence:

- (a) When the gas bubbles were approaching each other.
- (b) The hydrodynamic interaction between approaching bubbles which can cause deformation on bubbles surfaces called the “dimple”.
- (c) Formation of a plane-parallel film by the gradual disappearance of the dimples
- (d) Coalescence of bubbles if attractive pressures overcome negative pressures along the film surface [117].

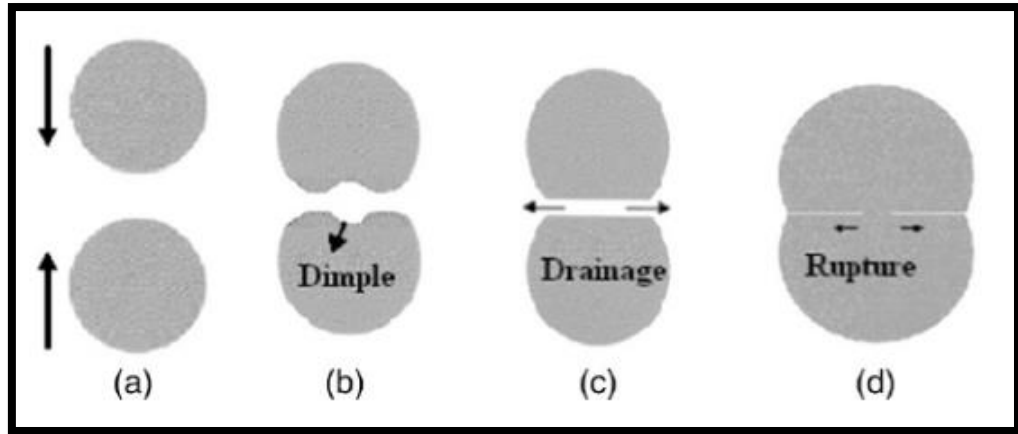


Figure 2.12: Bubble Coalescence Process [22]

The thin liquid film formed between two approaching bubbles is influenced by the capillary pressure. The capillary pressure arises from the curvature of bubbles during stage (b) in Figure 2.12 which can be defined as in equation (2.11) [118]:

$$P_c = \frac{2\sigma}{R} \quad (2.11)$$

Where:

P_c = Capillary pressure

σ = Surface tension of gas and liquid

R = Radius of curvature

When the film thickness is reduced to a thickness of 200nm to 300nm, the film drainage affected by the capillary will be slowing down. This is because the interactions between the two bubble's film surfaces will causes a pressure known as disjoining pressure to overcome the capillary force [119]. Depending on the balance of capillary pressure and disjoining pressure, if the film drainage takes a longer time for the bubbles to make contact, the liquid film will be assumed in a stable condition and the bubble coalescence will not take place [120]. Foam coarsening happened when there is a diffusion of gas from the smaller bubbles to a bigger bubble. This is because of the inner and outer pressure differences of the bubbles [41]. Hence, the smaller bubbles will disappear upon the contact with the bigger bubbles [121]. For a well-separated

droplet, this process is known as Ostwald ripening or called “coarsening” for cellular materials such as foams. Foam coarsening tends to increase the volume of certain size of bubbles at the expense of the other size of bubbles.

Foam drainage mechanism will start to occur when the foam starts to generate. This is because of the effect of the gravitational force, viscous force, and capillary pressure when the foam starts to generate. In the drainage process, the top of the foam will be the dry foam condition whereas, the bottom of the foam will be wet foam condition. This is because the liquid solution is flowing out from the bottom of the foam. Due to the foam drainage, the formation of the foam of the top section will always be polyhedral bubbles while, the bottom section of the foam will always be spherical shape due to the foam drainage. Hence, the foam drainage will always linked to the foam stability and other rheological properties of foam systems due to the formation of dry foam or the wet foam during the generation [122]. When the liquid films between the bubbles become very thin, the liquid films will eventually break. Therefore, the merging of two bubbles will be called bubble coalescence and the larger bubbles will start to appear in the foam and the number of bubbles decreases over time due to merging of bubbles and foam coarsening effect [123]. In general, the larger bubbles will continue to grow at the expense of smaller bubbles and at the end, smaller bubbles will disappear and eventually the foam collapsed [124].

2.4 Nanoparticles as a Foam Stabilizer in FAWAG Injection

In recent years, the usage of nanoparticles as a foam stabilizer is gaining attention due to its ability to overcome the limitations of conventional surfactant-stabilized foams. Nanoparticles are actually solid particles with a size of less than 100nm with its properties are being highly durable to the reservoir conditions [125]. The adsorbed nanoparticles helped to improve the foam stability by reducing the direct contact between the fluids to prevents liquid drainage, gas diffusion, and the rate of film rupture and bubbles coarsening [28]. Compared to the surfactants, nanoparticles are less prone to adsorption by the reservoir rocks and clay minerals. However, nanoparticles are still being influenced by many other factors such as concentration, size, and type of

nanoparticles [126]. Therefore, in this section, we will be discussing the mechanism of nanoparticles as a foam stabilizer for FAWAG injection, effect of nanoparticles stabilized foam against external factors and nanoparticles properties affecting foam stability.

2.4.1 Mechanism of Nanoparticles as a Foam Stabilizer in FAWAG Injection

When the foam that is stabilized by nanoparticles, it is largely dependent on the activity of nanoparticles at the foam lamellae. There are four type of mechanisms of nanoparticles that helped to improve foam stability which are high particle detachment energy, particle arrangement during film drainage, reduced capillary pressure and increased maximum capillary pressure of coalescence [127].

2.4.1.1 High Particle Detachment Energy

Particle detachment energy is defined as the total energy required to remove the adsorbed particles from the gas-liquid interface of the foam [128] and particle detachment energy can be defined as in equation (2.12) [129]:

$$W_r = \pi R^2 \gamma_{\alpha\beta} (1 - |\cos \theta|)^2 \quad (2.12)$$

Where:

W_r = Energy required to remove the particle from the gas-liquid interface

R = Radius of the particles

$\gamma_{\alpha\beta}$ = Surface tension of two fluids

θ = Particle contact angle at the interface of the fluids

Based on the equation, the radius of particles, surface tension and contact angle of two fluids are the main contributors to the increase of detachment energy. If the radius of particles or surface tension is high, the particle detachment energy will be higher.

According to Sun et al., if the nanoparticles size was 10nm, the contact angle will be close to 90° and the detachment energy from the equation will be $103kT$ which was 100 times higher than the detachment energy of surfactant molecules which was $1kT$ [130]. This is because when the contact angle is close to 90° , the $\cos \theta$ will be near zero and the detachment energy will be higher whereas, if the contact angle is close to 0° , the $\cos \theta$ will be near to one and the detachment energy will be low. Therefore, when the nanoparticles' detachment energy is high, a higher energy or force is required to remove the adsorbed nanoparticles from the interface of two fluids. Meanwhile, in the conventional foaming applications, surfactant molecules can be adsorb and desorb easily from the gas-water due to low detachment energy, however the adsorption of nanoparticles at the interface will be irreversible due to the high adsorption energy of nanoparticles [131]. Hence, the foams with nanoparticles tend to have a higher foam stability than foams without presence of nanoparticles.

2.4.1.2 Particle Arrangement During Film Drainage

The second effect of nanoparticles in improving foam stability is the nanoparticles arrangement at the gas-liquid interface. When nanoparticles were absorbed at the gas-liquid interface, some of the nanoparticles will formed a different structure arrangement because of the nanoparticle's aggregation, agglomeration and repulsion effect between the nanoparticles [132] as described in Figure 2.13 [115]. Figure 2.13(a) showed the nanoparticles were absorbed in a monolayer arrangement at the gas-liquid interface. The foam stability of the monolayer of bridging nanoparticles is largely dependent on the spatial resistance to stop the nanoparticles from breaking and exiting the bridge layer. For Figure 2.13(b), the nanoparticles was formed into a series of monolayer layer in the gas-liquid interface called bilayer layer. The bilayer layer of close-packed nanoparticles has a higher resistance against the dragging force of foam coalescence or foam coarsening effect than monolayer arrangement. Although, the bilayer layer of nanoparticles has a higher foam stability effect than monolayer nanoparticles, the arrangement of nanoparticles structure in Figure 2.19(c) has the highest foam stability effect between these three arrangements and called a series of aggregated nanoparticles layer [33]. This is because the aggregated nanoparticles at the gas-liquid interface tend

to create a thick solid film that will provide a steric barrier to film thinning and inter-bubble diffusion. Therefore, the presence of nanoparticles at the gas-liquid interface will help to slow down the gravitational effects and liquid drainage by reducing the direct contact between the fluids (gas and liquid). The formation of the nanoparticle arrangement is largely dependent on the interfacial rheological properties and capillary pressure of the foam. [115].

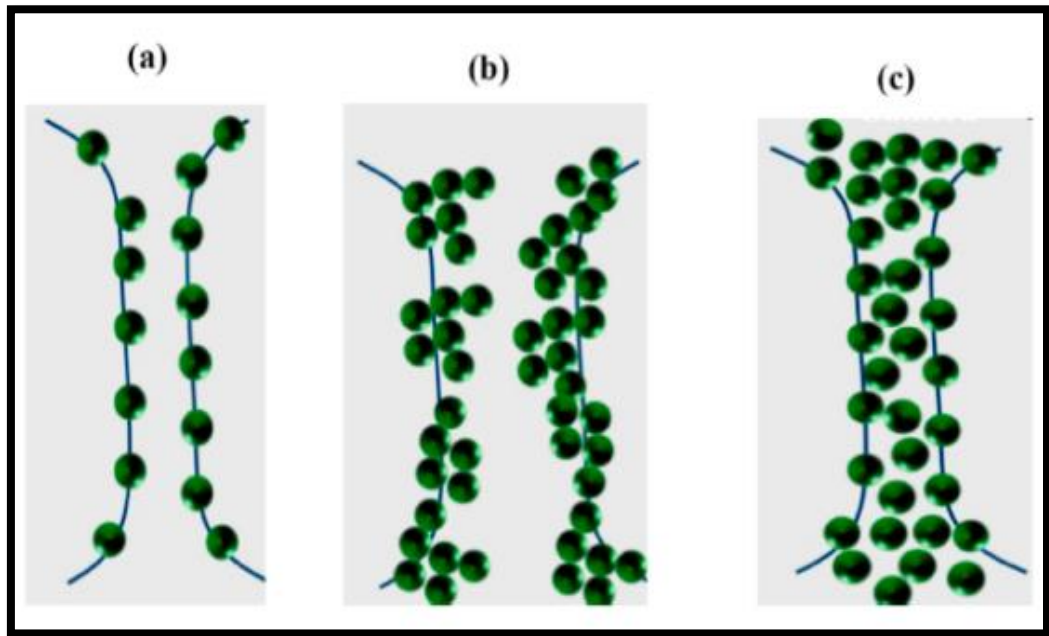


Figure 2.13: Particle Arrangement of nanoparticles in air-water interface [115]

2.4.1.3 Reduced Capillary Pressure

Capillary pressure is defined as the pressure difference across the gas-liquid interface of the foam due to the influence of capillary forces. If the capillary pressure increases, the faster the rate of foam coalescence. Capillary pressure can be defined as per equation (2.12) [133]:

$$P_c = \frac{\gamma}{R} (1 - \phi)^{0.5} \quad (2.12)$$

Where:

P_c = Capillary pressure

R = Foam film radius

γ = Interfacial tension

ϕ = Foam quality

Based on the equation (2.12), the capillary pressure will increase if the interfacial tension between two fluids increases, or the film radius decreases. Therefore, the interfacial tension between two fluids will be an important parameter to increase the foam stability [134]. However, the presence of nanoparticles in the foam will help to reduce the foam film radius due to higher stability control between the gas-liquid film [135]. This is because the adsorption and aggregation of nanoparticles between two bubbles help to reduce the capillary suction effect, Gibbs–Marangoni effect, and an increase in disjoining pressure. Furthermore, the capillary pressure is expected to be reduced due to the effect of the decrease in films thinning and lamellae drainage (drainage velocity in the lamellae) from the low value of foam film radius as shown in the equation (2.13) [136]:

$$V = \frac{dh_f}{dt} = \frac{h_f^3}{3 u_e R^2} \Delta P_{film} \quad (2.13)$$

Where:

V = Liquid drainage velocity,

h_f = Lamellae thickness,

R = Foam film radius

u_e = Viscosity of the aqueous phase

ΔP_{film} = Film pressure.

Film pressure can be calculated using equation (2.14) [134]:

$$\Delta P_{film} = 2 (P_c - \pi_d) \quad (2.14)$$

Where:

P_c = Capillary pressure

π_d = Disjoining pressure.

The liquid drainage velocity will be largely dependent on the film pressure and film pressure will be largely dependent on the increment of disjoining pressure and decrement of capillary pressure. Even though the presence of nanoparticles increases the film radius, the disjoining pressure will also increase to alleviate the drawback. Hence, with the presence of nanoparticles, the liquid drainage velocity will still be reduced thus, reduces the liquid drainage.

2.4.1.4 Maximum Capillary Pressure of Foam Coalescence

The capillary pressure of foam coalescence can be defined as the energy required to decrease the distance between two bubbles to almost zero and can be expressed as in equation (2.15) [137]:

$$P_c^{max} = \beta \frac{2 \gamma_{aw}}{R} \cos \theta \quad (2.15)$$

Where:

P_c^{max} = Maximum capillary pressure

γ_{aw} = Interfacial tension of air and water

θ = Nanoparticle's wettability in the air-water interface

R = Nanoparticle's radius

β = Theoretical packing parameter

When the maximum capillary pressure increased, the foam coalescence effect will be extended to a longer duration and thus, the foam stability will be increased. This is because when the capillary pressure reaches the maximum capillary pressure, the thin liquid film ruptures [138]. Based on the equation (2.15), the maximum capillary pressure can be increased if the nanoparticles present at the air-water interface of the foam, (β) increased. The nanoparticles presented at the air-liquid interface is largely dependent on the arrangement of nanoparticles in the air-liquid interface as shown in Figure 2.13. Furthermore, the maximum capillary pressure is depended on the value of interfacial tension and size of nanoparticles. If the interfacial tension decreases, the maximum capillary pressure will also decrease. This is because when the interfacial tension decreases, the capillary pressure will also decrease [139]. If the nanoparticle's size decreases to less than 100nm, the maximum capillary pressure will be higher than when the nanoparticle's size is above 1 μ m [140].

2.4.2 Effect of Nanoparticles on Foam Stability Against External Parameters

When nanoparticles migrated to the gas-liquid interface, the foam stability increases. This is because the foam with presence of nanoparticles has a higher tolerance against the effect of reservoir conditions such as temperature, salinity of brine, and adsorption of surfactant by the reservoir rock. [141]. Hence, in this section, we will be discussing the effect of nanoparticles on foam stability against reservoir condition.

Reservoir temperature is one of the critical parameters that reduced the foam stability. When the reservoir temperature is high, the surfactants in the foam will degraded. When nanoparticles were added into the foam, the foam stability will still decreases compared to the foam stability in ambient condition. This is due to the thermal agitation of the nanoparticles and insufficient adsorption of the nanoparticles and surfactant molecules at the gas-liquid interface when the reservoir temperature is high [18]. The effect of reservoir temperature on nanoparticles stabilized foam can be described into three reasons [142]:

1. The insufficient adsorption of nanoparticles at the lamellae because of the energetic movement of the nanoparticles gained in high temperature condition.
2. The reduction in the foaming solution viscosity with increasing of temperature. Therefore, the rate of liquid drainage will increase and resulted in bubble coalescence and thin film rupture.
3. The increasing rate of gas diffusion and evaporation of water from the thin liquid films will result in decrease of foam stability.

Even though, the stability of nanoparticles stabilized foam decreases with increasing of reservoir temperature, the foam stability with nanoparticles is still higher compared to foam without the presence of nanoparticles at the same reservoir temperature [143]. Furthermore, the apparent viscosity of nanoparticles foaming solution has a higher value (18 cp) compared to the apparent viscosity of foaming solution without nanoparticles (2 cp) at the same reservoir temperature [144].

High salinity of the brine is another critical parameter that will affect the foam stability [145]. The foamability and stability of the foam tend to decrease with the increasing of salt concentration in the brine solution when the concentration of the salinity increases from 0.5wt% to 5.0wt% [146], [147]. However, when nanoparticles were added into the foam, foam stability tend to increase with increasing of salt concentration [148]. When the salinity of the brine reaches a critical concentration called transition salt concentration, the stability of nanoparticles stabilized foam will be the highest and beyond the critical concentration, the foam stability will start to decrease [145]. This is because the foam stability was controlled by the sum of repulsive electrostatic forces and Van der Waals forces of the nanoparticles [149]. In the presence of the salts in the solution, the electrostatic repulsion force between nanoparticles becomes lower than the Van der Waals force of attraction between nanoparticles and therefore, it promotes the aggregation of nanoparticles in the gas-liquid interface [150]. This is because of the screening of the inherent charges of nanoparticles with the salts decreases the electrostatic repulsion force between nanoparticles [151]. However, when the nanoparticles start to aggregate in the gas-liquid interface, the aggregated nanoparticles will start to form a network of aggregated nanoparticles arrangement in the gas-liquid interface as shown in Figure 2.19(c) and will helped to increase the foam stability instead. This is because when the electrostatic repulsion between nanoparticles decreases, the energy barrier for nanoparticles adsorption and agglomeration at the gas-liquid interface will allow the formation of a series network of aggregated nanoparticles [152]. According to Kostakis et al., the increase of NaCl salt in the foaming solution resulted in the decrease of zeta potential and therefore allow nanoparticles adsorption at the air-water interface with ease [140]. Meanwhile, the stability of the foam without nanoparticles tend to decrease with increasing salinity of brine. This is because the presence of monovalent, divalent or multi-valent cation salts will react with surfactant and the surfactant will start to precipitate in the reservoir [153].

The foam stability decreases with the presence of crude oil even though the nanoparticles are added into the foam. However, the stability of the nanoparticles stabilized foam are much higher than the stability of the foam without any nanoparticles in the presence of the crude oil [128]. This is because the nanoparticles in the foam prevented the crude oil droplets from entering, or spreading into the foam which was

described in the entering, spreading and bridging coefficients model [154] discussed earlier. Based on Yekeen et al., the reason of the increase in foam stability for the foam with nanoparticles was because the nanoparticles in the foam were preventing the spreading of the oil droplets in the foam even though there was an accumulation of the oil in the foam plateau borders of the foam [149]. Therefore, the stability of the foam with nanoparticles remains higher than those without in as the nanoparticles also help to drain the oil droplets from the foam film and migrate the oil droplets to the plateau borders of the foam.

The stability of foam is greatly influenced by surfactant adsorption by the reservoir rock in porous media. The higher the adsorption rate of surfactant onto the rock, the less surfactant is adsorbed at the gas-liquid interface of the foam and thus, the foam stability will be greatly reduced [149]. The retention of nanoparticles in the porous media is described as the fierce collision and friction effect between nanoparticles and reservoir rock which may have led to a decrease in surfactant adsorption by the reservoir rock [155]. If the adsorption of surfactant by the nanoparticles on the reservoir rock's surface increases, the adsorption of the surfactant by the reservoir rock will decrease and vice versa [156]. However, when the nanoparticles and surfactant molecules were mixed, the nanoparticles and surfactant will form a negatively charged clusters and the mixture tend to suspend in the solution rather than residing on the reservoir rock surface and leads to a decrease of surfactant adsorption by the reservoir rock when the nanoparticles are presence in the solution [149]. However, if the concentration of the nanoparticles is too high, the interfacial tension between the two fluids of the foam will increase. This is because most of the surfactant will be adsorbed by the nanoparticles thus reduces the concentration of free surfactant in the foaming solution [157].

2.4.3 Influence of Nanoparticle's Parameters on Stability of the foam

The parameters of the nanoparticles can influence the stability of the foam. Nanoparticles are similarly to the surfactant, where different types and concentration, will influence of the stability of the foam. In addition, for nanoparticles, the size of the nanoparticles will also influence the foam stability. The nanoparticles are chemical compounds and therefore, the concentration of nanoparticles in the foaming solution will greatly affect the foam stability [158]. For example is Tang et al.'s experiment, the foam stability increased with the increase of nanoparticles concentration from 0.003 to 0.5wt % using silicon oxide with the size of nanoparticles kept at a constant of 400nm diameter size [159]. This is because the liquid drainage from foam films reduces when the nanoparticles concentration increases [160]. When the concentration of nanoparticles increases, the presence of nanoparticles at the liquid-gas interface will also increase and form aggregate particles instead of a monolayer bridging particles [161]. However, an optimum concentration of nanoparticles is required to achieve the highest foam stability. For example, in Figure 2.14, the foam stability decreased with the increase of nanoparticles concentration from 0.1wt% to 1.0wt% [162]. Another example is the Frye et al. experiment, when the concentration of silica oxide nanoparticles is less than 1wt %, the foam stability is much lower compared to the stability with concentration of 1wt% or higher [163]. Similarly, to surfactants, when the concentration of nanoparticles is beyond the optimum concentrations, the excess nanoparticles will start to agglomerate and formed a bigger particle network either in the liquid phase or at the gas-liquid interface, which interferes with bubbles formation. At above optimum concentration also, a rapid rate of liquid discharge will start to occur due to the action of exerted gravity by the heavy agglomerated nanoparticles in the interface of gas-liquid [164]. When the nanoparticles were migrating out of the foam, the surfactant molecules in the gas-liquid interface also decreased because most of the surfactant molecules were adsorbed by the nanoparticles and therefore, it will cause the foam coalescence phenomena to occur [147].

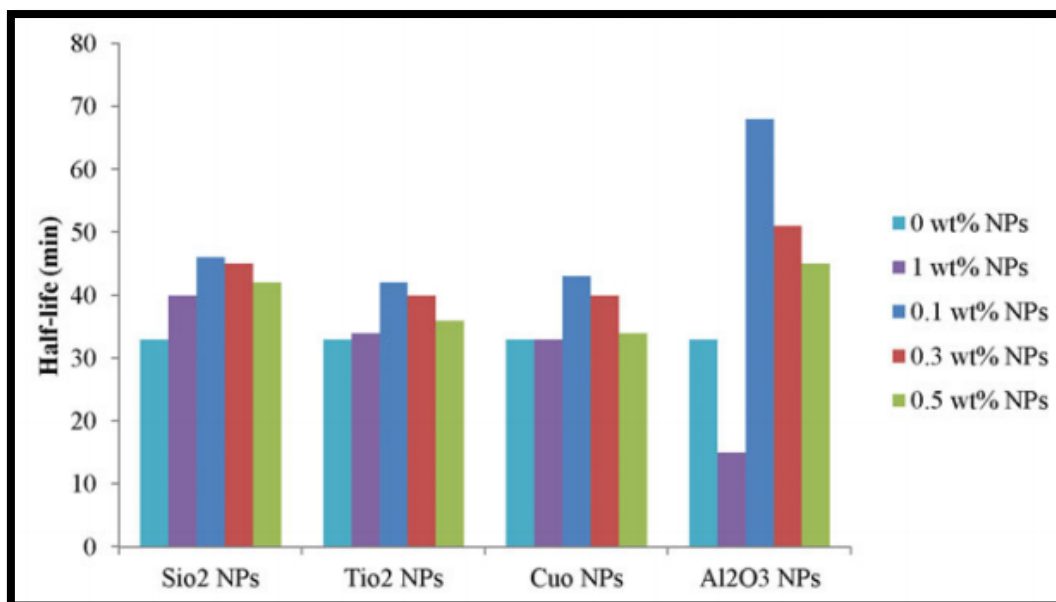


Figure 2.14: Comparison of foam half-life with different concentration and different type of nanoparticles [162]

The size of nanoparticles is another factor affecting the foam stability [28]. In Figure 2.15 showed that foam with nanoparticles size of 20nm has higher foam stability than the foam with nanoparticle size of 100nm and 500nm [165]. Furthermore, when the concentration of CTAB surfactant increases from the ratio of 1:1 to 1:30, the foam with 20nm size of nanoparticles has the highest foam half-life compared to the other nanoparticles. This is because the foam stability increases when the nanoparticles size is smaller. Smaller nanoparticles will tend to migrate to the gas-liquid interface of the foam easier than the larger-size nanoparticles [166]. This is because the smooth movement of the smaller nanoparticles to the gas-liquid interface of foam than the larger size nanoparticles [167]. Therefore, more nanoparticles were able to migrate into the gas-liquid interface than the larger size nanoparticles. This is because with less concentration of large size nanoparticles, the movement of nanoparticles into the interface will be easier and improved the stability of the foam by adsorption and accumulation of nanoparticles at foam lamellae.

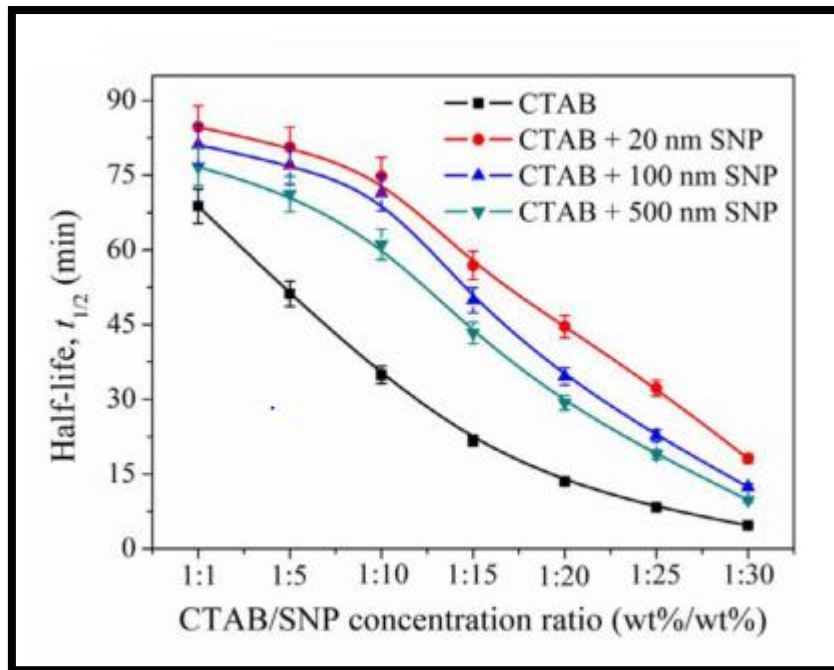


Figure 2.15: Foam half-life vs CTAB concentration with nanoparticles at different size (20nm, 100nm and 500nm) [165]

Similarly, to surfactants, the different types of nanoparticles will have different foam stability results. The most common nanoparticles used for foam stability is silicon oxide nanoparticles [144]. This is because the properties of the silicon oxide can be changed easier compared to the other types of nanoparticles. Furthermore, the foam with silicon oxide nanoparticles produces the highest foam stability compared to foam with aluminium oxide, titanium oxide or copper oxide nanoparticles based on Bayat et al. [168]. In Figure 2.16 showed that foam with silicon oxide has the highest foam stability compared to aluminium oxide, titanium oxide and copper oxide nanoparticles [168]. Meanwhile in Figure 2.17, the foam with silicon oxide nanoparticles has the highest oil recovery compared to foam with aluminium oxide, titanium oxide or copper oxide nanoparticles [168].

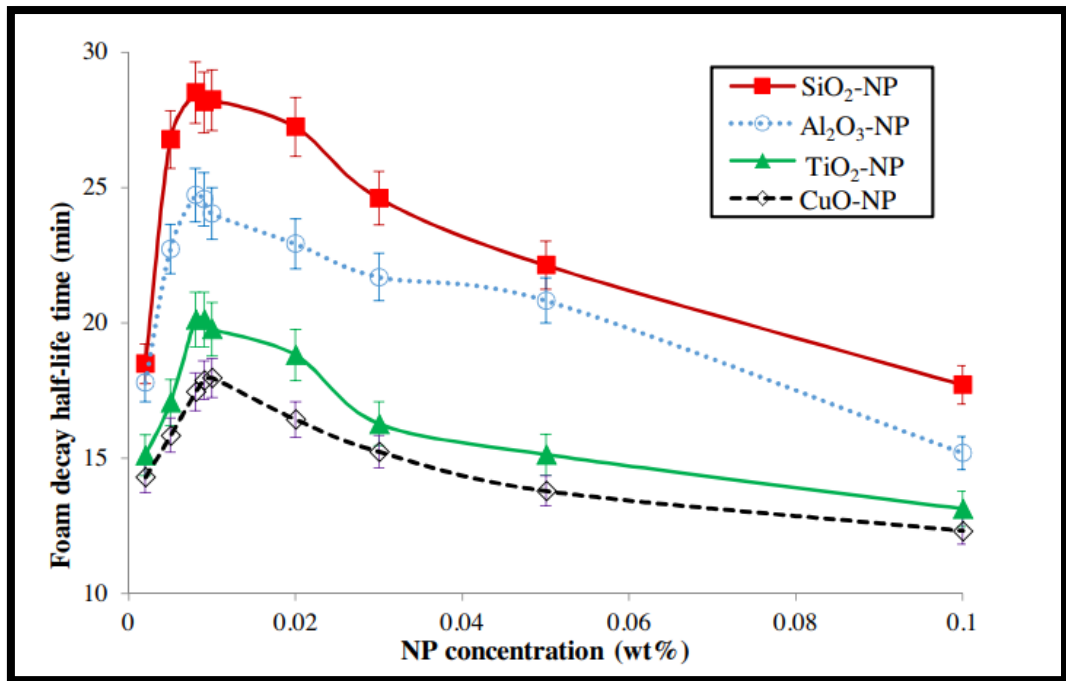


Figure 2.16: Foam half-life vs nanoparticles (NP) concentration with different type of nanoparticles [168]

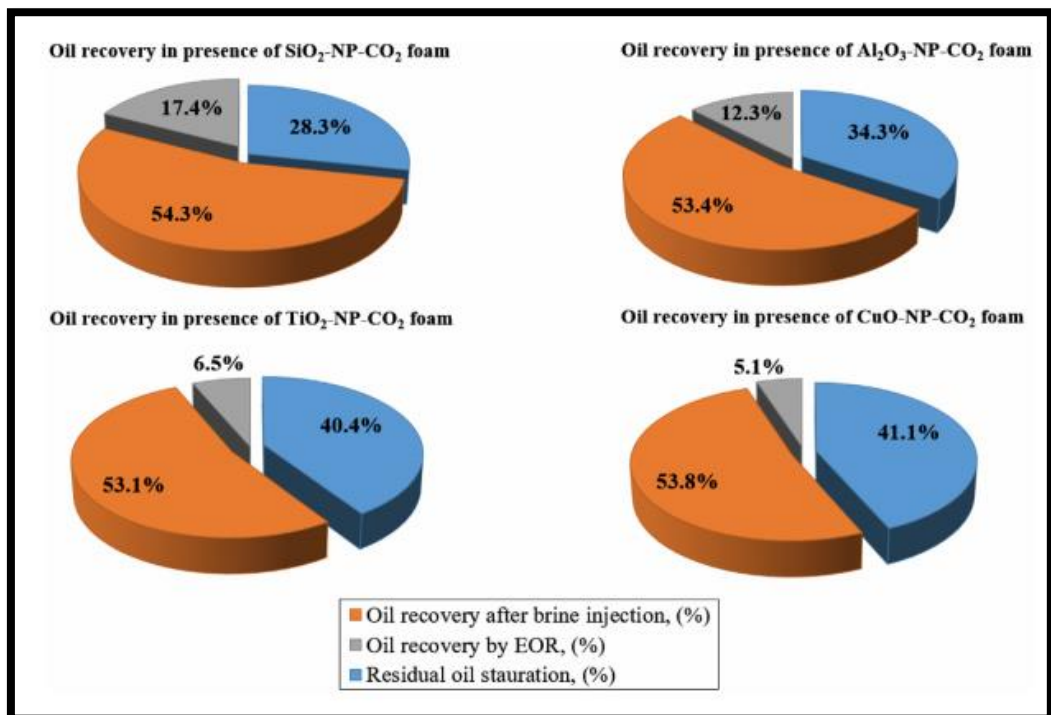


Figure 2.17: Oil recovery comparison with different types of nanoparticles [168]

However, there are other experimental works that produced a higher foam stability using aluminium oxide nanoparticles compared to that with silicon oxide, copper oxide or titanium oxide nanoparticles [162]. This is because the aluminium oxide nanoparticles has higher Hamaker constant compared to silicon oxide which enables the formation of a stronger network structure in foam film [169]. In Figure 2.14 showed that foam with aluminium oxide has the higher foam half-life compared to foam with silicon oxide, copper oxide or titanium oxide. In Figure 2.18 showed that foam with aluminium oxide nanoparticles has the highest oil recovery compared to foam with silicon oxide, copper oxide or titanium oxide nanoparticles [162]. Therefore, the available literatures were not enough to make an absolute conclusion that foam with silicon oxide or aluminium oxide nanoparticles will produced the highest foam stability. The only major conclusion is that foam with nanoparticles will have a better stability than foam without nanoparticles, irrespective of the types of the nanoparticles in the foam.

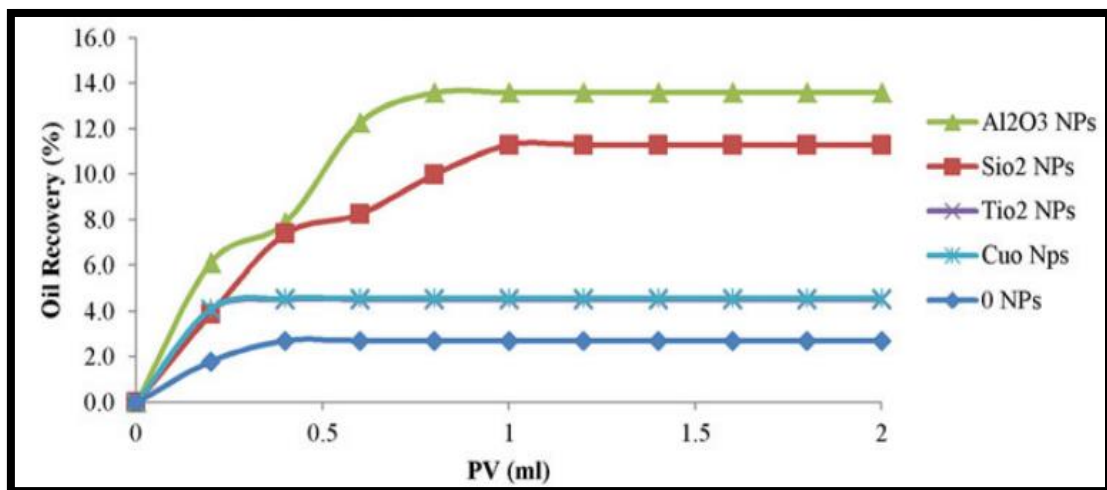


Figure 2.18: Oil recovery vs the pore volume (PV) of foam injected into the porous media with different types of nanoparticles [162]

2.5 Nanoparticles Assisted Foam Injection Using Fly Ash Nanoparticles

Despite the advantages of nanoparticles, the application of nanoparticles as a foam stabilizer on a commercial scale will require an abundant and inexpensive alternative source to produce a large quantity for field-scale application [29]. Coal fly ash is a by-product of burning coal and it can serve as an alternative source for low-cost large-scale production of nanoparticles [30]–[32]. However, the disadvantage of using fly ash nanoparticles compared to silicon oxide or aluminium oxide nanoparticles is the size of the fly ash sample. The size of nanoparticles played an important parameter because it helped to improve the stability of the foam [159]. Based on Singh et al. experiment, the diameter of the fly ash particles was between 18 μ m to 90 μ m, which is considered too large for the use to improve foam stability and therefore, the weak foam was generated and lower oil was produced compared to foam with other types of nanoparticles [170]. Therefore, to improve the performance of fly ash particles as a foam stabilizer, various techniques were used to produce fly ash nanoparticles with the size than 100nm such as dry grinding, wet grinding, alkaline mixing, and acid mixing. Based on Ishaq et al. experiment, the acidic treated fly ash and alkaline treated fly ash produced a higher foam stability compared to mechanical grinded wet or dry fly ash nanoparticles as shown in Figure 2.25 [171]. According to the Figure 2.25, the foam stability results of using mechanical grinded wet fly ash, acidic treated fly ash and alkaline treated fly ash were 92 minutes, 235 minutes, and 165 minutes, respectively. The stability of the foam with raw fly ash sample without any treatment was less than 50 minutes and the foam without any fly ash sample was between 100 minutes to 150 minutes which was much higher than when fly ash particles are added into the foaming solution. Therefore, it proved that the size of the nanoparticles played an important role affecting the foam stability. This is because the larger size nanoparticles will not be able to migrate into the gas-liquid interface since the diameter was larger than the foam lamellae. In addition, from the Figure 2.25, the foam with chemically treated fly ash produced the higher foam stability than foam with mechanically treated fly ash, raw fly ash or without any nanoparticles. When foam with fly ash sample is used for enhanced oil recovery (EOR) purposes, a high volume of foam solution is needed to improve oil recovery. In Figure 2.26 showed the pressure drop or pressure difference in the porous media when the foam is injected [170]. In figure 2.26(a) shows the foam without nanoparticles

producing a maximum pressure drop of 10psi meanwhile, in figure 2.26(b) shows the foam with fly ash nanoparticles producing up to a maximum pressure drop of 20psi. This showed that foam with nanoparticles regardless of size would help to improve the foam mobility compared to foam without nanoparticles. In Figure 2.27 showed the foam with AOS-LAPB surfactant mixed with fly ash sample has a higher oil recovery than foam with AOS-LAPB mixed with iron oxide nanoparticles [172]. However, the volume of foam injected for foam with fly ash sample was four times higher than the volume of foam injected for foam with iron oxide. This is because foam with fly ash sample has low foam half-life compared to foam with iron oxide and in the porous media, the foam with fly ash sample is more unstable compared to foam with iron oxide [172]

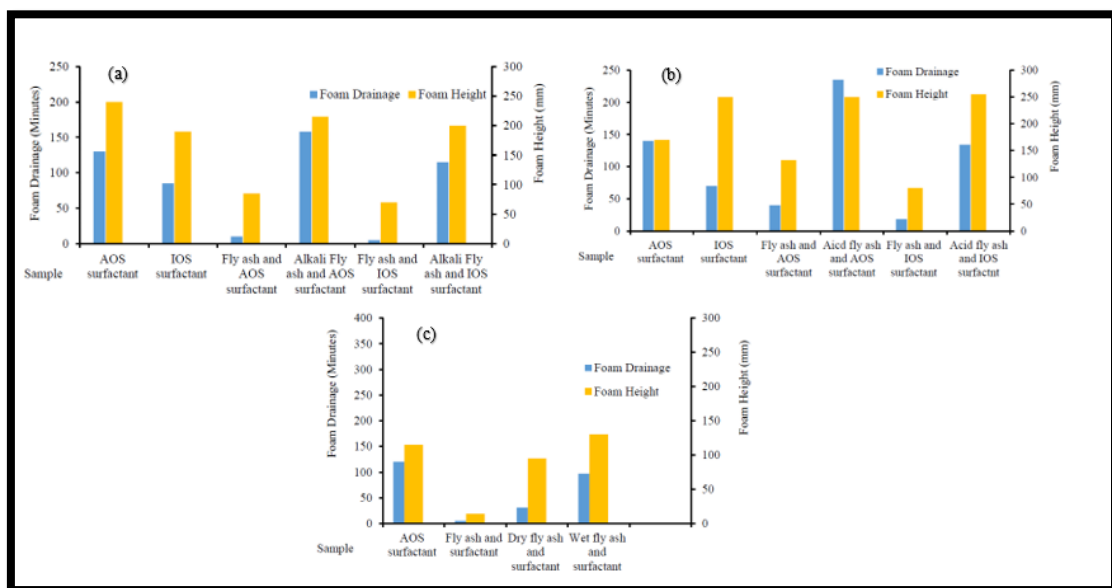


Figure 2.25: Nitrogen foam stability and foam height measurement in the presence of tapis crude oil with different type of surfactants fly ash nanoparticles, (a) alkali treated fly ash, (b) acidic treated fly ash and (c) dry and wet grinded fly ash [171]

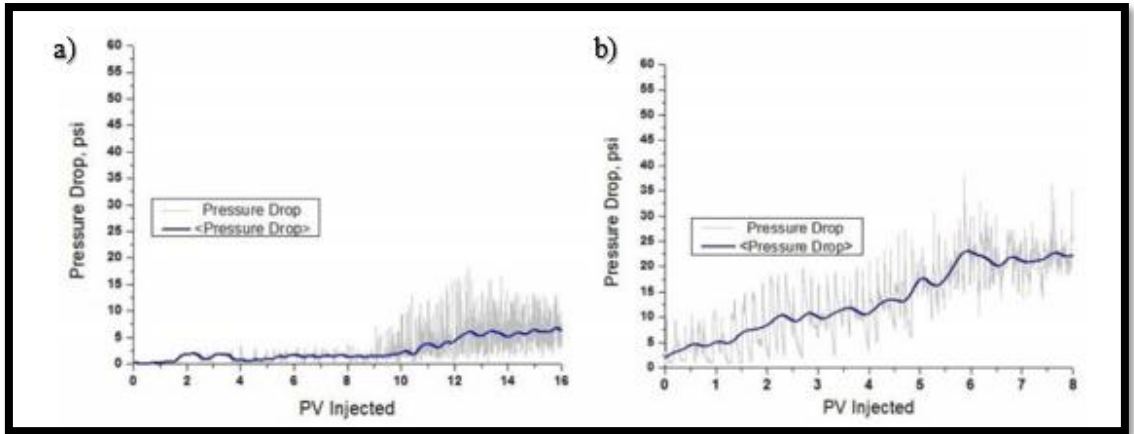


Figure 2.26: Pressure drop vs volume of foam injected a) foam without fly ash nanoparticles b) foam with fly ash nanoparticles [170]

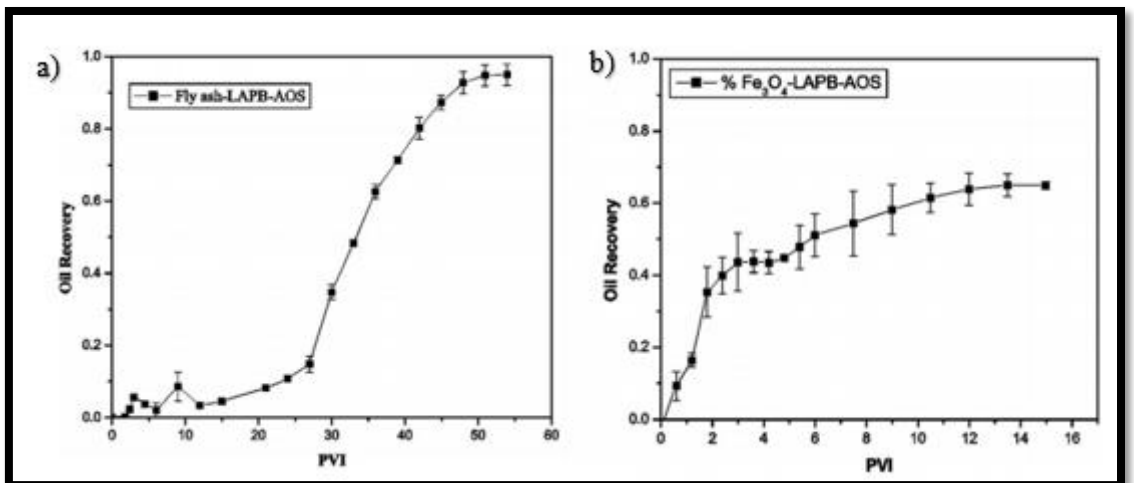


Figure 2.27: Oil recovery vs pore volume of foam injected, a) foam of AOS-LAPB + Fly ash, b) foam of AOS-LAPB + Iron oxide [172]

2.6 Chapter Summary

In nanoparticles study, the most important parameters of using nanoparticles as the foam stabilizer were the concentration of nanoparticles, size of nanoparticles and type of nanoparticles. From the results, the foam with silicon oxide and aluminium oxide nanoparticles produced the highest foam stability. One of the reasons in selecting fly ash particles as a foam stabilizer is because the main composition of fly ash particles is silicon oxide, and second highest composition is aluminium oxide. Secondly, a chemical synthesis was proposed to synthesis the nanoparticles from fly ash sample because foam with chemically treated fly ash has the highest foam stability compared to foam with mechanically treated fly ash, and raw fly ash as discussed.

CHAPTER 3

MATERIALS METHODOLOGY

3.1 Chapter Overview

In this research, we will be incorporating the experimental works, reservoir simulation and data analysis. Figure 3.1 will be discussing the detail procedure of all the experiments conducted from sample preparation until data obtained from the experimental works. The most important factor affecting foam injection in the porous media is the foam stability. Therefore, in this research, we will be mainly investigating the foam stability and foamability using various nanoparticles with an aim to extend the foam stability. The first section which is highlighted in blue background will be discussing the workflow of synthesising nanoparticles and characterization of nanoparticles such as the size and composition of the nanoparticles. In the second section which is highlighted in orange background, we will be discussing the experimental works related to the properties of the foam such as foam stability, foamability and IFT of the solution which may affect the foam stability or oil recovery when injected into the porous media. The third section which is highlighted in green background will be investigating the major governing factor of foam injection affecting oil recovery using Eclipse software.

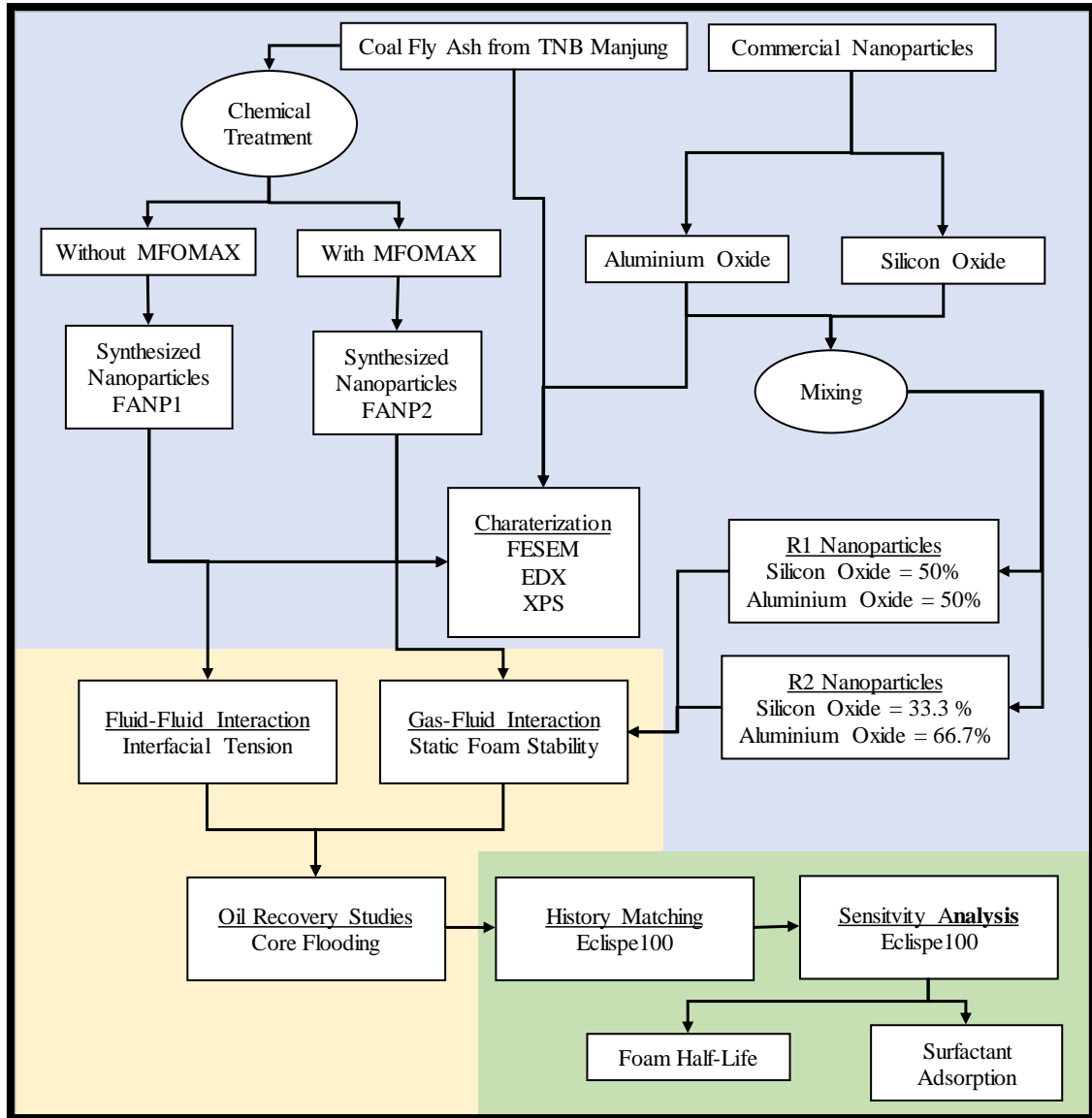


Figure 3.1: Research methodology of the research

3.2 Chemicals and Materials

Table 3.1 showed the chemicals and materials used for the experimental works. The MFOMAX surfactant solution was supplied by the Petronas Research Sdn Bhd company with a concentration of 20wt%. The surfactant is currently being patented hence no detailed content was provided by the company. However, the general description of the MFOMAX surfactant properties by the company is that it is a zwitterionic surfactant with some polymeric content in its structure [173]. The coal fly ash sample was supplied by the coal plant in Manjung, Perak, Malaysia. The Baronia crude oil and the Berea sandstone core samples were supplied by Petronas Research Sdn Bhd, Malaysia.

Table 3.1: Chemicals and Materials

Materials/ Chemicals	Supplied By
Coal Fly Ash	Manjung Tenaga Nasional Berhad (TNB), Malaysia
Sodium Chloride (NaCl)	Merck Millipore, USA
Calcium Chloride ($CaCl_2$)	R&M, Switzerland
Sodium Hydroxide (NaOH)	Sigma Aldrich, USA
Sulphuric Acid (H_2SO_4)	Sigma Aldrich, USA
Aluminium Oxide (Al_2O_3)	Sigma Aldrich, USA
Silicon Oxide (SiO_2)	US Research Nanomaterials, USA
Ethanol	Thermoscientific, USA
Whatmann Filter Paper	Thermoscientific, USA
MFOMAX surfactant	Petronas Research Sdn Bhd, Malaysia
Berea Sandstone	Petronas Research Sdn Bhd, Malaysia
Baronia Crude Oil	Petronas Research Sdn Bhd, Malaysia

The composition of the crude oil was described in Table 3.2 with a density of 0.8169 g/cm³ with an API of 39.4° in room temperature [174]. When the temperature increased up to 90°C, the density and API of the crude oil were 781.2 kg/m³ and 44.0° respectively.

Table 3.2: Composition of Baronia Composition of Baronia Crude Oil in term of Hydrocarbon Chain

Type of Hydrocarbon Chains	Percentage (%)	Type of Hydrocarbon Chains	Percentage (%)
C ₅₊	15.62	C ₁₈	0.3
C ₇₊	14.39	C ₁₈ – C ₂₀	7.19
C ₁₁	1.58	C ₂₀	0.22
C ₁₁ – C ₁₂	8.36	C ₂₀ – C ₂₂	3.64
C ₁₂	4.88	C ₂₂	0.38
C ₁₂ – C ₁₄	15.78	C ₂₂ – C ₂₄	0.73
C ₁₄	7.04	C ₂₄	0.07
C ₁₄ – C ₁₆	12.7	C ₂₄ – C ₂₆	0.19
C ₁₆	0.75	C ₂₆	0.01
C ₁₆ – C ₁₈	6.16	C ₂₆₊	0.03

The obtained Berea sandstone core samples were in cylindrical in size with a diameter of 1.5 inches and a length of 6.0 inches and the composition of the Berea sandstone samples were described in Table 3.3 [175].

Table 3.3: Composition of Berea sandstone

Composition of Berea Sandstone	Concentration (wt%)	Composition of Berea Sandstone	Concentration (wt%)
SiO ₂	84.60	CaO	0.20
Al ₂ O ₃	11.50	Fe ₂ O ₃	0.16
Na ₂ O	1.64	Cr ₂ O ₃	0.09
MgO	0.66	SO ₃	0.36
K ₂ O	0.60		

The properties of nitrogen gas was described in Table 3.4 because the nitrogen gas was mainly used for foam generation in this research.

Table 3.4: Properties of Nitrogen Gas

Density (g/ml) at 25°C and 14.7psi	Viscosity (cp) at 25°C and 14.7psi	Purity of nitrogen gas (%)
0.001251	0.0177	99
Critical Temperature (°C)	Critical Pressure (psia)	
-146.9	492.3	

3.3 Synthesis of Nanoparticles from Coal Fly Ash using Chemical Treatment

The aim of chemical treatment is to synthesis a nanoparticle size sample from the coal fly ash because the size of coal fly sample is larger than $1\mu\text{m}$ [170], [172], [176], [177]. Furthermore, for a material to be classified as a nanoparticle, the diameter of the material must be less than 100nm. The chemical treatment procedure is divided into two steps which are alkaline leaching and acid titration as shown in Figure 3.2.

Before the start of chemical treatment, the coal fly ash sample was washed with sulphuric acid (H_2SO_4) at a temperature of 100°C . This was done to remove any metallic impurities and any loss-on-ignition (LOI) components attached on the fly ash sample. The loss-on-ignition (LOI) is a standard method to evaluate the carbon content in fly ash sample according to the ASTM D3174-82 [170]. The leached fly ash was leached in an alkaline solution using sodium hydroxide (NaOH). The mixture was then filtered using the Whatman filter paper and neutralise with distilled water until the pH reached 7. The colourless filtrate was then collected and used for acid titration process. During the acid titration process, the sulphuric acid was slowly added into the filtrate, until the formation of the white gel appeared. The white gel was then used calcinated to produce the synthesized nanoparticles. Therefore, in this section, we will be describing the procedure of synthesising two synthesized nanoparticles FANP1 and FANP2 using chemical treatment.

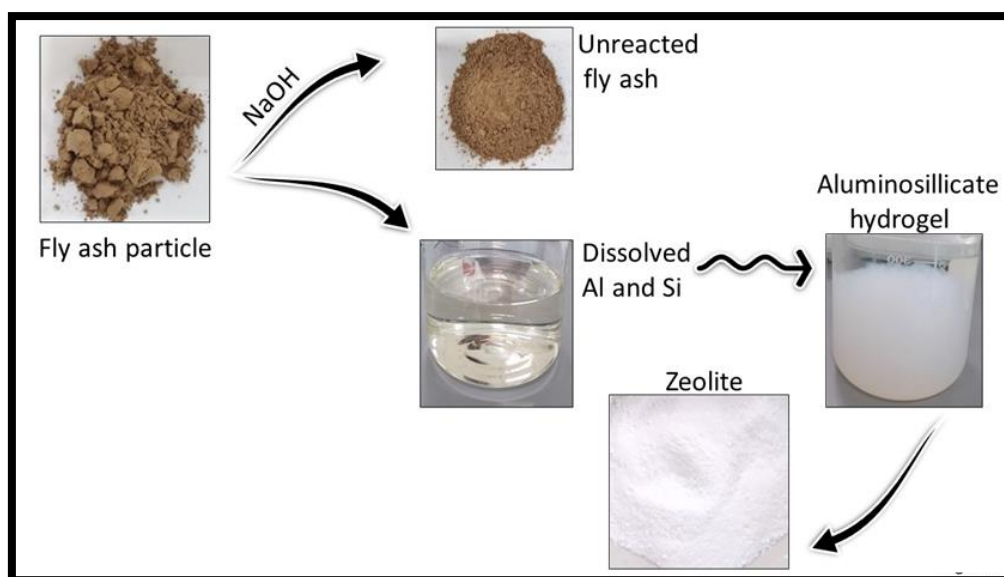


Figure 3.2: Procedure of how nanoparticles are synthesized from coal fly ash

3.3.1 Synthesis of FANP1 Nanoparticles using Chemical Treatment

The synthesis process for FANP1 nanoparticles using the chemical treatment was describe in Figure 3.3. Firstly, the coal fly ash sample was washed with sulphuric acid with a concentration of 10wt% and under a continuous stirring condition at the temperature of 100°C. The leached fly ash was then filtered using the Whatmann filter paper and the residue was washed with distilled water until the pH values reached 7. The residue was mixed with 2.5M of sodium hydroxide, followed by heating at a temperature of 100°C for five hours. The mixed solution was filtered again using the Whatmann filter paper and the filtrate was used for the acid titration process. The filtrate then undergoes a titration process using 2.0M of sulphuric acid with a continuous stirring condition at the temperature of 100°C, until a white gel appeared [37]. The white gel was then aged for 24 hours to get the uniform-size zeolite. After aging for 24 hours, the white gel was washed with distilled water and ethanol solution until the pH value reached the value of 7. Lastly, the white gel was then filtered using Whatman

filter paper to remove the filtrate and undergoes the calcination process at the temperature of 400°C for two hours [178].

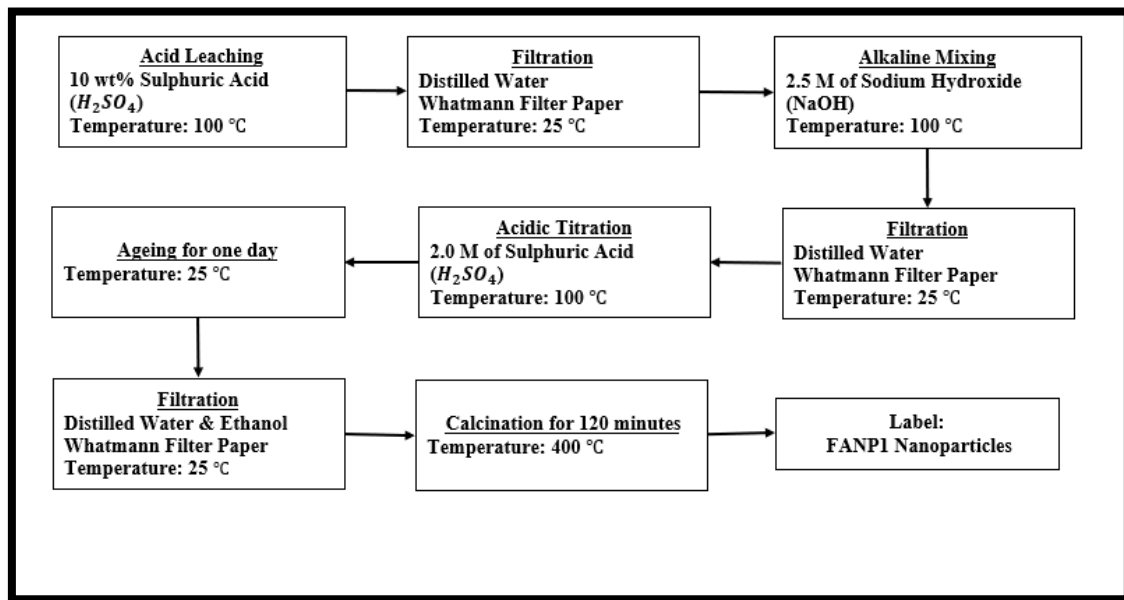


Figure 3.3: Methodology of Synthesized Nanoparticles FANP1

3.3.2 Synthesis of FANP2 Nanoparticles using Chemical Treatment

The process of synthesising FANP2 nanoparticles using the chemical treatment procedure is describe in Figure 3.4. Before the chemical treatment, the coal fly ash sample was washed with sulphuric acid with a concentration of 10wt% and under a continuous stirring condition at the temperature of 100°C. The leached fly ash was then filtered using the Whatmann filter paper and the residue was extracted and washed with distilled water until the pH values reached 7. The residue was mixed with 2.5M of sodium hydroxide in a beaker and the residue was heated at a temperature of 100°C for five hours. The mixed solution was filtered again using the Whatmann filter paper and the filtrate was extracted. The filtrate was then mixed with 2wt% of MFOMAX surfactant and the mixed solution undergoes the acid titration process using 2.0M of

sulphuric acid with a continuous stirring condition at the temperature of 100°C, until a white gel appeared [37]. The white gel was then aged for 24 hours to get the uniform-size zeolite. After aging for 24 hours, the white gel was washed with distilled water and ethanol solution until the pH value reached the value of 7. Lastly, the white gel was then filtered using Whatman filter paper to remove the filtrate and undergoes the calcination process at the temperature of 400°C for two hours [178].

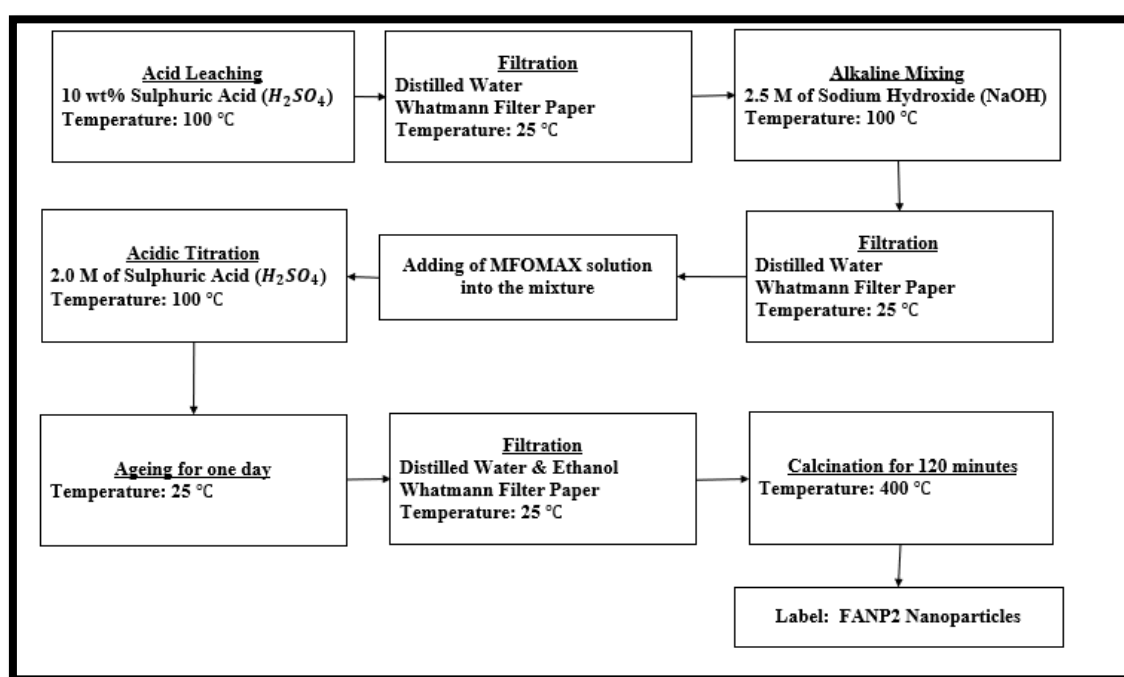


Figure 3.4: Methodology of Synthesized Nanoparticles FANP2

3.4 Preparation of Foaming Solution

Six types of nanoparticles were used as a foam stabilizer for the foam injection experiment which were described as followed:

- Base: No nanoparticles and only contain MFOMAX surfactant.
- CFA: Coal fly ash sample as foam stabilizer.
- FANP1: Synthesized nanoparticles FANP1 that was produced using chemical treatment as described in Section 3.3.1.
- FANP2: Synthesized nanoparticles FANP2 that was produced using chemical treatment as described in Section 3.3.2.
- R1: Consist of 50% of commercial nanoparticles SiO₂ and 50% of commercial nanoparticles Al₂O₃.
- R2: Consist of 66.7% of commercial nanoparticles SiO₂ and 33.3% of commercial nanoparticles Al₂O₃.

The foaming solution was made by the mixture of several fluids that have different properties which were listed:

- Brine with salinity of 3.3wt% that consist of 95% NaCl and 5% CaCl₂.
- MFOMAX surfactant with a concentration of 0.5wt%.
- Nanoparticles with a concentration of 556ppm, 1250ppm, or 2143ppm.

The foaming solution was stirred for 12 hours using the magnetic stirrer. Followed by 2 hours of sonication using ultrasonic cleaner TPC-120, TELSONIC to stabilize nanoparticles in solution at room condition [179]. In Table 3.5 showed the concentration ratio between the MFOMAX surfactant and nanoparticles. Four different concentration ratios of nanoparticles were used for the experiment which were 100:0, 90:10, 80:20 and 70:30. For R1 nanoparticles, when the concentration of the nanoparticles was 556ppm, the concentration of silicon oxide nanoparticles was 278ppm and for aluminium oxide was 278ppm. For R2 nanoparticles, when the

concentration was 556ppm, the concentration of silicon oxide nanoparticles was 371ppm and the concentration for aluminium oxide was 185ppm. These phenomena will be same when the concentration of nanoparticles increased up to 1250ppm and 2143ppm. The reason was the composition of R1 nanoparticles was 50% of silicon oxide nanoparticles and 50% of aluminium nanoparticles. For R2 nanoparticles, the composition of R2 nanoparticles was 66.7% of silicon oxide and 33.3% of aluminium oxide.

Table 3.5: Concentration Ratio Between Surfactant and Nanoparticles

Type of Nanoparticles	Labelling	Concentration of Nanoparticles (ppm)	Concentration of MFOMAX (ppm)	Concentration ratio between MFOMAX and Nanoparticles
Base	Base	0 ppm	5000 ppm	100:0
CFA	CFA-a	556 ppm	5000 ppm	90:10
	CFA-b	1250 ppm	5000 ppm	80:20
	CFA-c	2143 ppm	5000 ppm	70:30
FANP1	FANP1-a	556 ppm	5000 ppm	90:10
	FANP1-b	1250 ppm	5000 ppm	80:20
	FANP1-c	2143 ppm	5000 ppm	70:30
FANP2	FANP2-a	556 ppm	5000 ppm	90:10
	FANP2-b	1250 ppm	5000 ppm	80:20

	FANP2-c	2143 ppm	5000 ppm	70:30
R1	R1-a	556 ppm	5000 ppm	90:10
	R1-b	1250 ppm	5000 ppm	80:20
	R1-c	2143 ppm	5000 ppm	70:30
R2	R2-a	556 ppm	5000 ppm	90:10
	R2-b	1250 ppm	5000 ppm	80:20
	R2-c	2143 ppm	5000 ppm	70:30

3.5 Characterization of Nanoparticles and Coal Fly Ash

After the synthesis process of nanoparticles, the size of the nanoparticles will be measured using the FESEM (Emission Scanning Electron Microscope) equipment. The composition of the nanoparticles will be measured using the EDX (Energy-Dispersive X-ray Spectroscopy) and X-ray Photoelectron Spectrometer (XPS) equipment. The aim was to determine whether the synthesized nanoparticles and commercial nanoparticles can be classified as nanoparticles as discussed in Section 3.3. Furthermore, the size and composition nanoparticles will influence the foam stability as discussed in section 2.4.3.2 and 2.4.3.3. The last experiment for characterization was sedimentation experiment. The objective of the experiment was to determine whether the nanoparticles was suspended in the liquid solution or agglomerated and sedimented on bottom of the foaming solution. This is because when the nanoparticles agglomerated due to the gravitational force, the nanoparticles will be migrated out of the foam lamellae and thus, the foam stability decreased.

3.5.1 Nanoparticle's Size Measurement

The size of nanoparticles will be observed using the Emission Scanning Electron Microscope (FESEM) equipment. The experiments were done at the temperature of 25°C and the pressure of 1 atm. Before starting the measurement, the nanoparticles were coated with thin layer of gold using the Biorad RC500 equipment. The usage of gold particles was used to reduce the charge build-up on the nanoparticles under the electron beam at the high voltage needed to obtain high magnification and to improve the conductive character of the nanoparticles that contain metallic elements. After, coating the nanoparticles with gold particles, the procedure of size measurement was described as followed:

1. The glass plate was used to place the nanoparticles on top of it and the glass plate was mounted onto microscopy stubs using carbon sticky tape.
2. The FESEM equipment and the computer connected to the FESEM equipment were turned on.
3. The SmartSEM[®] program was used for size measurement and, in the program, the docking panel was selected to load the nanoparticles sample on the glass plate into the specimen chamber.
4. The Vent button was selected in the program to vacuum the air in the specimen chamber and the electron gun was switched on.
5. The EHT value was set at 5.00 kV and the magnified image was set at 50.00 K.X for the size measurement.
6. The detector panel was selected in the SmartSEM[®] program to measure the size of nanoparticles.

7. The image was then saved by selecting the Freeze button and save the image into the word document.

3.5.2 Nanoparticle's Composition Analysis

The composition of nanoparticles will be observed using the Energy-Dispersive X-ray Spectroscopy (EDX) and X-ray Photoelectron Spectrometer (XPS) equipment. The usage of two equipment to analyse the composition was to differentiate some chemical compounds that produced the same energy wavelength such as oxygen atom in term of O₂ and O₃ will produced the similar energy wavelength [180]. The composition experiments were done at the temperature of 25°C and the pressure of 1 atm. The EDX equipment can be operated using the procedure in Section 3.5.1 because the EDX equipment was connected to the FESEM equipment. The measurement can be done by opening the EDX program after the FESEM measurement and the data can be saved together with the size measurement into a word file document. The EDX equipment was used to measure the peaks of each electromagnetic emission created by the nanoparticles as each chemical elements will has its own unique atomic structure, thus allowing a unique set of peaks on the electromagnetic emission spectrum [181]. Meanwhile, the XPS equipment will be measuring the kinetic energy and number of electrons that escaped from the molecules by irradiating a material with a beam of X-rays to determine the composition of the nanoparticles. The procedure of operating the XPS is as followed:

1. The nanoparticles sample was mounted on the XPS stub after cleaning the stub.
2. The XPS and computer connected to the XPS equipment were turned on.
3. The nitrogen pump connected to the XPS equipment was turned on and the stub containing the sample was placed onto the load lock arm.

4. The sample was then moved into the specimen chamber and in the XPS program, the vacuum button was selected to vacuum the specimen chamber.
5. The ion gun was switched to standby mode. In the X-ray gun panel, the emission (mA) was set to “1” and anode HT (kV) was set to “10”.
6. The ion gun was then turned on. The emission (mA) and the anode HT were slowly increased up to 10mA and 15kV respectively while monitoring the SAC pressure.
7. In the X-ray Gun panel, the “on” button to start injecting electrons and in the Acquisition panel, the “on” button was pressed to start the measurement.
8. The microscope was magnified up to 50.00 K.X. The microscope was adjusted until the picture of the sample was clearer.
9. After capturing the data, the “recipes” button was selected to export the data in excel format and the data was saved in the excel file.

3.5.3 Sedimentation of Synthesized Nanoparticles Experiment

The sedimentation experiment was done by measuring the turbidity of the foaming solution, using the Hach Model 2100A turbidimeter. The definition of turbidity is the measurement of water transparency lost due to the presence of suspended particles in the water. The experiments were done at the temperature of 25°C and the pressure of 1 atm. Three type of nanoparticles will be used for the experiment which were CFA-a, FANP1-a and FANP2-a with a concentration ratio of 90:10. The procedure of the sedimentation experiment was done as followed:

1. 25ml of the foaming solution was prepared.
2. The foaming solution was then put into the specimen chamber of turbidimeter.
3. The lid of the specimen chamber was closed, and the button with the label “Scan” was pressed to start measuring the turbidity reading.
4. The reading was recorded, and the turbidity measurement was repeated at the interval of 10 minutes for 2 hours.

3.6 Interfacial Tension (IFT) Measurement

The interfacial tension (IFT) measurement was done using the pendant-drop method. Before the IFT experiment, the density data was required for the IFT measurement, therefore, the density was measured using the DM 40 density meter. The density experiments were done at the temperature of 90°C and pressure of 1800 psi. The procedure of density experiment was done as followed:

1. Before the experiment, toluene was injected into the equipment to clean the equipment.
2. Nitrogen gas was then injected into the equipment to remove any remaining liquid residue in the equipment.
3. 20ml of the solution was injected into the sample container.
4. The sample container was closed tightly, and the pressure was set at 1800psi.
5. After maintaining the pressure at 1800psi, the temperature was then set at 90°C.
6. When the temperature reaches 90°C, the density readings was collected.

The IFT experiments were done at the temperature of 90°C and pressure of 1800 psi using the HTHP pendant drop IFT-700 equipment. The IFT procedure was done as followed:

1. Toluene solution was injected into the equipment to remove any residue in the equipment.
2. Nitrogen gas was injected into the equipment to blow any remaining liquid residue in the equipment.
3. Two types of fluid solutions for droplet fluid and bulk fluid were prepared and the fluids were injected into two separate sample containers, respectively.
4. The bulk fluid was injected into the fluid chamber.
5. The computer connected to the IFT equipment to connect the equipment and camera was turned on.
6. The density of two fluids were inserted into the IFT software.
7. The pressure of the equipment was set at 1800psi.
8. After maintaining the pressure at 1800psi, the temperature was then set to 90°C.
9. When the required temperature and pressure were achieved, the valve connected to the capillary needle was opened.
10. The droplet fluid was then injected into the fluid chamber.
11. The droplet was created and monitored through the PC camera window.
12. The camera was adjusted to detect and monitor the clearer picture of the droplet.
13. Through the IFT software, the IFT data were captured and saved into a excel document.

3.7 Static Foam Stability Measurement

The static foam stability experiments were done using the FoamScan equipment manufactured by Teclis, France. In the static foam stability experiment, the foamability and foam stability (Foam half-life) were measured to determine the effectiveness of the foam when using nanoparticles. The foamability was calculated by measuring the time taken for the foam to reach 150 ml of foam volume and the foam stability was calculated by measuring the time taken for the foam volume to decrease from 150 ml to 75 ml of foam volume [182]. Although the morphology of the foam flowing in the porous media is different from static foam, the static foam stability experiment can be used as a screening tool to compare and evaluate the foaming tendency of different chemical formulations because it has the highest accuracy to measure the half-life of the foam in reservoir condition compared to other measurement methods [183]. The temperature of the experiments was set at 90°C while the pressure was set at 3 bar. The static foam stability procedure was described as followed:

1. Before the experiment, distilled water was injected to the FoamScan equipment to wash off any residue.
2. Nitrogen gas was then injected into the Foamsan equipment to remove any residue left behind.
3. 60ml of foaming solution containing 10wt% of Baronia oil was injected into the liquid column of the equipment.
4. The computer connected to the equipment was turned on and the FoamScan equipment was pressurized up to 3bar.
5. When the pressure reading stabilized, the temperature was increased up to 90°C.
6. The camera was calibrated, and grey scale was adjusted so that the camera can differentiate the liquid solution and the foam.

7. Nitrogen gas was then injected from the bottom of the equipment at a flow rate of 50 cc/min until the foam volume generate up to 150 ml.
8. The FoamScan software will captured the time taken for when the foam reached up to 150ml of foam volume and the time taken when the foam volume reduced to 75ml of foam volume.
9. The data was then saved into the excel document.

3.8 Core Flooding Experiment

Core flooding experiments or known as core displacement experiments were done to investigate the efficiency of nanoparticles in improving the gas mobility control and oil recovery before the application into the pilot filed.

3.8.1 Core Cleaning Methodology

Five Berea sandstone cores were prepared for core flooding experiments. Before the core flooding experiment, the Berea sandstone cores were cleaned to remove any impurities, chemicals, and oil stain. The core cleaning process was done using the CO₂ and Solvent Core Cleaner equipment, Vinci Technologies. The core cleaning process was done by submerging the core samples into the solvent solution (Toluene) for a few hours. The purpose of using the Toluene was to dissolve any impurities into the solvent. The CO₂ gas was injected into the core samples was to apply some pressure for the solvent to invade into the smaller pores of the core sample so that the solvent will dissolve any chemicals or oil stain in the pore of the core by forming the oil-solvent emulsion. The cycle of injecting solvent and CO₂ gas were repeated for seven days. During the depressurization process, the solvent was drained out and CO₂ gas was injected again to blow out any liquid out from the core samples. The core samples were

taken out and dried in the oven for a few days to remove any remaining solvent left in the core samples.

3.8.2 Porosity and Permeability of Berea Core Measurement

After the core cleaning process, the weight of the Berea core sample was measured using the mass balance. After the measurement, the core was submerged into a brine solution with a salinity of 3.3wt% (95% of NaCl and 5% of CaCl₂) in the desiccator equipment attached with vacuum pump. When the lid of the desiccator equipment is closed, the vacuum pump was turned on to vacuum the air in the desiccator equipment for a few hours. The sample core was then left to submerged in the brine solution for a few days until there were no gas bubbles coming out of the core sample when the vacuum pump was turned on. The core sample was taken out and was weighted using the mass balance to calculate the porosity of the core which was measured using the equation (3.2):

$$\phi = \frac{W_{after} - W_{before}}{\rho_{brine}} \quad (3.2)$$

Where:

ϕ = Porosity,

W_{after} = Weight of the core after submerging into the brine

W_{before} = Weight of the core before submerging into the brine

ρ_{brine} = Density of the brine solution.

The permeability of the core was measured by measuring the water permeability of the core. The water permeability was calculated using the HTHP core flooding equipment, Sanchez Technologies. The salinity of the brine solution used for the water permeability measurement was 3.3wt% and contained 95% of NaCl and 5% of CaCl₂. The core sample was put into a rubber sleeve and placed inside the core holder. The core holder was then placed into the equipment. The brine solution was injected with three different flow rates which were 0.2 ml/min, 0.5 ml/min, 1.0 ml/min at the atmospheric conditions. Equation (3.3) was used to calculate the water permeability [184]:

$$\frac{q \mu}{A} = k \frac{\Delta P}{L} \quad (3.3)$$

Where:

q = Injection flow rate

A = Area of the core

μ =Viscosity of the brine solution

ΔP = Differential pressure of inlet pressure and outlet pressure

L = Length of the core

k = Water permeability

3.8.3 Foam Injection Experiment

After measuring the water permeability, the equipment was heated up to 90°C and slowly pressurized up to 1800 psi. When the readings of the temperature and pressure become stable, Baronia crude oil was injected into the core sample at a flowrate of 0.2

ml/min, until there was no water produced at the outlet of the equipment. The initial oil saturation (S_{or}) was calculated by subtracting the total volume of oil injected with the total volume of oil produced at the outlet of the equipment. The irreducible water (S_{wrr}) was calculated by subtracting the total volume of brine (water) injected with the total volume of the brine produced at the outlet of the equipment. The core sample was then left to age for two days. Brine solution was injected thereafter, as primary recovery followed by nitrogen gas injection as secondary recovery. Finally, a cycle of foaming solution was injected followed by nitrogen gas injection as the EOR injection. All the injected solutions were injected at a flow rate of 0.2 ml/min [185]. The MRF value can be calculated using the equation (3.4) for the foam mobility calculation:

$$MRF = \frac{\Delta P_{foam}}{\Delta P_{without\ foam}} \quad (3.5)$$

Where:

ΔP_{foam} = Pressure drops across the core during SAG injection

$\Delta P_{without\ foam}$ = Pressure drops across the core during gas injection

A higher pressure drops and a higher MRF value will indicate a strong foam front inside the core whereas, a sustained pressure drops and MRF trend indicate the stability of the foam [186].

3.9 History Matching and Sensitivity Analysis

Schlumberger Eclipse 100 software was used for the foam history matching from one of the core flooding experiment. The foam model used in this work is a Local-equilibrium model, also known as "implicit texture (IT) model" [187], which does not able to clearly capture the dynamic behaviour of foam but assumes that foam creation

and coalescence has reached equilibrium. This assumption was considered valid at the timescale of a field scale applications as shown in equation (3.5) [188]:

$$u_g^f = \frac{u_g}{FM} \quad (3.5)$$

Where:

u_g^f = Gas viscosity with foam

u_g = Viscosity of gas

FM = Non-dimensional of mobility reduction factor

The IT model relates the value of FM to several functions such a surfactant concentration, water saturation, oil saturation, and capillary number as shown in equation (3.6) [189]:

$$FM = \frac{1}{1 + f_{mmob} + F_{surf} + F_{dry} + F_{oil} + F_{cap}} \quad (3.6)$$

Where:

f_{mmob} = Reference mobility factor

F_{surf} = Mobility reduction factor due to surfactant concentration

F_{dry} = Mobility reduction factor due to water saturation

F_{oil} = Mobility reduction factor due to oil saturation

F_{cap} = Mobility reduction factor due to capillary number

After history matching, the sensitivity analysis will be done to provide a better understanding and interpretation of foam injection. The foam stability and surfactant adsorption by the reservoir rock were the two factors in forecasting the oil recovery using the Eclipse 100.

3.10 Chapter Summary

This chapter was a platform to expose the methodology used in this research to achieve mentioned objectives. It presented different chemicals, materials and equipment employed in this study in detail. All the equipment and procedure used in this study, was provided in this chapter with detail starting from sample preparation up to data analysis were described in detail such as nanoparticles characterization, foam stability, foamability, IFT, core flooding and reservoir simulation.

CHAPTER 4

RESULT AND DISCUSSION

4.1 Chapter Overview

The Chapter 4 will be discussing the results done from the experimental works and simulation run as described in Chapter 3. The result and discussion can be divided into 3 sections related to the respective objectives.

- I. Characterization of nanoparticles after nanoparticles synthesis using chemical treatment.
- II. Experimental works such as foam stability experiment, IFT experiment and oil recovery to evaluate the performance of nanoparticles on foam stability and oil recovery.
- III. History matching and oil forecasting to determine the main governing factor of foam injection on oil recovery using Eclipse100.

4.2 Nanoparticle's Size Measurement

Figure 4.1 showed the FESEM image of CFA nanoparticles, and the size of the CFA nanoparticles was around 13.63 μm . The size of the CFA nanoparticles was considered too large to be classified as a nanoparticle [176]

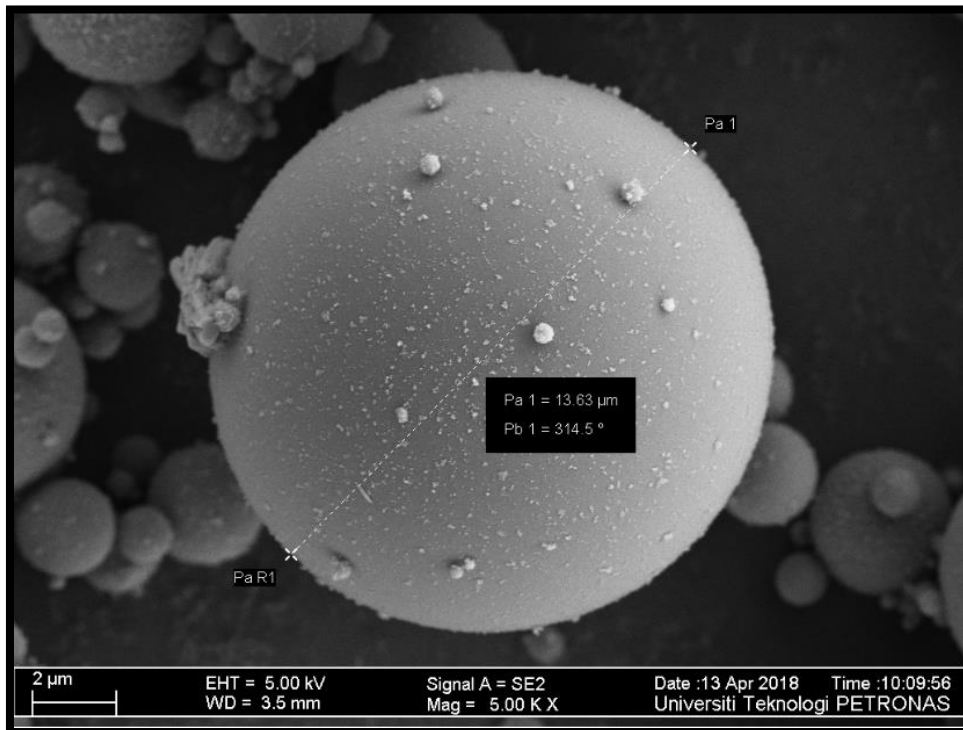


Figure 4.1: FESEM Image of CFA nanoparticles [176]

In Figure 4.2 showed the FESEM image of synthesized nanoparticles FANP1 that was produced using chemical treatment as discussed in Section 3.3.1. The size of FANP1 nanoparticles was between 10nm to 20nm. In Figure 4.3 showed the FESEM image of synthesized nanoparticles FANP2 that was coated with MFOMAX surfactant and was produced using chemical treatment as discussed in Section 3.3.2. The size of FANP2 nanoparticles was between 40nm to 60nm. Based on the Figure 4.2 and Figure 4.3, the FANP2 synthesized nanoparticles was slightly larger than the FANP1 synthesized nanoparticles. This is because FANP2 nanoparticles was coated with MFOMAX surfactant during the chemical treatment. This phenomena was similar to the Ahmed et al experiment [190]. In the Ahmed et al experiment, the size of normal silicon oxide nanoparticles was between 50nm to 125nm, but when the silicon oxide nanoparticles were coated with ENORDETTTM O-342 surfactant, the size of the coated

nanoparticles was increased up to 145nm. Based on the FESEM results, it showed that the synthesized nanoparticles FANP1 and FANP2 were successfully produced into the size of less than 100nm which can be classified as nanoparticles when chemical treatment method was used.

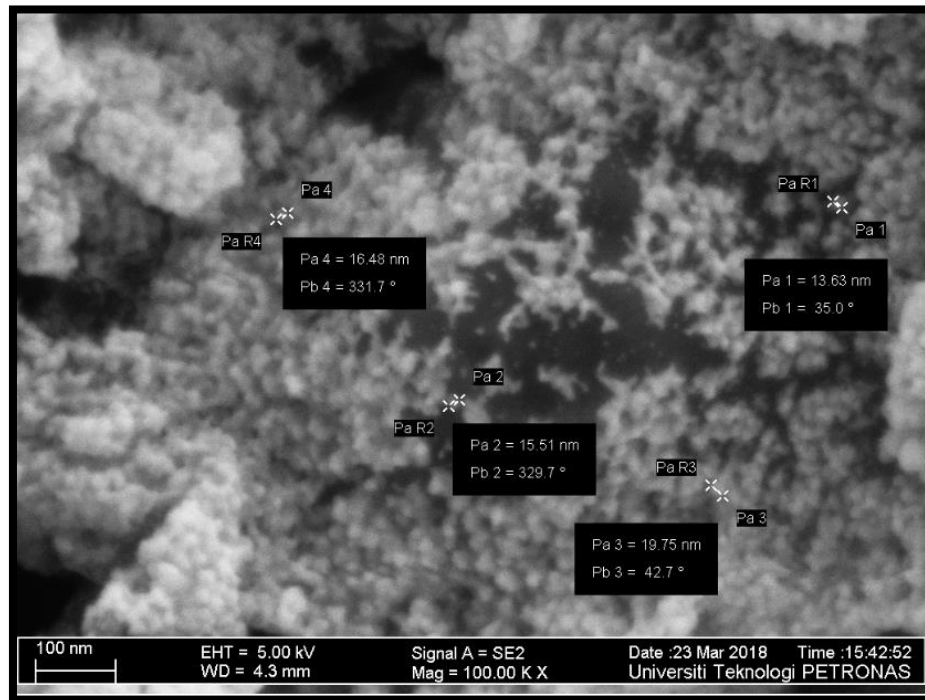


Figure 4.2: FESEM Image of FANP1 nanoparticles

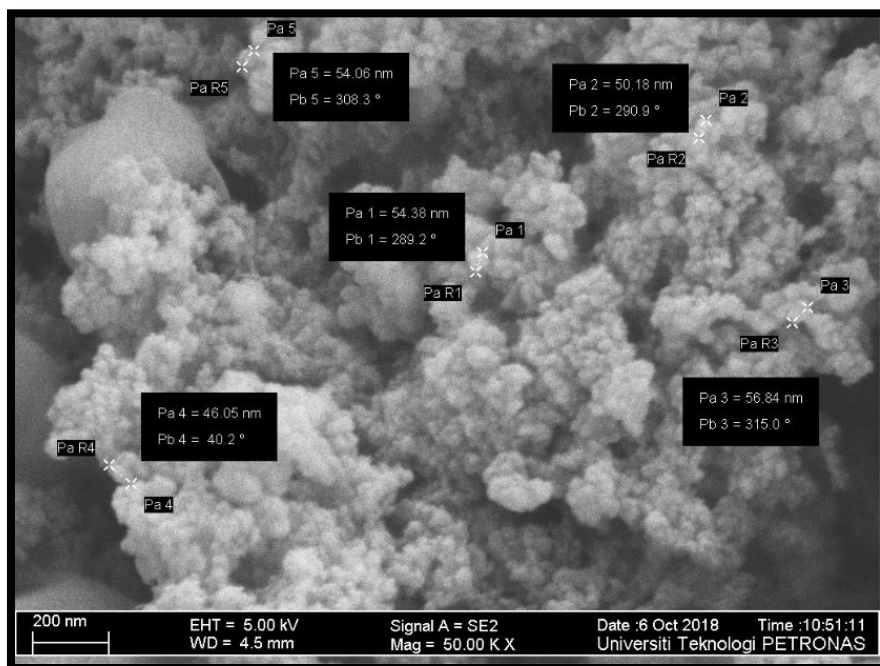


Figure 4.3: FESEM Image of FANP2 nanoparticles

Figure 4.4 and Figure 4.5 showed the FESEM image of SiO_2 and Al_2O_3 nanoparticles bought from Sigma Aldrich and US Research Nanomaterials, respectively. In Figure 4.4 showed that the size of SiO_2 nanoparticles was between 10nm to 55nm. In Figure 4.5 showed the image of Al_2O_3 nanoparticles and the size of the nanoparticles was between 20nm to 30nm. Therefore, it showed that the commercial nanoparticles SiO_2 and Al_2O_3 have the size of less than 100nm.

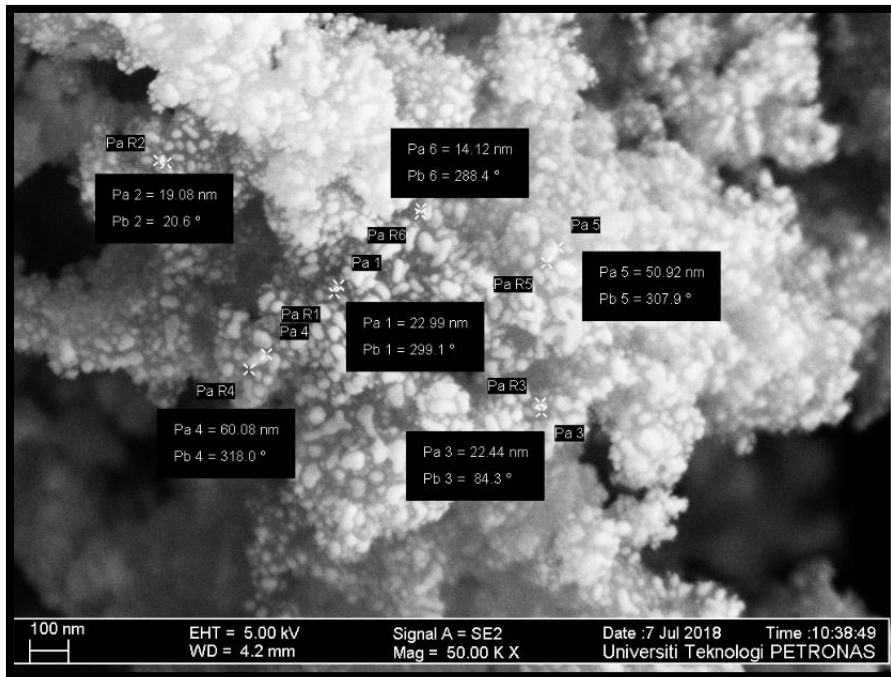


Figure 4.4: FESEM Image of SiO_2 nanoparticles

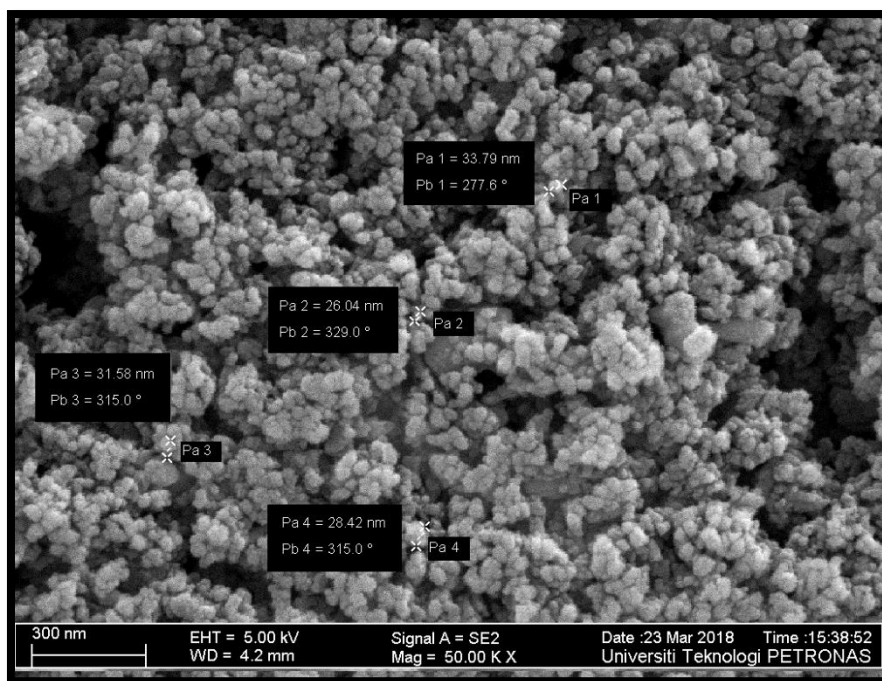
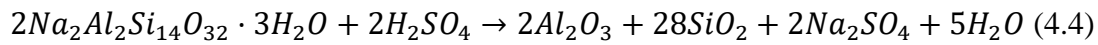
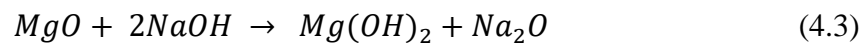
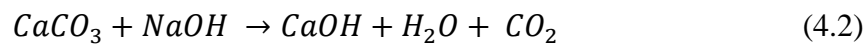
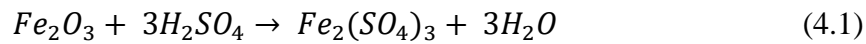


Figure 4.5: FESEM Image of Al₂O₃ nanoparticles

4.3 Nanoparticle's Composition Analysis Study

Table 4.1 showed the composition of CFA, FANP1, FANP2, SiO₂ and Al₂O₃ nanoparticles using EDX analysis. From the EDX analysis, the main composition of the CFA nanoparticles was SiO₂ (43.26%) component followed by 20.59% of Al₂O₃, 11.11% of iron (II) oxide (Fe₂O₃), 3.76% of calcium carbonate (CaCO₃) and 8.79% of other components such as magnesium oxide (MgO), loss-on-ignition (LOI), and etc. For the synthesized nanoparticles of FANP1 and FANP2, both synthesized nanoparticles only contained three chemical components which were SiO₂, Al₂O₃ and Na₂SO₄. Meanwhile the remaining chemical components such Fe₂O₃, MgO and K₂O were absent in the composition of the synthesized nanoparticles. The Fe₂O₃ component was removed when the coal fly ash sample was washed with sulphuric acid before the chemical treatment as shown in Equation (4.1). This is because Fe₂O₃ is a maghemite, hematite, and magnetite component that will can be easily dissolved in the presence of diluted acid solution [191]. The CaCO₃ component was removed when the leached fly ash sample was mixed with sodium hydroxide and formed calcium hydroxide (CaOH) as explained in Equation (4.2). Calcium hydroxide is relatively insoluble in water

especially under a higher temperature condition. Therefore, calcium hydroxide was separated through filtration after mixing with sodium hydroxide using Whatmann filter paper. MgO component was removed by mixing with the alkaline solution and formed Mg(OH)₂ as explained in Equation (4.3) which was insoluble materials and therefore, can be filtered out as a residual using Whatmann filter paper [192]. Meanwhile for LOI, it was burn away during the heating process and during the primary washing with dilute sulphuric acid.



Based on Table 4.1, the composition of the FANP1 nanoparticles was 40.71% of SiO₂, 34.65% of Al₂O₃ and 24.64% of Na₂SO₄ whereas, the composition of FANP2 nanoparticles was 29.54% of SiO₂, 51.53% of Al₂O₃, and 18.93% of Na₂SO₄. FANP2 nanoparticles has lower silicon oxide content because the MFOMAX surfactant attracted the silicon oxide component out from the filtrate, therefore, the composition of FANP2 will consist of high aluminium oxide content, when the white gel was formed during the chemical treatment process. However, due to the confidentiality of the surfactant, the reaction of component in MFOMAX with SiO₂ component could not be discussed until the patent of MFOMAX is approved. The presence of Na₂SO₄ could be the remains of unreacted sodium silicate as shown in Figure (4.4). Lastly, the composition of commercial silicon oxide nanoparticles was 100% of SiO₂ and the composition of commercial aluminium oxide nanoparticles was 100% of Al₂O₃.

Table 4.1: Composition of nanoparticles using EDX analysis

Composition	Percentage (%)				
	CFA	FANP1	FANP2	SiO ₂	Al ₂ O ₃
Silicon Oxide	43.26	40.71	29.54	100.00	-
Aluminium Oxide	20.59	34.65	51.53	-	100.00
Iron (II) Oxide	11.11	-	-	-	-
Calcium Carbonate	3.76	-	-	-	-
Sodium Sulphate	-	24.64	18.93	-	-
Other Components	8.79	-	-	-	-
Total Percentage	100.00	100.00	100.00	100.00	100.00

Figure 4.6 showed the XPS results of CFA (blue line), FANP1 (green line) and FANP2 (red line) nanoparticles. Based on the XPS graph, the CFA nanoparticles produced 7 energy peaks which were 78.77, 106.73, 309.47, 352.3, 532.2, 712.42, and 1072.38 eV represent the aluminium (Al2p), silica (Si2p), carbon (C1s), oxygen (O1s), calcium (Ca2p), iron (Fe2p) and sodium (Na1s). For FANP1 nanoparticles, the XPS graph showed four energy peaks which were 67.98, 106.77, 533.98 and 1073.02 eV and the energy peaks represent the aluminium (Al2p), silica (Si2p), oxygen (O1s) and sodium (Na1s) respectively. For FANP2 nanoparticles, the XPS graph also showed four energy peaks which were 69.19, 107.23, 536.61 and 1076.68 eV and the energy peaks represent the aluminium (Al2p), silica (Si2p), oxygen (O1s) and sodium (Na1s).

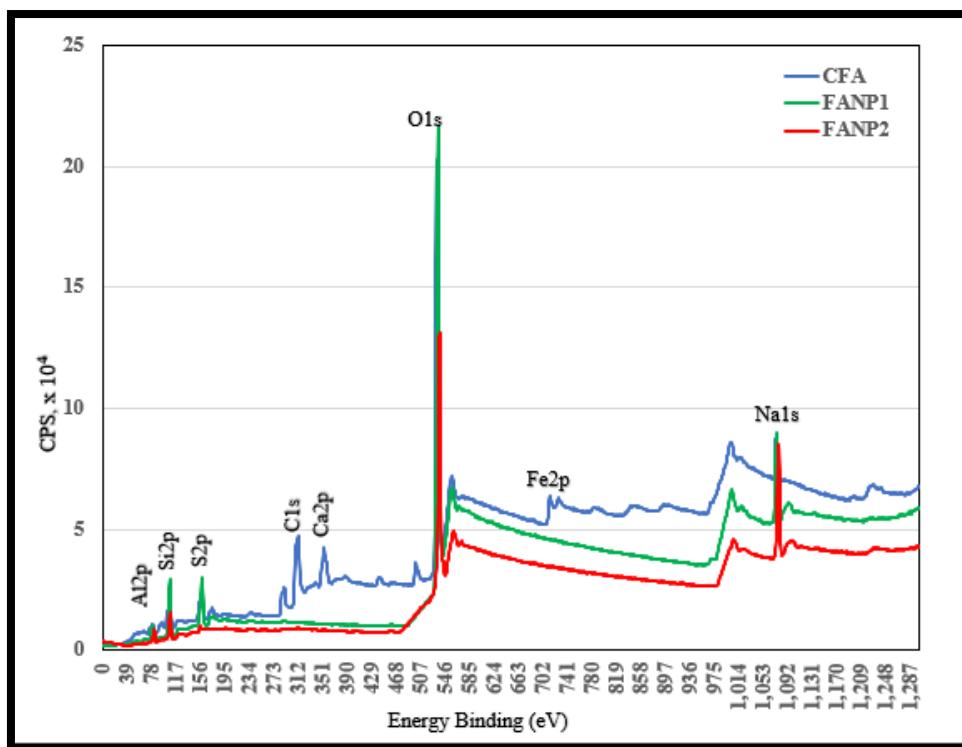


Figure 4.6: XPS analysis of CFA, FANP1 and FANP2 nanoparticles

Table 4.2 described the details of the chemical components for each energy peak of CFA nanoparticles. The EDX results confirmed the presence of aluminium oxide, silicon oxide, calcium carbonate, iron oxide, albite, and wollastonite in the CFA nanoparticles. However, the sodium (Na1s) detected by CFA nanoparticles was a different sodium component compared to synthesized nanoparticles.

Table 4.2: XPS energy peak analysis on CFA nanoparticles

Element	Chemical Formula	Binding Energy, (eV)	Ref.
Silica, Si2p	Silicon Oxide, SiO ₂	106.73	[180]
Aluminium, Al2p	Aluminium Oxide, Al ₂ O ₃	78.77	[193]
Carbon, C1s	Calcium Carbonate, CaCO ₃	309.47	[194]
Iron, Fe2p	Iron (II) Oxide, Fe ₂ O ₃	712.42	[195]
Sodium, Na1s	Albite, NaAlSi ₃ O ₈	1072.38	[196]
Calcium, Ca2p	Wollastonite, CaSiO ₃	352.3	[196]
	Calcium Carbonate, CaCO ₃	352.3	[197]

In Table 4.3 and 4.4 showed the XPS composition result of FANP1 and FANP2 nanoparticles, respectively. Both the synthesized nanoparticles showed three chemical components which were silicon oxide, aluminium oxide, and sodium sulphate. The XPS experiment was not performed on commercial nanoparticles silicon oxide and aluminium oxide. This is because the EDX experiment had confirm the composition of the commercial nanoparticles with the material safety data sheet provided by the supplier.

Table 4.3: XPS energy peak analysis on FANP1 nanoparticles

Element	Chemical Formula	Binding Energy, (eV)	Ref.
Silica, Si2p	Silicon Oxide, SiO ₂	106.77	[180]
Aluminium, Al2p	Aluminium Oxide, Al ₂ O ₃	67.98	[193]
Sodium, Na1s	Sodium Sulphate, Na ₂ SO ₄	1073.02	[198]

Table 4.4: XPS energy peak analysis on FANP2 nanoparticles

Element	Chemical Formula	Binding Energy, (eV)	Ref.
Silica, Si2p	Silicon Oxide, SiO ₂	107.23	[180]
Aluminium, Al2p	Aluminium Oxide, Al ₂ O ₃	69.19	[193]
Sodium, Na1s	Sodium Sulphate, Na ₂ SO ₄	1076.68	[198]

4.4 Sedimentation Experiment of Synthesized Nanoparticles and Coal Fly Ash

Figure 4.7 showed the turbidity results of CFA, FANP1 and FANP2 nanoparticles for the sedimentation experiment. Based on Sia et al when a higher turbidity value, it indicated a higher suspended particle in the liquid solution [199]. The NTU (Nephelometric Turbidity Unit) represent the unit value of turbidity. In Figure 4.7, the first reading of CFA nanoparticles was 639 NTU and it was the highest NTU reading among the three types of nanoparticles. This is because CFA nanoparticles has a larger particles size distribution (PSD) compared to the synthesized nanoparticles. The PSD value was affected by the concentration of the nanoparticles and the size of the nanoparticles [200]. When the size of the CFA nanoparticles was larger than 1 μ m, meanwhile the size of the synthesized nanoparticles of FANP1 and FANP2 were less than 100nm, the PSD of CFA nanoparticles will be larger than the synthesized nanoparticles. Therefore, a higher concentration of FANP1 and FANP2 were needed to achieve the NTU value of 639. However, the sedimentation experiment was to measure the duration of the nanoparticles can suspended in the solution and not the number of particles suspended in the solution. When the time= 0, the NTU reading of FANP1 and FANP2 were 185 NTU and 190 NTU, respectively. When the time was 120 minutes, the NTU reading recorded for CFA, FANP1 and FANP2 nanoparticles were 259 NTU, 103 NTU and 82 NTU, respectively. The decremental NTU value from time= 0 to time= 120 minutes for CFA nanoparticles was 59.47% or a 380 NTU difference. Meanwhile for FANP1 nanoparticles, the NTU difference when the time= 0 and time= 120 minutes was 44.32% or an 82 NTU difference. For FANP2 nanoparticles, when the time was zero compared to when the time was 120 minutes, the NTU difference was 30.53%

decrement or a 58 NTU difference. Based on the result, CFA nanoparticles has the highest sedimentation compared to the synthesized nanoparticles. This is because the CFA nanoparticles was affected by the gravitational force due to the its higher weight and larger size of CFA nanoparticles [201]. Meanwhile FANP2 nanoparticles has the highest stability to suspend in the solution for a longer time compared to FANP1 and CFA nanoparticles. This is because FANP2 nanoparticles was coated with MFOMAX surfactant. According to Ahmed et al. experiment. it stated that the presence of surfactant layers on the nanoparticles would helped to reduce the Van der Waals attraction force between the nanoparticles themselves and therefore improved the dispersion stability in the liquid phase [202]. Furthermore, when the nanoparticles coated with MFOMAX surfactant, it can used to reduce the agglomeration between the nanoparticles. This is because of the higher repulsion force between the double bonds of aromatic rings and the CH₂ monomers on the surface of nanoparticles and therefore, increased the nanoparticle's mobility and reduced the agglomeration between the nanoparticles [203]. Therefore, FANP1 nanoparticles will have a lower sedimentation rate compared to FANP1 and CFA nanoparticles.

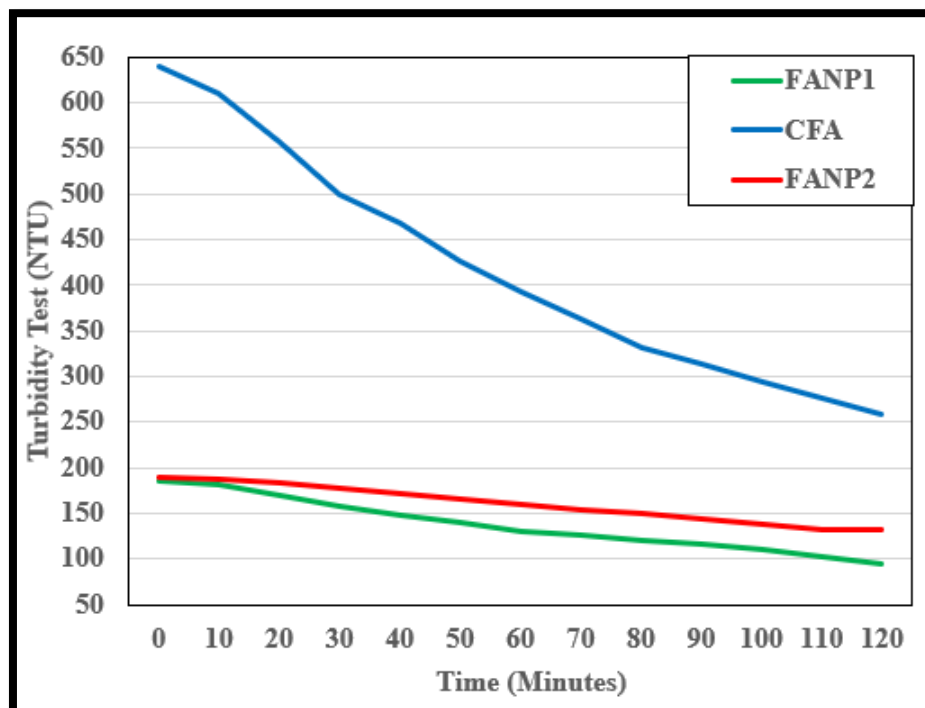


Figure 4.7: Turbidity experiment for CFA, PFA and SFA nanoparticles

4.5 Interfacial Tension (IFT) Measurement

For a successful EOR injection, the EOR injection needed not only produced a good volumetric sweep efficiency and displacement efficiency but the injection also need to produce a sufficient energy to mobilize the immobilised fraction of the oil in the unswept region [204]. This is because in the oil reservoir, there were a lot of oil residual trapped in the pore network. Therefore, in order to mobilise the trap oil, a good capillary pressure is needed to recover the immobilised oils and one of the important parameters of increasing the capillary pressure is the interfacial tension (IFT) [205]. IFT can be defined as the surface free energy that exists between two immiscible liquids [206]. Figure 4.8 showed the IFT of foaming solution with different type of nanoparticles and Baronia crude oil. Based on the Figure 4.8, foaming solution with base sample has the lowest IFT reading compared to other foaming solution which was 0.21mN/m. The IFT readings for CFA-a, CFA-b, and CFA-c nanoparticles were 0.66, 0.68 and 0.74mN/m, respectively. The CFA nanoparticles has the highest IFT value when compared to other type of foaming solutions regardless the concentration of nanoparticles. This is because the size of CFA nanoparticles was larger than other type of nanoparticles, therefore, it resulted into the increases of IFT value. These results were similar to the Bhuiyan et al. experiment where the IFT increases when the size of aluminium oxide increased from 13nm to 50nm and when the silicon oxide, the size increased from 5nm~10nm to 10nm~20nm [207]. This is because the smaller nanoparticles will exhibit a higher surface charge density compared to its larger size counterpart [208]. Therefore, the electrostatic repulsion force between nanoparticles and surfactant molecules will increased and the diffusion of surfactant molecules toward the interface of the fluids will be much easier [209]. For FANP1 nanoparticles, the IFT readings for FANP1-a, FANP1-b and FANP1-c were 0.49, 0.54 and 0.58mN/m, respectively. Meanwhile, the IFT readings for FANP2-a, FANP2-b, and FANP2-c were 0.35, 0.38 and 0.43mN/m, respectively. For the R1 nanoparticles, the IFT readings for R1-a, R1-b, and R1-C were 0.39, 0.44 and 0.47mN/m, respectively. For the R2 nanoparticles, the IFT readings for R2-a, R2-b, and R2-c were 0.44, 0.46 and 0.49mN/m, respectively. The aim of having mixing nanoparticles of R1 and R2 nanoparticles were to compare the effectiveness of synthesized nanoparticles which were having the same concentration ratio of silicon oxide and aluminium oxide as R1 and R2 nanoparticles as showed in Table 4.1.

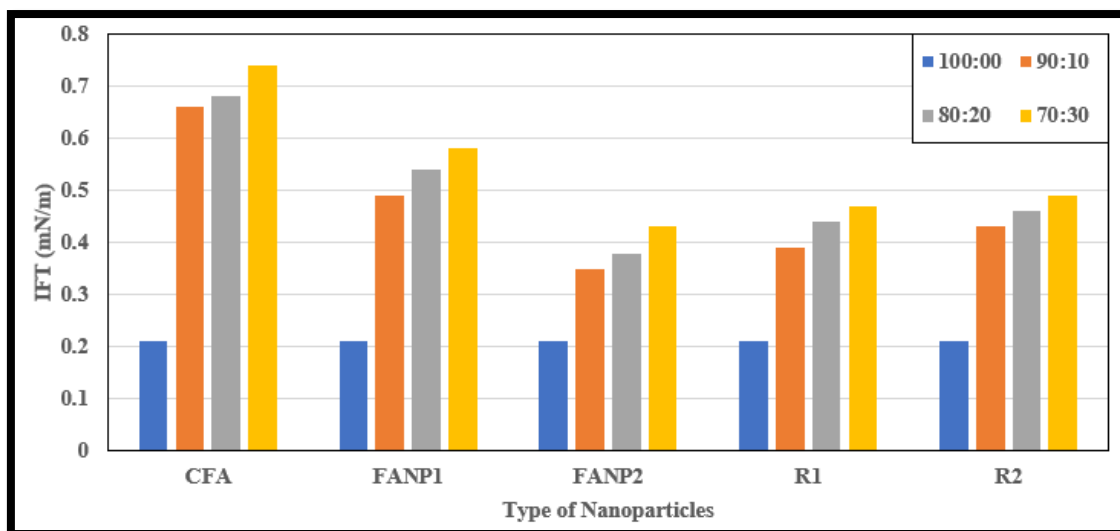


Figure 4.8: Interfacial tension of foam solution with different type of nanoparticles

According to the Figure 4.8, the IFT reading increased with increased of the concentration of nanoparticles regardless the type of nanoparticles. This is because, when more nanoparticles were added into the solution, the nanoparticles in the interface will try to get closer to each other due to the Van der Waals force of attraction and agglomerated [207]. Therefore, this phenomena will lead to an unevenly distribution of the surfactant molecules at the interface of the fluids and cause an increment of IFT value [210]. FANP2 nanoparticles has the lowest IFT values when compared to the other types of nanoparticles. This is because of the effect of the MFOMAX surfactant-coated nanoparticles. When the FANP2 nanoparticles was coated by a large amount of surfactant molecules, the nanoparticles will act as a carrier for the MFOMAX surfactant molecules towards the fluids interface, thus, the IFT value will reduced greatly [211]–[213]. In addition, the reason foaming solution with R1 nanoparticles has a lower IFT value compared to R2 nanoparticles. This was due to the chemical compatibility between the silicon oxide nanoparticles and surfactant. These results were similar to the Ragab et al., Alomair et al. and Bayat et al. IFT experiments between SiO₂ nanoparticles and Al₂O₃ nanoparticles [214]–[216]. Therefore, FANP2 nanoparticles will has the lowest IFT value compared to other nanoparticles.

Figure 4.9 showed the ANOVA two-way calculation for IFT measurement. The two variables' conditions for the ANOVA calculation were the types of nanoparticles and concentration of the nanoparticles. In Figure 3.9, the first table showed the IFT values collected for the ANOVA calculation. Five IFT measurement were collected for concentration of the nanoparticles. The null hypothesis (H_0) for the experiment was that the IFT values be the same across the table and the alternative hypothesis (H_a) was that the IFT value will be different across the first table in Figure 3.9. The second table in the Figure 3.9 showed the calculation of ANOVA. Lastly, the F values calculated across the column of the first table and the F value across the row of the first table were higher than the accepted value. Therefore, both the F values rejected the null hypothesis, and the alternative hypothesis was accepted. Based on the ANOVA calculation, it showed that the presence of nanoparticles in the solution will influence the IFT value.

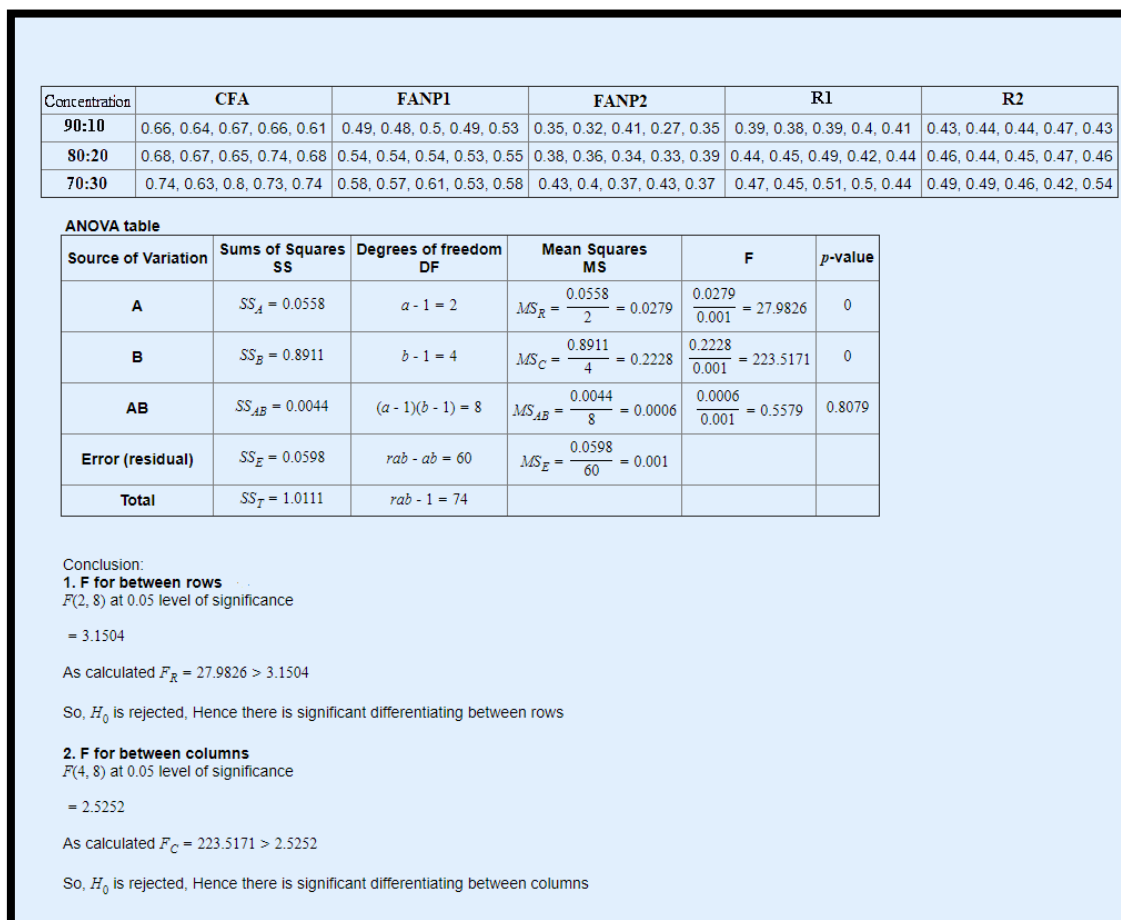


Figure 4.9: ANOVA of the IFT measurement with different types and concentration of nanoparticles

4.6 Static Foam Stability Measurement

Figure 4.10 showed the foam stability with five different nanoparticles and three types of concentration of the nanoparticles. The foam stability of the base sample (Ratio 100:00) was 404 seconds. In the absence of nanoparticles, the foam half-life of base sample was the lowest when compared with surfactant in the presence of nanoparticles regardless the types or concentration of the nanoparticles. This is because when the nanoparticles were added into the foaming solution, the nanoparticles moved to the interface of the gas-liquid of the foam and aggregated to form a monolayer or a network of aggregate nanoparticles [217]. When the nanoparticles formed a layer of nanoparticles, the foam drainage was reduced because, the nanoparticles were resisting the dragging force of the liquid [131]. The foam stability of CFA-a, CFA-b and CFA-c were 472 seconds, 614 seconds, and 494 seconds. The foam stability of the CFA nanoparticles was higher than base sample by 30 seconds to 150 seconds according to the concentration of CFA. The reason CFA has higher foam stability than base sample was the presence of nanoparticles at the gas-liquid interface which slowed down the gravitational force and liquid drainage by reducing the direct contact between fluids [127]. However, when CFA nanoparticles was compared to other types of nanoparticles, the foam stability of CFA nanoparticles was the lowest. This can be because the size of CFA nanoparticles was larger than other type of nanoparticles. The size of CFA nanoparticles was between $5\mu\text{m}$ to $20\mu\text{m}$, and the size of other nanoparticles were less than 100nm. Smaller nanoparticles tend to have higher foam stability because the smaller nanoparticles were able to flow into the small lamellae space easier compared to the larger size nanoparticles. In addition, the nanoparticle's size has an effect on the apparent viscosity of the foam [166], [218]. For FANP1 nanoparticles, the foam stability for FANP1-a, FANP1-b and FANP1-c were 669 seconds, 1142 seconds, and 923 seconds. Meanwhile, for FANP2 nanoparticles, the foam stability of FANP2-a, FANP2-b, and FANP2-c were 757 seconds, 875 seconds, and 702 seconds. For R1 nanoparticles, the foam stability for R1-a, R1-b and R1-c were 554 seconds, 962 seconds, and 627 seconds. For R2 nanoparticles, the foam stability for R2-a, R2-b and R2-c were 615 seconds, 738 seconds, and 587 seconds.

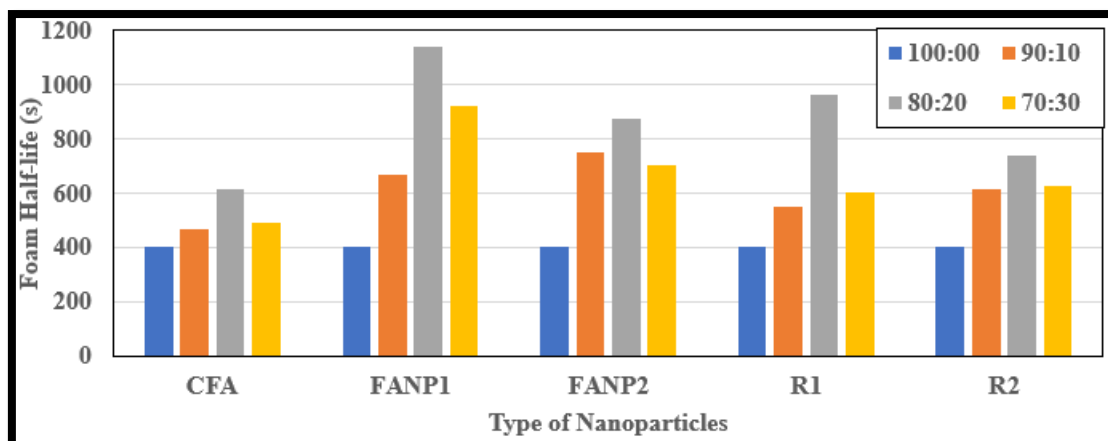


Figure 4.10: Foam stability experiment with different type and concentration of nanoparticles

Based on the Figure 4.10, when the nanoparticles concentration ratio was increased from 90:10 to 80:20, the foam stability of the nanoparticles was increased too. However, when the nanoparticle concentration ratio increased from 80:20 to 70:30, the foam stability of the nanoparticles decreases. Based on the figure, it showed that when the concentration ratio of the nanoparticles was 80:20, the foam stability of the nanoparticles was the highest. Therefore, the optimum concentration ratio of nanoparticles was 80:20 and this phenomenon was the same for all types of nanoparticles. At low concentration of nanoparticles, the adsorbed nanoparticles at the gas-liquid interface were insufficient to improve the foam stability. However, when the concentration of nanoparticles was above the optimum concentration, the foam stability will either remains the same or decreased with the increasing concentration of nanoparticles [219]. When the concentration nanoparticles exceed the beyond the optimum concentration, more nanoparticles will agglomerated to form a larger nanoparticles network in the gas-liquid interface [125]. When more nanoparticles were in the interface, the interface become heavier and therefore, the liquid drainage will be increased dramatically under the force of gravitational energy due to the heavily agglomerated nanoparticles. In addition, when the concentration of nanoparticles exceed the optimum concentration, the main mechanism of the foam stability was changed from particles detachment energy and capillary pressure to gravity drainage

[220]. Therefore, based on Figure 4.10, we can conclude the concentration ratio of 80:20 was the optimum concentration for all types of nanoparticles.

Based on the Figure 4.10, nanoparticles with higher silicon oxide content in the composition tend to have a higher foam stability. This observation can be seen between the synthesized nanoparticles (FANP1 and FANP2 nanoparticles) and the commercial nanoparticles (R1 and R2 nanoparticles). Both FANP1 and R1 nanoparticles which have higher silicon oxide content produced a higher foam stability compared to FANP2 and R2 nanoparticles. These results were same as the Yekeen et al. experiment. In Yekeen et al. experiment, the foam stability of silicon oxide or modified silicon oxide nanoparticles tend to have a higher foam stability than the foam stability of aluminium oxide nanoparticles [152]. The reason silicon oxide nanoparticles has a better effect on foam stability compared to aluminium oxide was due to the higher interaction energy between two particles according to the DLVO theory [221]. The definition of DLVO theory stated that the net interaction between two particles is a summation of electrostatic double layer (EDL) and the van der Waals force of attraction. The higher the positive values of the interaction energy, implies that the EDL force is greater than the van der Waals force of attraction [222]. Figure 4.11 showed the DLVO theory done by Bayat et al's experiment for aluminium oxide and silicon oxide nanoparticles [223].

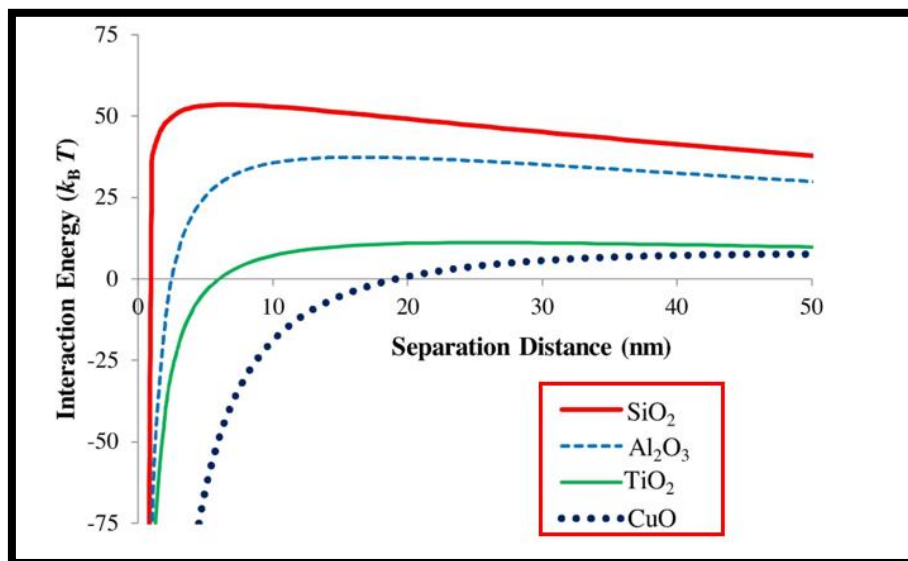


Figure 4.11: Nanoparticles and nanoparticles interaction energy profile generated by DLVO theory [223]

The reason FANP1-b and FANP2-b nanoparticles have higher foam stability compared to R1-b and R2-b nanoparticles were due to the presence of sodium sulphate electrolyte in the composition of the synthesized nanoparticles (FANP1 and FANP2 nanoparticles). This is because of the ionic effect of electrolytes where the electrolytes interacts with the counter-charges on the zwitterionic MFOMAX surfactant thereby reducing the electrostatic force which involved in film formation and trapping of gas [224]. Therefore, the synthesized nanoparticles (FANP1 and FANP2) have higher foam stability compared to the commercial nanoparticles (R1 and R2).

The foam stability of FANP1 nanoparticles produced the highest foam stability compared to other type of nanoparticles. Although FANP1 nanoparticles has higher sedimentation rate compared to FANP2 nanoparticles, the FANP1 nanoparticles has higher foam stability compared to FANP2 nanoparticles. This can be attributed to the particle arrangement at the liquid-gas interface as shown in Figure 4.12 [132]. FANP1 nanoparticles has higher sedimentation rate was because FANP1 nanoparticles has higher aggregation rate compared to FANP2 nanoparticles. When the FANP1 nanoparticles aggregated in the gas-liquid interface, FANP1 nanoparticles tend to form a network of aggregate nanoparticles as shown in Figure 4.12 due to the high aggregation rate of the nanoparticles. However, for FNP2 nanoparticles, it was expected the FANP2 nanoparticles to form a monolayer or a bilayer of nanoparticles at the gas-liquid interface due to lower agglomeration rate. The formation of network of aggregate nanoparticles tend to have a resistance against the dragging force of the fluids in the lamellae compared to monolayer and bilayer of nanoparticles [33]. This is because the aggregated nanoparticles will form a thick solid film at the lamellae to provide a steric barrier to reduce film thinning and inter-bubble diffusion. Therefore, the presence of aggregated nanoparticles will be more effective at slowing down the liquid drainage by reducing the direct contact between fluids [115]. Thus, the foam with FANP1 nanoparticles produces the highest foam stability compared to foam with other types of nanoparticles.

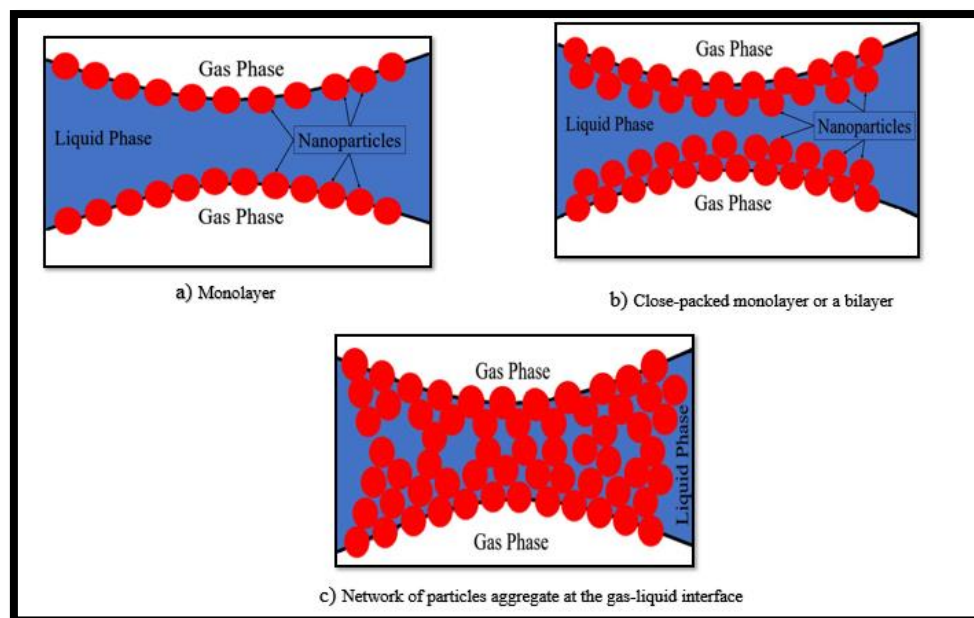


Figure 4.12: Nanoparticles adsorption at the gas-liquid interface in form of (a) Monolayer (b) Close-packed monolayer or a bilayer (c) Network of particles aggregate at the gas-liquid interface [132]

4.7 Study of Foam and Oil Interaction

For the calculation of the entering, spreading, bridging coefficients and lamella number models were used to correlate the static foam stability in the presence of the crude oil so that it would be able to replicate the foam stability in the porous media. The Table 4.5 showed the calculation of the entering, spreading, bridging and lamella number models. The equation of the entering, spreading, bridging and lamella number models were discussed in Section 2.3.2. According to the Equation (2.12), (2.13) and (2.14) described that FANP2-b and R1-b nanoparticles have the highest foam stability because the value of the entering, spreading, and bridging were less than zero. Meanwhile, R2-b nanoparticles and base sample have a moderate stable foam because the spreading, and bridging values were less than zero, but the entering value was higher than zero. This indicated that the oil droplets were able to enter the gas-liquid interface of foam but the oil droplets were not able to spread through the gas-liquid interface of the foam [225]. Foam produced with FANP1-b and CFA-b nanoparticles have the weakest foam according to the entering, spreading, and bridging coefficients model.

This is because the entering, spreading, and bridging values for FANP1-b and CFA-b were all positive values. If the bridging values for FANP1-b and CFA-b were positive, the foam films will be destroyed completely when the oil droplets completely enter the lamellae surface [61]. However, when the model was compared to the results collected in Section 4.6, the calculation values were entirely different with the experimental results collected. In the experiment, FANP1 nanoparticles has the highest foam stability, and the base sample has the lowest foam stability but in the coefficients model, the base sample has the highest foam stability and the FANP1 nanoparticles has the lowest foam stability. These results were similarly to the Singh et al. experiment with three different type of crude oils (A, B, C), using the same type surfactant at a fixed concentration [128]. The calculated values of entering, spreading, and bridging values were all positive value and therefore, it indicates that all the foams will be highly unstable. However, in the foam stability experiment, the foams were in a stable condition. The reason that the entering, spreading, and bridging calculation were different with the experimental works was because the model does not included the antifoaming properties of the crude oil [154]. In Yekeen et al. experiment also showed the entering, spreading and bridging values were not accurate when compared to the foam stability experiment [149]. In the lamella number model, the values calculated were same with the experimental results in Section 4.6. According to the lamella number model, the lower the calculated value, the higher the foam stability. Therefore, the FANP1-b nanoparticles has the highest foam stability and base sample has the lowest foam stability. These values were same with Singh et al. experiment, where, the lamella number values were same with the experiment results [154].

Table 4.5: Nanoparticles stabilized foam interaction between oil and foam at concentration ratio of 80:20

	Base	CFA-b	FANP1-b	FANP2-b	R1-b	R2-b
γ_{gw}	17.64	30.10	18.90	15.70	17.35	17.66
γ_{ow}	0.21	0.68	0.54	0.38	0.44	0.42
γ_{og}	17.80	17.80	17.80	17.80	17.80	17.80
Entering	0.05	12.98	1.64	-1.72	-0.01	0.28
Spreading	-0.37	11.53	0.56	-2.48	-0.89	-0.56
Bridging	-5.63	589.63	40.66	-70.21	-15.62	-4.79
Lamella No.	12.60	6.64	5.25	6.19	5.91	6.31

4.8 Foamability of Nanoparticle Assisted Foam Injection Measurement

Foamability is defined as the capacity of the solution to produce the amount of foam required. In this experiment, the foamability was measured based on the time required to generate foam up to 150ml of foam volume. Figure 4.13 showed the time taken for the foam to reach the foam volume of 150ml. The time taken for the base sample was 80 seconds. For CFA nanoparticles, the CFA-a, CFA-b and CFA-c were 82 seconds, 81 seconds, and 86 seconds, respectively. For FANP1 nanoparticles, the FANP1-a, FANP1-b, and FANP1-c were 82 seconds, 84 seconds, and 81 seconds, meanwhile, the foamability of FANP2-a, FANP2-b and FANP2-c were 78 seconds, 75 seconds, and 79 seconds. The foamability results of R1-a, R1-b, R1-c, R2-a, R2-b, and R2-c nanoparticles were 87 seconds, 86 seconds, 92 seconds, 82 seconds, 68 seconds, and 87 seconds, respectively. Based on the Figure 4.13, there was no clear relationship between the foamability and presence of nanoparticles in the foam. A similar observation was reported by Bee Chea et al. experiment. In the foamability experiment, different types and concentration of nanoparticles were used for the experiment, however, the foamability results does not affected by the nanoparticles [226]. In addition to that, similar results were observed by Guo et al. experiment using the nano-fly ash sample [172]. Hence, we can deduce that nanoparticles have no effect on foamability.

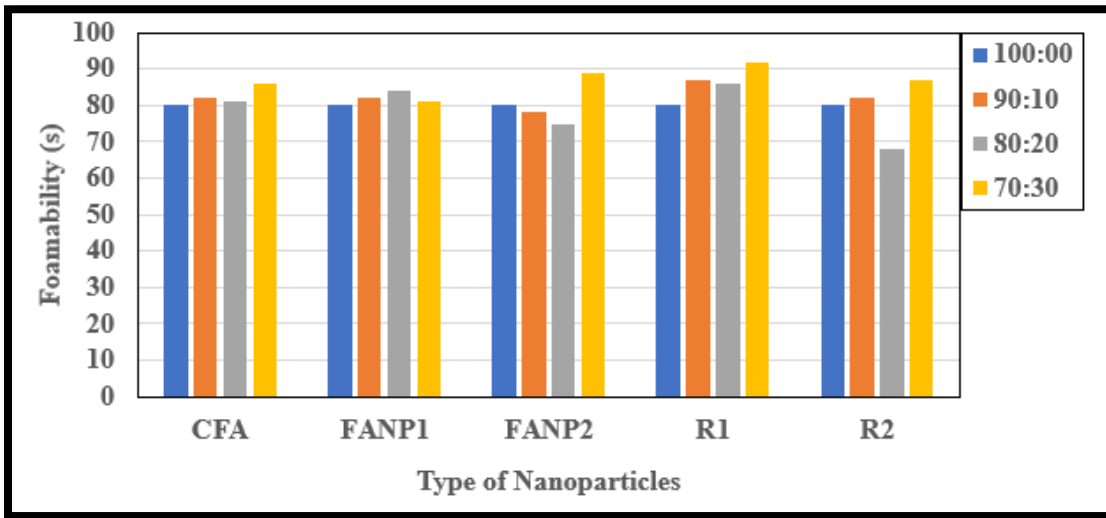


Figure 4.13: Foamability of foam with different concentration and type of nanoparticles

4.9 Core Flooding Experiment

Based on previous screening experiments, five types of foaming solution were used to determine the effectiveness of the nanoparticles on foam stability and oil recovery. The nanoparticles used for the core flooding experiment were base sample, FANP1-b, FANP2-b, R1-a, and R1-b nanoparticles. In the core flooding experiment, two parameters were measured to determine the strength of the foam which were mobility reduction factor (MRF) and oil recovery measurement. Table 4.6 showed the properties of the Berea sandstone core after cleaning the core samples. The porosity of five sandstone core samples were between 22.0% to 23.0% and the permeability were between 215md to 235md using the equation (3.2) and (3.3) respectively.

Table 4.6: Properties of the Berea sandstone core

Core Number	1	2	3	4	5
Type of nanoparticles	Base	FANP1-b	FANP2-b	R1-b	R2-b
Concentration	100:00	80:20	80:20	80:20	80:20
Permeability (md)	232	218	229	233	232
Porosity (%)	22.11	22.18	22.49	22.77	22.64
Dead Volume (ml)	4.3	4.3	4.3	4.3	4.3
Pore Volume (ml)	38.17	38.25	38.50	39.04	38.97
Initial oil saturation, S_{oi} (%)	55.99	55.35	56.31	55.71	55.81
Irreducible water saturation, S_{wirr} (%)	44.01	44.65	43.87	44.29	44.19

4.9.1 Mobility Reduction Factor (MRF)

Figure 4.14 showed the pressure drop of gas injection and foam injection the experiment. The purpose of showing the gas injection of five different core flooding experiment were to make sure the parameters of the core flooding were the same before proceeding to the SAG injection. During the initial of gas injection, the pressure drops increased up to 1psi because it indicated the flow resistance of the gas due to the formation of gas front encountering the oil. After 16ml of cumulative volume of gas injection, the pressure drops below 1psi and the pressure drops remain at a stable condition at the 0.30psi. This was due to the early gas breakthrough [184]. When the foam was injected into the porous media, the pressure drops slowly increased regardless the presence of nanoparticles because the foam was slowly generated in the porous media. The fluctuating pressure drops during the foam injection indicated the phenomena of both foam generation and coalescence taking place simultaneously in the porous media [111]. The decrement of the pressure drops indicated the foam collapsing in the porous media. The foam with base sample has the lowest maximum pressure

drops difference which was 2.4 psi. Meanwhile, for foam with R2 nanoparticles, the maximum pressure drop was 4.6 psi and foam with R1 nanoparticles, the maximum pressure drop was 7.2 psi. For synthesized nanoparticles, the maximum pressure drops for foam with FANP2 nanoparticles was 5.2 psi and for foam with FANP1 the maximum pressure drops was 8.0 psi.

The foam with FANP1 has the highest pressure drops and it indicated the formation of strong foam. Strong foam offered a higher resistance against the gas flow and trapping the gas into the foam. The foam with base sample produced the lowest pressure drops and it indicated a weak formation of foam. Furthermore, the foam with FANP1 with highest pressure drops propagates for a longer duration. This is because when a strong foam was formed, the crude oil droplets will have little effect on the foam stability. In the core flooding experiment, the foam with base sample collapsed after 27.48ml of total volume of injection, and the pressure drops decreases until it reaches the same pressure drops as the gas injection which indicates collapsed of the foam whereas, the foam with the presence of nanoparticles start to collapse at the range of between 35.0ml to 40.0ml of total volume injection into the porous media. Therefore, it indicated that the foam with the presence of nanoparticles will have a stronger foam and a higher tolerance against the presence of the crude oil in the porous media.

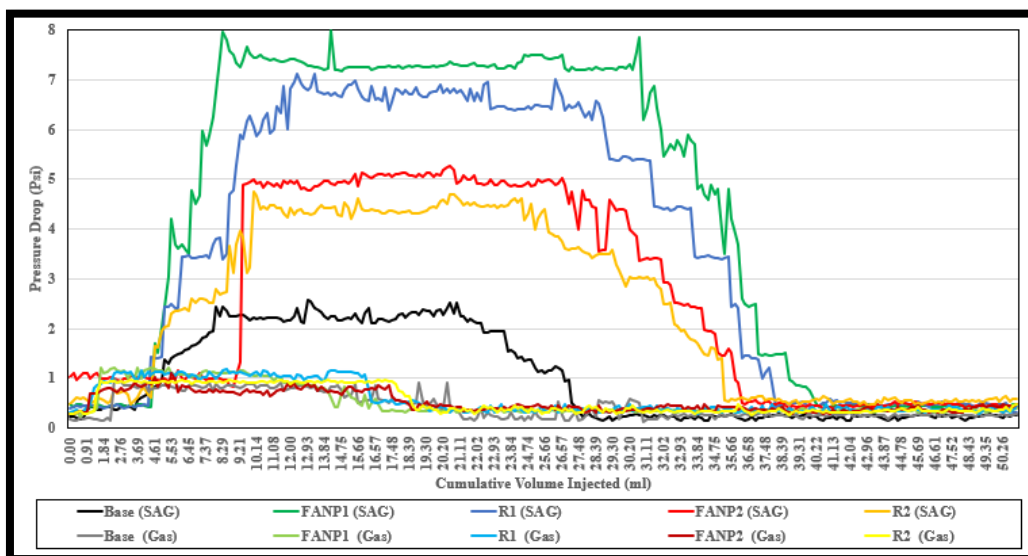


Figure 4.14: Pressure drops of foam injection and gas injection for different type of nanoparticles

MRF value was used to determine the effectiveness of nanoparticles in strengthening the foam. The MRF values were calculated based on the comparison of pressure drop during foam injection against the pressure drop of gas injection in the same core as shown in Equation (3.5). A higher pressure drops or MRF value will indicate a strong foam front inside the core whereas, a sustained pressure drops and MRF trend indicate a higher foam stability [186]. If the MRF values is equal to one or less than one, it indicates the absence of foam in the porous media because the pressure drop of the foam injection is the same as the pressure drop during gas injection. Figure 4.15 showed the MRF values of the foam with different types of nanoparticles against the cumulative volume of foam injected into the porous media. The highest MRF value produced was FANP1 nanoparticles which was 24.4 followed by the foam with R1 nanoparticles which was 21.9. Meanwhile, the maximum MRF value produced by the foam with FANP2 and R2 nanoparticles were 15.4 and 14.5, respectively. Lastly, the foam with base sample produced the lowest MRF value which was 12.1. Based on Figure 4.15, the MRF value of the foam with nanoparticles showed a steady increase in MRF value and followed by a steep increase of MRF value. These phenomena indicate the foam generation in the porous media. For foam with base sample, the MRF value steady increases up to the maximum of 12.1 before the MRF value decreases again. This is because the foam was weakened by the oil droplets flowing into the foam lamellae [227]. The higher the concentration of the oil droplets flowing in the foam lamellae, the higher the chance for the foam to collapse. This phenomenon was same with foam with other type of nanoparticles. The MRF values start to decrease when the total of foam injection was 30ml. This is because, the foam quality decreases at this stage. When the MRF value is high, it indicates a higher apparent viscosity [228] which translates into a higher foam apparent viscosity, and a higher foam quality [229]. With a higher foam quality, the volume of gas trapped in the foam also increased. According to Gong et al., the foam quality is governed by the fractional flow of liquid and gas. If the foam has at least 50% to 80% of gas in the foam, the apparent viscosity will be high. If the gas content in the foam is not between 50% to 80%, the apparent viscosity will be reduced and therefore, the control of gas mobility will be reduced. The fluctuation of MRF value means that the foam was carrying higher oil saturation in the foam which result in the foam stability decreased. When the foam is carrying higher oil saturation,

the foam tends to be unstable with the increasing oil saturation sipping in into lamellas until the foam completely collapsed when the saturation of oil in the foam was beyond the critical foaming oil saturation [56]. The critical foaming oil saturation can be defined as the maximum concentration of the crude oil can be carried by the foam.

Although the nanoparticles retention was not measured, we believe that the nanoparticles retention may not be an important phenomena as based on the previous experimental work done by Singh et al, where 99.57% of the nanoparticles used for the foam injection were recovered with the remaining of less than 1% were retained in the porous media [230]. Murphy et al reported that the nanoparticles recovered from injection were 95% and 96% for two different type of coated silica nanoparticles [231]. In Bayat et al. experiment, when aluminium oxide nanoparticles were injected into the porous media, the retention of aluminium oxide nanoparticles would be high [201]. However, according to the EDX analysis in the Bayat et al. experiment showed that the retention of aluminium oxide nanoparticles in the quartz sandstone was less than 2% while the retention of titanium oxide was estimated at 25% according to the EDX analysis [201]. Therefore, we believed that high MRF is not resulted from nanoparticles retention phenomena.

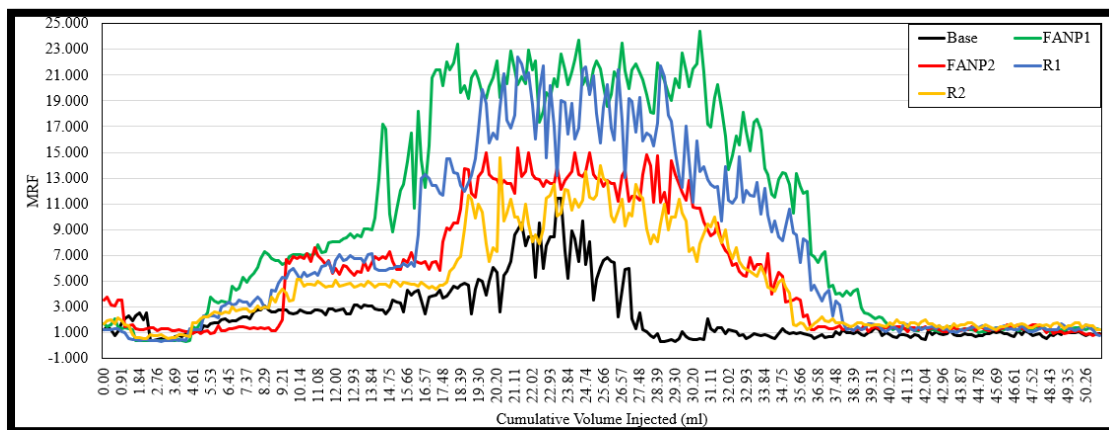


Figure 4.15: MRF of SAG with different type of nanoparticles

4.9.2 Oil Produced by SAG Injection Measurement

Table 4.7 showed the oil recovered by using water injection, gas injection and foam injection with different type of nanoparticles. During the water injection, the oil recovery for water injection for experiments were between 57% to 58%. Meanwhile, the oil recovery for gas injection for all core flooding experiments were between 14% to 16%. The foam with R1 nanoparticles has the highest oil recovery which was 12.18%. However, the foam with FANP1 nanoparticles which has the highest MRF value produced about 9.75% of oil whereas, the foam with FANP2 produced about 11.48% of oil. The foam with R2 nanoparticles produced the lowest oil production among the foam with the presence of nanoparticles which was 8.75%. Although, the oil recovered by the foam with R2 nanoparticles was the lowest, the oil recovered using the foam using R2 nanoparticles was still higher than oil recovered using the foam with base sample. The oil recovery of foam with base sample was 6.69%. Based on the table, we can conclude that the foam in the presence of the nanoparticles will have a higher oil recovery than foam without the presence of any nanoparticles. Although the foam with FANP1 nanoparticles has a higher MRF value than the foam with R1 nanoparticles, R1 nanoparticles produced a higher oil recovery than FANP1 nanoparticles. Therefore, it can conclude that although a higher MRF value can helped to produce a higher oil recovery, there are other factors that will affect the oil recovery such as the reduction of interfacial tension (IFT) between the suspensions and oil phase, and reducing oil viscosity with the nanoparticles surfactant solution [216]. So that the oil droplets will can carried out by the foam aqueous medium [232]. Furthermore, the effect of capillary number, adsorption of the surfactant onto the rock, and wettability of the rock will have an effect on oil recovery [233].

Surfactant partitioning can be described as when the surfactants molecules were introduced to another fluid, the surfactants molecules will start to partition in the interface of the two fluids [234]. As a result, the surfactant molecules will start to remove any hydrophobic parts of the surfactant from the contact of water and therefore, it will decrease the energy of the interface or interfacial tension between the two fluids. According to Belhaj et al. experiment mentioned that surfactant partition is affected by two parameters which were critical micelle concentration and interfacial tension

between two fluids [235]. The coefficient of surfactant partition increases when the concentration of the surfactant increases towards the CMC value of the specific surfactant whereas, the coefficient of surfactant partition will decrease as the concentration of the surfactant increase above the CMC value. Furthermore, when the IFT value decreases, the coefficient of surfactant partition increased and vice versa [235]. However, according to Schramm et al. foam experiment stated that the surfactant partitioning was considered to be negligible in the presence of foam-foaming surfactant and crude oil if the foam-forming surfactant adsorptions by the crude oil and reservoir rocks have already been satisfied, then any foam destabilization effect or physical changes of the foam are attributed to the invasion of crude oil into the foam, temperature of the reservoir, and salinity of the brine [84]. Therefore, in foam injection experiment, the volume of surfactant injection was used until the experiment only produced surfactant solution.

Table 4.7: Oil recovery of foam injection with different types of nanoparticles

Oil Recovery (%)	Base	FANP1	FANP2	R1	R2
Water Injection	57.00	57.58	57.70	57.84	57.29
Gas Injection	15.25	14.83	14.86	14.94	15.17
Initial Residual Oil Saturation (S_{or})	27.75	27.59	27.44	27.22	27.54
Foam Injection	6.69	9.75	11.48	12.18	8.75
Final S_{or} After Foam Injection	21.06	17.84	15.96	15.03	18.79
Oil recovered percentage using Foam Injection from initial S_{or}	24.11	35.34	41.82	44.76	31.18

4.10 History Matching

Based on the result of the core flooding experiment, foam with FANP2 nanoparticles was used for history matching and oil forecasting. Some assumptions were made in the simulation compared to the experiment such as:

1. The porous media was assumed in three phases.
2. The flow in all the injections were considered in steady state.
3. The foam injection was assumed as the co-injection of foam into the porous media.
4. The simulator does not model foam generation in the porous media.
5. The gas, oil and water were present in the beginning of the simulation, purpose to enable the foam model in the simulation.
6. The reservoir has isotropic and uniform permeability and porosity.
7. The injection was assumed to be in a cylindrical geometry for a rectangular shaped grid block, and uniform properties in the grid block.
8. The presence of C1 to C4 hydrocarbons were present in the simulation model meanwhile in the experiment, C1 to C4 hydrocarbon were absent in the Baronia oil content for the experiment.

In Table 4.8, the total oil collected from water injection, gas injection and foam injection were 31.42%, 17.70% and 5.22% respectively. While in the simulation run, the total oil recovery for water injection, gas injection and foam injection were 33.65%, 15.70% and 5.14%. The percentage difference between experimental and simulation results for water injection is 2.23%, 2.00% and 0.08%.

Table 4.8: Oil recovery comparison between experimental and simulation run

Oil Recovery Percentage (%)	Experimental	Simulation
Total Oil recovery by Water injection	31.42	33.65
Total Oil recovery by Gas injection	17.70	15.70
Total Oil by Foam injection	5.22	5.14
Final Oil Recovery (Water + Gas + Foam Injection)	54.34	54.49

4.11 Sensitivity Analysis

The sensitivity analysis was done using the history matching foam injection simulation model and equation (3.6) to determine the major influence of foam in oil recovery. According to equation (3.6), FM or Foam Mobility was depended on the surfactant concentration (F_{surf}), water saturation (F_{dry}), oil saturation (F_{oil}), capillary number (F_{cap}) and mobility reference factor (f_{mmob}). However, in this simulation run, the water saturation, capillary number and reference factor will be defaulted. Since the Berea core is a horizontal homogenous permeability core, the water saturation will have little effect on oil recovery. Therefore, the foam stability on water saturation was not used for reservoir simulation run. In the simulation model, the capillary number was calculated by measuring the surface tension of the foam, and since no equipment were able to measure the surface tension of the foam, the data was set at a constant according to the Eclipse 100 software. The effect of surfactant concentration was model based on adsorption of the core and the maximum concentration of the surfactant was 0.5wt% which was the concentration of surfactant injected. For oil saturation, the static foam stability data was used to model the foam. This is because the core flooding equipment

could not measure dynamic foam stability. The sensitivity analysis was done to provide a better understanding and interpretation of foam injection.

4.11.1 Forecasting of Oil Recovery Study using Surfactant Adsorption by Reservoir Rock

Figure 4.16 showed the oil recovery of foam injection and the different surfactant adsorption rates. HS case was referred to foam history matching model in Section 4.10. For HS with -25% case, the surfactant adsorption by the reservoir rock was reduced by 25% in the HS case. For HS with -50% case, the surfactant adsorption by the reservoir rock was reduced by 50% in the HS case and for HS with -75% case, the surfactant adsorption by the reservoir rock was reduced by 75% in the HS case. The oil recovery for foam injection in HS case was 0.684cc in Figure 4.16. The oil recovery for HS with -25%, -50%, and -75% cases were 0.72cc, 0.79cc, and 0.89cc, respectively. Although the volume of oil recovered for three different adsorption rates were less than 1.00cc, in terms of percentage, the oil recovery was increased by 5.84%, 15.75% and 30.69% for the HS with -25%, -50% and -75% cases, respectively when compared to HS case. Therefore, it can be concluded that when the surfactant adsorbed onto the rock decreases, the oil recovery will increase.

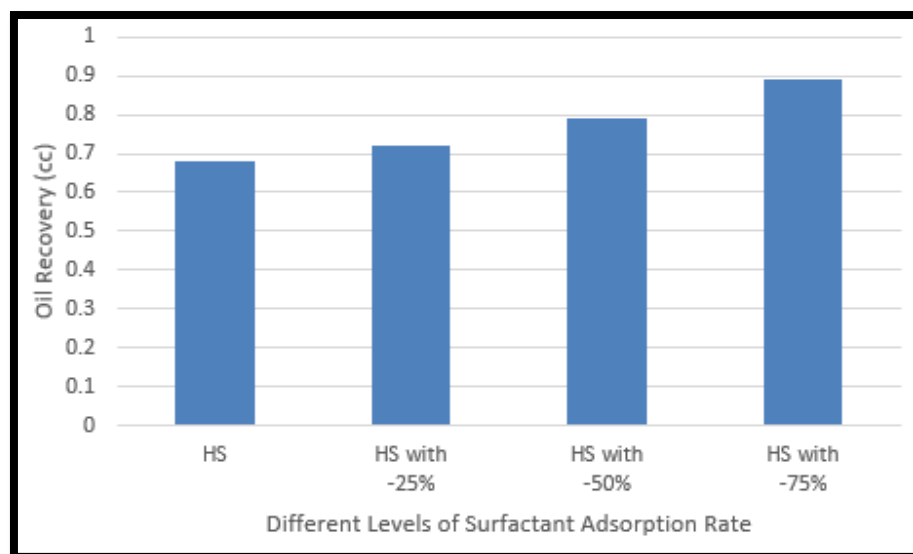


Figure 4.16: Oil recovery for different levels of surfactant adsorption rate

4.11.2 Forecasting of Oil Recovery Study using Half-life of Foam Study

Figure 4.17 indicated the oil recovered by different stability of foam half-life cases in the presence of oil. HS case was referred to the foam history matching model in Section 4.10. The foam half-life of HS case was changed to 10 hours, 15 hours, 20 hours, and 24 hours of foam half-life. In the Figure 4.17, the oil recovered by HS case was 0.684cc. Meanwhile for HS case with foam half-life of 10 hours, 15 hours, 20 hours, and 24 hours were 0.70cc, 0.74cc, 0.77cc and 0.78cc, respectively. The oil recovery increment of when the foam half-life were 10 hours, 15 hours, 20 hours, and 24 hours when compared to HS case were 2.34%, 8.19%, 12.57%, and 14.04%, respectively. When the foam half-life was extended to 24 hours, the increment of oil recovery predicted was increased by 14.04%, the oil recovery was less than the oil recovered when the surfactant adsorption was reduced by 75% which was 30.69% increment of oil recovery. This indicated that when the optimum foam stability was achieved, the oil recovery will reach a plateau [236]. Therefore, the increment of oil recovery for 10 hours, 15 hours, 20 hours, and 24 hours were 0.016cc, 0.04cc, 0.03cc, and 0.01cc, respectively. As a conclusion, the optimum half-life would be required to generate the maximum oil recovery and, in this case, 20 hours of foam half-life is the optimum limit.

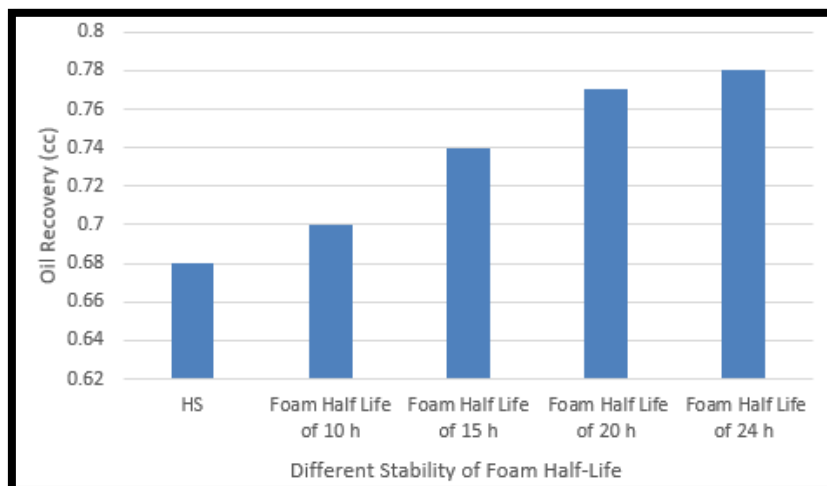


Figure 4.17: Oil recovery comparison with different stability of foam half-life

4.12 Chapter Summary

In this chapter, we have presented the results from the characterization of nanoparticles to extensive experimental work mainly involving the effect of nanoparticles on foam stability and oil recovery. Furthermore, a history matching and sensitivity analysis were done to study the main factor governing oil recovery using foam injection. The size of the synthesized nanoparticles was observed to be less than 100nm and the composition of components was reduced to three composition mainly silicon oxide, aluminium oxide, and sodium sulphate. Moreover, in the sedimentation test, the synthesized nanoparticles were more stable in suspending solution than the CFA nanoparticles. In experimental works, FANP1 nanoparticles produced the highest foam stability, and MRF value compared to other foam with other type of nanoparticles. Meanwhile, the foam with FANP2 nanoparticles produced a lowest IFT value. In core flooding experiment, foam with the presence of nanoparticles produced a higher oil recovery compared to foam without presence of nanoparticles. The foam with 1 R1 nanoparticles produced the highest oil recovery followed by FANP2, FANP1, R2 nanoparticles and lastly foam with base sample. Therefore, it indicates that a higher MRF value can helped to produce a higher oil recovery, there are other factors that will affect the oil recovery such as the reduction of interfacial tension (IFT) between the suspensions and oil phase, and reducing oil viscosity with the nanoparticles surfactant solution. A sensitivity analysis is done, and it was determined that the surfactant adsorption is the main governing factor for oil recovery using FAWAG injection.

CHAPTER 5

CONCLUSION AND RECOMMENDATION

5.1 Conclusion

The synthesized nanoparticles from coal fly ash using the chemical treatment were a successful process in synthesising nanoparticles with the size less than 100nm. The two size of synthesized nanoparticles for FANP1 and FANP2 nanoparticles were between 10nm to 20nm and 40nm to 60nm, respectively. The size of synthesized nanoparticles was similarly to the commercial nanoparticle's silicon oxide and aluminium oxide which were between 10nm to 55nm and 20nm to 30nm. Furthermore, the main composition of the synthesized nanoparticles were silicon oxide, aluminium oxide, and sodium sulphate. The sedimentation results showed that the FANP2 nanoparticles has the highest stability in the solution due to longer suspension duration in the liquid followed by FANP1 nanoparticles and CFA nanoparticles.

In the IFT experiment, it proved that when the foaming solution was added with nanoparticles, the IFT reading will increased. The foaming solution with base sample has the lowest IFT which was 0.21mN/m. Furthermore, the IFT value of foaming solution increased with increasing of nanoparticles concentration. As more nanoparticles were added into the foaming solution, the nanoparticles at the interface increased. As a result, the nanoparticles will try to get closer to each other and the Van der Waals force of attraction will increased and will lead to an unevenly distribute surfactant molecules at the interface of the two fluids that will increased the IFT value [210]. The foaming solution with FANP2 nanoparticles has the lowest IFT value if it was compared with other foaming solution in the presence of different type nanoparticles. This is because of the effect of the surfactant-coated nanoparticles of

FANP2. When FANP2 nanoparticles was coated by a large amount of surfactant, the nanoparticles can act as a carrier of MFOMAX surfactant moving towards the oil and surfactant interface. When the surfactant is released from carrier and the IFT value will be reduced greatly [211]–[213].

The static foam stability experiment was performed to investigate the effect of nanoparticles as an additive in foam stability and foamability. The static foam stability experiment was also used as a screening tool to select the best composition of nanoparticles for the core flooding experiments. The results from the static foam experiments showed that the nanoparticles have the potential of a foam stabilizer to increase the foam stability with the MFOMAX surfactant. Of all the mixture ratio tested, the highest performance for foam stability and foamability was FANP1-b. The optimum concentration ratio for the foam stability experiment was 80:20. In the foamability measurement, the foamability of foam with base sample was 80 seconds. However, the presence of nanoparticles has no effect on foamability as there was a no trending of increment or decrement of foamability with different type of nanoparticles or concentration of nanoparticles. According to the lamella number calculation showed that foam with FANP1 nanoparticles has the most stable foam compared to other foams since the lamella number calculated was 5.25.

The core flooding experiments were conducted at the reservoir condition of 90°C and 1800psi. The foam with FANP1 nanoparticles has the highest MRF value which was 24. Meanwhile, the MRF of foam with base sample was 11. In the presence of nanoparticles, the MRF of foam increases by a twofold compared to foam without nanoparticles. Meanwhile, the MRF value of foam with R1, FANP2 and R2 were 21, 15, and 13, respectively. The higher the MRF value will indicates a higher foam apparent viscosity which translates into a higher foam quality. A higher foam quality indicates a higher gas volume stored in the foam. On the other hand, if the MRF value of foam was fluctuating. This is because the foam was believed to be carrying a higher oil saturation. Therefore, the instability of the MRF values indicates the instability of the foam due to the foam being weakened by the oil droplets flowing into the foam lamellae. The higher the concentration of the oil droplets in the foam lamellae, the higher the chance for the foam stability to decrease or foam collapse. The oil recovered

by the foam with R1 nanoparticles has the highest oil recovery compared to other foams.

The history matching, and sensitivity analysis were performed to investigate the major influence on oil recovery by the foam. History matching was done to validate the reservoir simulation model and to adjust the model until it closely reproduces the behaviour of the core displacement experiment. Overall, the history matching process of the simulation model has a 54.49% of oil production with the highest oil production percentage error coming from gas injection and water injection at around 2.0% error percentage. This because of the presence of gas in the porous media beginning of the simulation and the purpose gas is present in the beginning was part of the simulator requirement for foam injection model, and the presence of C1 to C4 in the hydrocarbon to produce natural gas in the simulator meanwhile in the experiment, the hydrocarbon of C1 to C4 are absence. In the sensitivity analysis, two major influence of foam on oil recovery were investigated which were surfactant adsorption and foam half-life. Owing to the fact that the increment of oil recovery by reducing the surfactant adsorption of 75% was 30.69% and oil recovery from foam stability with a half-life of 24 hours was only 14.04% increment, we can conclude that surfactant adsorption reduction was the main governing factor of oil recovery compared to foam stability.

5.2 Recommendation

The chemical synthesis process has successfully synthesis the nanoparticles with a size less than 100nm in diameter from the coal fly ash with a size more than 1µm in diameter. However, based on the oil recovery results, the synthesized nanoparticles have a lower oil recovery compared to commercial R1 nanoparticles. This may be attributed to the presence of sodium sulphate in the composition of nanoparticles because the sulphate molecular chain is one of the main components in anionic surfactant. However, this result was not fully studied and therefore, a further analysis of sodium sulphate on foam stability and fluid-oil interaction should be proper studied. Although the synthesis process was able to produce a nano-size particle, the impurity of sodium sulphate in the composition may reduce the oil recovery produced using the

foam with synthesized nanoparticles compared to the foam with R1 nanoparticles. Therefore, a further chemical synthesis method should fully focus on extracting silicon oxide and aluminium oxide out from the coal fly ash sample.

In the core flooding experiment, the nanoparticles retention and plugging were not studied. Therefore, the reduction of oil recovery from FANP1 nanoparticles may also be resulted from nanoparticles retention and permeability plugging by the nanoparticles in the porous media whereby, it resulted a higher MRF value with a lower oil recovery factor compared to commercial nanoparticles. Although some studies have been conducted on nanoparticles retention such as Singh et al, where 99.57% of the nanoparticles used for injection were recovered with the remaining of less than 1% retained in the porous media [230]. Murphy et al reported that the nanoparticles recovery from injection were 95% and 96% for two different type of coated silica nanoparticles [231].

APPENDIX A

Fuel 266 (2020) 117033



Contents lists available at ScienceDirect

Fuel

journal homepage: www.elsevier.com/locate/fuel



Full Length Article

Relationship between fly ash nanoparticle-stabilized-foam and oil production in core displacement and simulation studies



Guan Ming Phong^a, Rashidah M. Pilus^{a,*}, Afiq Mustafa^a, Lakshmi Priya Thangavel^b, Norani Muti Mohamed^b

^a Department of Petroleum Engineering, Universiti Teknologi Petronas, Malaysia

^b Department of Applied Science, Universiti Teknologi Petronas, Malaysia

ARTICLE INFO

Keywords:
Nanoparticles
Fly ash
FAWAG
Foam
EOR

ABSTRACT

In this study, the use of coal fly ash nanoparticles as a stabilizer to generate stable foam was explored. First, the fly ash nanoparticles will undergo two-step chemical treatment to synthesize a smaller nanoparticle of higher purity. The fabricated nanoparticle's size was 50 nm and the composition was 99% zeolites and 1% sodium compounds were characterized using Field-Emission Scanning Electron Microscope (FESEM), Energy-Dispersive X-ray Spectroscopy (EDX) and X-ray Photoelectron Spectrometer (XPS). Static foam stability test was done to screen the type and concentration of nanoparticle that has the potential for a foam stabilizer for further core displacement tests. The highest half-life of foam was by fabricated nanoparticles (FN) with a concentration of 80:20 at 875 s. The core displacement test was done to determine the effectiveness of fly ash nanoparticles on oil recovery. The oil recovery results showed that foam with the presence of FN nanoparticles produced a higher oil recovery than those without nanoparticles. The mobility reduction factor (MRF) value of foam with nanoparticles was two times higher than foam without nanoparticles. A sensitivity analysis is done to determine whether the factor governing oil recovery and MRF is the foam stability or surfactant adsorption. The oil recovered by foam injection increased by 30.69% when the surfactant adsorption was reduced by 75%, however, the oil recovery was only half of this value when the foam half-life was tripled. This may indicate that surfactant adsorption is still a major influence to be monitored on increasing oil recovery while focusing on foam stability.

1. Introduction

Gas Injection is one of the widely applied EOR injection methods other than water injection [1–4] because the sweep efficiency of water injection across the porous media is much lower than gas injection [5]. However, due to the inefficiency of gas injection in reservoir conditions, this method is not often promising due to the low density and viscosity characteristics of gas compared to water and crude oil [6]. These characteristics lead to gas injection suffering from the effect of viscous fingering and gravity segregation leading to early gas breakthrough and low oil recovery. Additionally, reservoir heterogeneity further contributes to poor volumetric sweep efficiency [7]. To alleviate the drawbacks of gas injection, foam injection is proposed to improve the oil recovery as it can reduce the viscous fingering and gravity segregation. The objective of foam application is to increase the displacing fluid viscosity and density for the fluid to achieve a more favorable mobility ratio during gas flooding. In other words, the foam serves as a mobility control agent in gas flooding [8,9]. Foam helps to reduce the

high mobility of gas phase in the porous media [10,11]. This is because in the form of foam, the gases are trapped in the foam and thus, the more stable foam further reduces the gas mobility in the porous media [12,13].

This concept of foam injection was first introduced in 1958 by Boud and Holbrook [14]. Foam is produced when gas enters the layers of liquids that expands to enclose or trap the gas with a film of the liquid membrane [15]. The foam forms a hexagonal structure of gas cells whose cell walls consist of lamellae with approximately plane parallel sides. When three or more gas bubbles meet, the lamellae are curved by forming the plateau border [16]. There are three types of mechanisms which lead to foam generation in the porous media which are snap-off, lamella-division and leave behind [17]. The snap-off mechanism normally occurs at the pore throat area when the gas is flowing through the pore throat to the pore body. If the capillary pressure at the front is lower than the capillary pressure at the throat, this difference in capillary pressure will allow the gas bubbles to snap off [18,19]. In order for the snap off mechanism to work, the ratio of pore throat to the pore

* Corresponding author at: Department of Petroleum Engineering, Universiti Teknologi Petronas, PERSIARAN UTP, 32610 SERI ISKANDAR, PERAK, MALAYSIA.
E-mail address: rashidah_mp@utp.edu.my (R. M. Pilus).

<https://doi.org/10.1016/j.fuel.2020.117033>

Received 8 August 2019; Received in revised form 2 January 2020; Accepted 4 January 2020

Available online 13 January 2020

0016-2361/© 2020 Elsevier Ltd. All rights reserved.

REFERENCES

- [1] J. Franklin M. Orr, *Theory of Gas Injection Processes*. Copenhagen, Denmark: Tie-Line Publications, 2007.
- [2] J. R. Christensen, E. H. Stenby, and A. Skauge, “Review of WAG field experience (SPE 71203),” *SPE Reserv. Eval. Eng.*, vol. 4, no. 2, pp. 97–106, 2001.
- [3] D. Rao, “Gas injection EOR - a new meaning in the new millennium,” *J. Can. Pet. Technol.*, vol. 40, no. 2, pp. 11–19, Feb. 2001.
- [4] F. I. Stalkup, “Status of Miscible Displacement (SPE 9992),” *JPT, J. Pet. Technol.*, vol. 35, no. 4, pp. 815–826, 1983.
- [5] Don W. Green and G. Paul Willhite, *Enhanced Oil Recovery*. Society of Petroleum Engineers, 1998.
- [6] L. W. Lake, *Enhanced oil recovery*. Prentice-Hall Inc., Englewood Cliffs, 1989.
- [7] L. W. Lake, Russell T. Johns, W. R. Rossen, and G. A. Pope, *Fundamentals of Enhanced Oil Recovery*. Society of Petroleum Engineers, 2014.
- [8] S. Wang, C. Chen, M. J. Kadum, B. J. Shiau, and J. H. Harwell, “Enhancing foam stability in porous media by applying nanoparticles,” *J. Dispers. Sci. Technol.*, vol. 39, no. 5, pp. 734–743, May 2018.
- [9] H. T. Horjen, “CO₂ Foam Stabilization with Nanoparticles and EOR in Fractured Carbonate Systems,” Master Thesis, Department of Physics and Technology, University of Bergen, 2015.
- [10] W. R. Rossen, “Foam in Porous Media,” in *Foams and Emulsions*, NSSE, Volu., J. F. Sadoc and N. Rivier, Eds. Springer, Dordrecht, 1999, pp. 335–348.
- [11] D. H. Smith, *Foams: Fundamentals and Applications in the Petroleum Industry*. Washington, DC: American Chemical Society, 1994.

- [12] G. Q. Tang and A. R. Kovscek, “Trapped gas fraction during steady-state foam flow,” *Transp. Porous Media*, vol. 65, no. 2, pp. 287–307, Nov. 2006.
- [13] A. Skauge, M. G. Aarra, L. Surguchev, H. A. Martinsen, and L. Rasmussen, “Foam-Assisted WAG: Experience from the Snorre Field (SPE 75157),” in *SPE/DOE Improved Oil Recovery Symposium, 2002*.
- [14] D. C. Bond, O. C. Holbrook, and C. Lake, “Gas Drive Oil Recovery Process,” US2866507A.
- [15] J.-P. Krause, “Foams. Theory, Measurements, and Applications. Edited by R. K. Prud’homme and S. A. Khan. VIII and 596 pages, numerous figures and tables. Marcel Dekker, Inc., New York, Basel, Hong Kong 1996. Price: 165.75 US \$.” *Food / Nahrung*, vol. 41, no. 1, pp. 55–55, 1997.
- [16] A. H. Falls, G. J. Hirasaki, T. W. Patzek, D. A. Gauglitz, D. D. Miller, and T. Ratulowski, “Development of a mechanistic foam simulator: The population balance and generation by snap-off (SPE 14961),” *SPE Reserv. Eng. (Society Pet. Eng.)*, vol. 3, no. 3, pp. 884–892, 1988.
- [17] J. N. Israelachvili, *Intermolecular and Surface Forces*. Academic Press, San Diego, Calif, 2011.
- [18] W. Yang, T. Wang, and Z. Fan, “Highly Stable Foam Stabilized by Alumina Nanoparticles for EOR: Effects of Sodium Cumenesulfonate and Electrolyte Concentrations,” *Energy and Fuels*, vol. 31, no. 9, pp. 9016–9025, 2017.
- [19] K. L. Stellner and J. F. Scamehorn, “Surfactant precipitation in aqueous solutions containing mixtures of anionic and nonionic surfactants,” *J. Am. Oil Chem. Soc.*, vol. 63, no. 4, pp. 566–574, 1986.
- [20] J. C. Amante, J. F. Scamehorn, and J. H. Harwell, “Precipitation of mixtures of anionic and cationic surfactants. II. Effect of surfactant structure, temperature, and pH,” *J. Colloid Interface Sci.*, vol. 144, no. 1, pp. 243–253, 1991.
- [21] L. L. Handy, J. O. Amaefule, V. M. Ziegler, and I. Ershaghi, “SPE 7867

- Thermal Stability of Surfactants for Reservoir Application (includes associated papers 11323 and 11597),” *Soc. Pet. Eng. J.*, vol. 22, no. 05, pp. 722–730, Oct. 1982.
- [22] R. Farajzadeh, A. Andrianov, R. Krastev, W. R. Rossen, and G. J. Hirasaki, “Foam-oil interaction in porous media-Implications for foam-assisted enhanced oil recovery (SPE 154197),” *74th Eur. Assoc. Geosci. Eng. Conf. Exhib. 2012 Inc. SPE Eur. 2012 Responsibly Secur. Nat. Resour.*, pp. 4996–5016, 2012.
- [23] A. S. Emrani, A. F. Ibrahim, and H. A. Nasr-El-din, “Evaluation of mobility control with nanoparticle-stabilized CO₂ foam (SPE 185551),” *SPE Lat. Am. Caribb. Pet. Eng. Conf. Proc.*, no. May, pp. 18–19, 2017.
- [24] R. Barati, S. J. Johnson, S. McCool, D. W. Green, G. P. Willhite, and J.-T. Liang, “Polyelectrolyte complex nanoparticles for protection and delayed release of enzymes in alkaline pH and at elevated temperature during hydraulic fracturing of oil wells,” *J. Appl. Polym. Sci.*, vol. 126, no. 2, pp. 587–592, Oct. 2012.
- [25] M. F. Zakaria, M. Husein, and G. Hareland, “Novel nanoparticle-based drilling fluid with improved characteristics (SPE 156992),” *Soc. Pet. Eng. - SPE Int. Oilf. Nanotechnol. Conf. 2012*, no. 2009, pp. 232–237, 2012.
- [26] A. Karimi *et al.*, “Wettability alteration in carbonates using zirconium oxide nanofluids: EOR implications,” *Energy and Fuels*, vol. 26, no. 2, pp. 1028–1036, Feb. 2012.
- [27] M. Khajepour, S. Reza Etminan, J. Goldman, and F. Wassmuth, “Nanoparticles as foam stabilizer for steam-foam process (SPE 179826),” in *Society of Petroleum Engineers - SPE EOR Conference at Oil and Gas West Asia, OGWA 2016*, 2016.
- [28] S. I. Karakashev, O. Ozdemir, M. A. Hampton, and A. V. Nguyen, “Formation and stability of foams stabilized by fine particles with similar size, contact angle and different shapes,” *Colloids Surfaces A Physicochem. Eng. Asp.*, vol.

- 382, no. 1–3, pp. 132–138, Jun. 2011.
- [29] D. Lee, H. Cho, J. Lee, C. Huh, and K. Mohanty, “Fly ash nanoparticles as a CO₂ foam stabilizer,” *Powder Technol.*, vol. 283, pp. 77–84, Oct. 2015.
- [30] R. Singh and K. K. Mohanty, “Nanoparticle-stabilized foams for high-temperature, high-salinity oil reservoirs (SPE 187165),” *Proc. - SPE Annu. Tech. Conf. Exhib.*, 2017.
- [31] C. Huh and H. Cho, “Silica, Fly Ash and Magnetite Nanoparticles for Improved Oil and Gas Production,” *Korean Soc. Miner. Energy Resour. Eng.*, vol. 55, no. 4, pp. 272–284, Aug. 2018.
- [32] I. Ahmad, M. B. Awang, M. Mumtaz, and M. Z. M. Noor, “Development and evaluation of fly ash particle for foam stability for possible application to foam flooding,” *J. Sci. Res. Dev.*, vol. 2, no. 14, pp. 166–171, 2015.
- [33] Z. AlYousef, M. Almobarky, and D. Schechter, “Enhancing the Stability of Foam by the Use of Nanoparticles,” *Energy & Fuels*, vol. 31, no. 10, pp. 10620–10627, Oct. 2017.
- [34] O. W. Flörke *et al.*, “Silica,” in *Ullmann’s Encyclopedia of Industrial Chemistry*, Weinheim, Germany: Wiley-VCH Verlag GmbH & Co. KGaA, 2008.
- [35] S. (Simon) Aldridge and A. J. (Anthony J. Downs), *The group 13 metals aluminium, gallium, indium and thallium : chemical patterns and peculiarities*. Wiley, 2011.
- [36] J. Alegbe, O. S. Ayanda, P. Ndungu, N. Alexander, O. O. Fatoba, and L. F. Petrik, “Chemical, Mineralogical and Morphological Investigation of Coal Fly Ash Obtained from Mpumalanga Province, South Africa,” *Res. J. Environ. Sci.*, vol. 12, no. 3, pp. 98–105, Mar. 2018.
- [37] T. Lakshmipriya, N. Mohamed, R. Bashiri, R. M. Pilus, and A. Mustaffa, “Extraction of zeolite nanoparticles from industrial waste of coal fly ash by

alkali reduction.,” *3rd Int. Conf. Appl. Surf. Sci.*, 2019.

- [38] M. R. Atri and S. N. Ashrafizadeh, “The importance of foams and antifoaming in bioprocesses,” *Pakistan J. Biotechnol.*, vol. 7, no. 2, pp. 19–39, 2010.
- [39] R. K. Prud’homme, “Foams: Theory: Measurements: Applications.” p. 610, 1995.
- [40] A. Saint-James, D. J. Durian, and D. A. Weitz, “Foams,” in *Kirk-Othmer Encyclopedia of Chemical Technology*, Hoboken, NJ, USA: John Wiley & Sons, Inc., 2012.
- [41] A. Saint-Jalmes, “Physical chemistry in foam drainage and coarsening,” *Soft Matter*, vol. 2, no. 10, pp. 836–849, 2006.
- [42] G. Kontogeorgis and S. Kiil, “Chapter 13: Foams,” in *Introduction to Applied Colloid and Surface Chemistry*, John Wiley & Sons, Ltd, 2016, pp. 283–302.
- [43] L. L. Schramm and F. Wassmuth, “Foams: Basic Principles,” in *Foams: Fundamentals and Applications in the Petroleum Industry*, L. L. Schramm, Ed. Advance in Chemistry, 1994, pp. 3–45.
- [44] P. Walstra, “Principles of Foam Formation and Stability,” in *Foams: Physics, Chemistry and Structure*, 1989, pp. 1–15.
- [45] D. Exerowa and Pyotr M. Kruglyakov, “Chapter 1. Formation and structure of foams. Pressure in the liquid and gas phases of foams,” in *Studies in Interface Science*, vol. 5, no. C, Elsevier, 1998, pp. 1–41.
- [46] D. Exerowa and Pyotr M. Kruglyakov, “Chapter 7. Foam stability and the stabilising ability of surfactants,” in *Studies in Interface Science*, vol. 5, no. C, Elsevier, 1998, pp. 502–570.
- [47] S. A. Magrabi, B. Z. Dlugogorski, and G. J. Jameson, “Bubble size distribution and coarsening of aqueous foams,” *Chem. Eng. Sci.*, vol. 54, no. 18, pp. 4007–4022, Sep. 1999.

- [48] S. Qin, B. B. Hansen, and S. Kiil, “Foaming in wet flue gas desulfurization plants: Laboratory-scale investigation of long-term performance of antifoaming agents,” *AIChE J.*, vol. 59, no. 10, pp. 3741–3747, Oct. 2013.
- [49] G. J. Hirasaki, “Steam-foam process,” *JPT, J. Pet. Technol.*, vol. 41, no. 5, pp. 449-456 19505, May 1989.
- [50] W. R. Rossen, “Foam generation at layer boundaries in porous media,” *SPE J.*, vol. 4, no. 4, pp. 409–412, Dec. 1999.
- [51] F. Vardar-Sukan, “Foaming: Consequences, prevention and destruction,” *Biotechnology Advances*, vol. 16, no. 5–6. Elsevier Sci Ltd, pp. 913–948, 01-Sep-1998.
- [52] V. J. Van Der Bent, “Comparative study of Foam Stability in bulk and porous media,” Delft University of Technology, 2014.
- [53] L. A. Lyon, “Handbook of Applied Surface and Colloid Chemistry. Volumes 1 and 2 Edited by Krister Holmberg (Chalmers University of Technology). John Wiley & Sons: West Sussex. 2002. xii + 1110 pp. \$600.00. ISBN 0-471-49083-0.,” *J. Am. Chem. Soc.*, vol. 124, no. 50, pp. 15143–15144, Dec. 2002.
- [54] J. J. Bikerman, “Formation and Structure,” in *Foams*, Berlin, Heidelberg: Springer Berlin Heidelberg, 1973, pp. 33–64.
- [55] “The Collected Works of J. Willard Gibbs,” *Nature*, vol. 124, no. 3117, pp. 119–120, Jul. 1929.
- [56] J. J. Sheng, “Foams and Their Applications in Enhancing Oil Recovery,” in *Enhanced Oil Recovery Field Case Studies*, Elsevier Inc., 2013, pp. 251–280.
- [57] V. B. Fainerman, D. (Dietmar) Möbius, and R. Miller, *Surfactants : chemistry, interfacial properties, applications*. Elsevier Science, 2001.
- [58] S. I. Karakashev and M. V. Grozdanova, “Foam and Antifoam theory,” *Adv. Colloid Interface Sci.*, vol. 176, pp. 1–17, 2012.

- [59] L. L. Schramm, *Emulsions, Foams, and Suspensions*. Wiley, 2005.
- [60] I. Cantat *et al.*, “Foams: Structure and Dynamics,” *Clim. Chang. 2013 - Phys. Sci. Basis*, vol. 1, no. 9, pp. 1–278, 2013.
- [61] K. Osei-Bonsu, N. Shokri, and P. Grassia, “Foam stability in the presence and absence of hydrocarbons: From bubble- to bulk-scale,” *Colloids and Surfaces A: Physicochemical and Engineering Aspects*, vol. 481, pp. 514–526, 2015.
- [62] A. Saint-Jalmes, “Physical chemistry in foam drainage and coarsening,” *Soft Matter*, vol. 2, no. 10, pp. 836–849, Sep. 2006.
- [63] J. F. Casteel and N. F. Djabbarah, “Sweep Improvement in CO₂ Flooding by Use of Foaming Agents,” *SPE Reserv. Eng.*, vol. 3, no. 04, pp. 1,186-1,192, Nov. 1988.
- [64] M. Kanda and R. S. Schechter, “On the Mechanism of Foam Formation in Porous Media,” in *SPE Annual Fall Technical Conference and Exhibition*, 1976.
- [65] H.-L. Chen, M.-J. Ke, T.-K. Chuang, and R. W. Flumerfelt, “Experimental Studies of Capillary Pressure Effects of Foams in Porous Media,” in *SPE California Regional Meeting*, 1990.
- [66] L. L. Handy, J. O. Amaefule, V. M. Ziegler, and I. Ershaghi, “Thermal Stability of Surfactants for Reservoir Application (includes associated papers 11323 and 11597),” *Soc. Pet. Eng. J.*, vol. 22, no. 05, pp. 722–730, Oct. 1982.
- [67] A. M. Al-Sabagh, N. M. Nasser, M. A. Migahed, and N. G. Kandil, “Effect of chemical structure on the cloud point of some new non-ionic surfactants based on bisphenol in relation to their surface active properties,” *Egypt. J. Pet.*, vol. 20, no. 2, pp. 59–66, Jun. 2011.
- [68] S. S. Adkins *et al.*, “Morphology and Stability of CO₂-in-Water Foams with Nonionic Hydrocarbon Surfactants,” *Langmuir*, vol. 26, no. 8, pp. 5335–5348, Apr. 2010.

- [69] S.-H. Chang, F. D. Martin, and R. B. Grigg, "Effect of Pressure on CO₂ Foam Displacements: A Micromodel Visualization Study," in *SPE/DOE Improved Oil Recovery Symposium*, 1994.
- [70] A. M. Elsharkawy, F. H. Poettmann, and R. L. Christiansen, "Measuring Minimum Miscibility Pressure: Slim-Tube or Rising-Bubble Method?," in *SPE/DOE Enhanced Oil Recovery Symposium*, 1992.
- [71] Z. Sun, "Capillary phenomena in porous media: Pore and grain scale studies," Georgia Institute of Technology, 2018.
- [72] T. Al-Sahhaf, A. Elkamel, A. S. Ahmed, and A. R. Khan, "The influence of temperature, pressure, salinity, and surfactant concentration on the interfacial tension of the n-octane-water system," *Chem. Eng. Commun.*, vol. 192, no. 4–6, pp. 667–684, Apr. 2005.
- [73] M. Srivastava, "Foam assisted low interfacial tension enhanced oil recovery," University of Texas, 2010.
- [74] N. Agharazi-Dormani, V. Hornof, and G. H. Neale, "Effects of divalent ions in surfactant flooding," *J. Pet. Sci. Eng.*, vol. 4, no. 3, pp. 189–196, Jul. 1990.
- [75] M. S. Kamal, I. A. Hussein, and A. S. Sultan, "Review on Surfactant Flooding: Phase Behavior, Retention, IFT, and Field Applications," *Energy & Fuels*, vol. 31, no. 8, pp. 7701–7720, Aug. 2017.
- [76] Y. Liu, R. B. Grigg, and R. K. Svec, "CO₂ Foam Behavior: Influence of Temperature, Pressure, and Concentration of Surfactant," in *SPE Production Operations Symposium*, 2005.
- [77] E. Torino, E. Reverchon, and K. P. Johnston, "Carbon dioxide/water, water/carbon dioxide emulsions and double emulsions stabilized with a nonionic biocompatible surfactant," *J. Colloid Interface Sci.*, vol. 348, no. 2, pp. 469–478, Aug. 2010.
- [78] R. Farajzadeh, A. Andrianov, H. Bruining, and P. L. J. Zitha, "Comparative

- Study of CO₂ and N₂ Foams in Porous Media at Low and High Pressure–Temperatures,” *Ind. Eng. Chem. Res.*, vol. 48, no. 9, pp. 4542–4552, May 2009.
- [79] S. A. Farzaneh and M. Sohrabi, “Visual Investigation of Improvement in Extra-Heavy Oil Recovery by Borate-Assisted CO₂-Foam Injection CO₂-Foam Injection,” *Transp. Porous Media 2018 1222*, vol. 122, no. 2, pp. 487–513, Feb. 2018.
- [80] S. A. Farzaneh and M. Sohrabi, “A Review of the Status of Foam Application in Enhanced Oil Recovery,” 2013.
- [81] F. Friedmann and J. A. Jensen, “Some Parameters Influencing the Formation and Propagation of Foams in Porous Media,” in *SPE California Regional Meeting*, 1986.
- [82] R. F. Li, W. Yan, S. Liu, G. J. Hirasaki, and C. A. Miller, “Foam mobility control for surfactant enhanced oil recovery,” *SPE J.*, vol. 15, no. 4, pp. 934–948, Dec. 2010.
- [83] R. E. Blauer and C. A. Kohlhaas, “Formation Fracturing with Foam,” in *Fall Meeting of the Society of Petroleum Engineers of AIME*, 1974.
- [84] L. L. Schramm, “Foam Sensitivity to Crude Oil in Porous Media,” 1994, pp. 165–197.
- [85] S.-H. Chang and R. B. Grigg, “Effects of Foam Quality and flow Rate on CO₂-Foam Behavior at Reservoir Conditions,” in *SPE/DOE Improved Oil Recovery Symposium*, 1998.
- [86] M. J. Rosen and J. T. Kunjappu, *Surfactants and interfacial phenomena*. Wiley, 2012.
- [87] J. Novosad, B. B. Maini, and A. Huang, “Retention Of Foam-Forming Surfactants At Elevated Temperatures,” *J. Can. Pet. Technol.*, vol. 25, no. 3, pp. 42–46, Jun. 1986.

- [88] V. Bergeron, M. E. Fagan, and C. J. Radke, "Generalized entering coefficients: a criterion for foam stability against oil in porous media," *Langmuir*, vol. 9, no. 7, pp. 1704–1713, Jul. 1993.
- [89] L. L. Schramm, "Foam Sensitivity to Crude Oil in Porous Media," 1994, pp. 165–197.
- [90] T. S. Kristiansen and T. Holt, "Properties of Flowing Foam in Porous Media Containing Oil," in *SPE/DOE Enhanced Oil Recovery Symposium*, 1992.
- [91] L. L. Schramm, A. T. Turta, and J. J. Novosad, "Microvisual and coreflood studies of foam interactions with a light crude oil," *SPE Reserv. Eng. (Society Pet. Eng.)*, vol. 8, no. 3, pp. 201–206, Aug. 1993.
- [92] A. D. Nikolov, D. T. Wasan, D. W. Huang, and D. A. Edwards, "The Effect of Oil on Foam Stability: Mechanisms and Implications for Oil Displacement by Foam in Porous Media," Jan. 1986.
- [93] W. D. Harkins and A. Feldman, "Films. The spreading of liquids and the spreading coefficient," *J. Am. Chem. Soc.*, vol. 44, no. 12, pp. 2665–2685, Dec. 1922.
- [94] P. M. Kruglyakov and N. G. Vilkovala, "The relation between stability of asymmetric films of the liquid/liquid/gas type, spreading coefficient and surface pressure," *Colloids Surfaces A Physicochem. Eng. Asp.*, vol. 156, no. 1–3, pp. 475–487, Oct. 1999.
- [95] P. R. Garrett, "The effect of polytetrafluoroethylene particles on the foamability of aqueous surfactant solutions," *J. Colloid Interface Sci.*, vol. 69, no. 1, pp. 107–121, Mar. 1979.
- [96] L. L. Schramm and J. J. Novosad, "Micro-visualization of foam interactions with a crude oil," *Colloids and Surfaces*, vol. 46, no. 1, pp. 21–43, Jan. 1990.
- [97] L. L. Schramm and J. J. Novosad, "The destabilization of foams for improved oil recovery by crude oils: Effect of the nature of the oil," *J. Pet. Sci. Eng.*, vol.

7, no. 1–2, pp. 77–90, Apr. 1992.

- [98] W. R. Rossen, Z. H. Zhou, and C. K. Mamun, “Modeling foam mobility in porous media,” in *Proceedings - SPE Annual Technical Conference and Exhibition*, 1991, vol. Gamma, no. 01, pp. 337–351.
- [99] S. . Vasshus, “Experimental study of foam generation and flow in carbonate fracture systems,” Master Thesis, Department of Physics and Technology, University of Bergen, 2016.
- [100] R. Liontas, K. Ma, G. J. Hirasaki, and S. L. Biswal, “Neighbor-induced bubble pinch-off: Novel mechanisms of in situ foam generation in microfluidic channels,” *Soft Matter*, vol. 9, no. 46, pp. 10971–10984, Dec. 2013.
- [101] M. Chen, Y. C. Yortsos, and W. R. Rossen, “A pore-network study of the mechanisms of foam generation,” *Proc. - SPE Annu. Tech. Conf. Exhib.*, pp. 4393–4412, 2004.
- [102] K. Mannhardt, J. J. Novosad, and L. L. Schramm, “Foam/Oil Interactions at Reservoir Conditions,” in *SPE/DOE Improved Oil Recovery Symposium*, 1998.
- [103] M. Chen, Y. C. Yortsos, and W. R. Rossen, “Insights on foam generation in porous media from pore-network studies,” *Colloids Surfaces A Physicochem. Eng. Asp.*, vol. 256, no. 2–3, pp. 181–189, Apr. 2005.
- [104] B. Li, G. J. Hirasaki, and C. A. Miller, “Upscaling of Foam Mobility Control to Three Dimensions,” in *SPE/DOE Symposium on Improved Oil Recovery*, 2006.
- [105] T. C. Ransohoff and C. J. Radke, “Mechanisms of Foam Generation in Glass-Bead Packs,” *SPE Reserv. Eng. (Society Pet. Eng.)*, vol. 3, no. 2, pp. 573–585, 1988.
- [106] D. Tanzil, G. J. Hirasaki, and C. A. Miller, “Mobility of foam in heterogeneous media: Flow parallel and perpendicular to stratification,” *SPE J.*, vol. 7, no. 2, pp. 203–212, Jun. 2002.
- [107] Q. Nguyen, “Dynamics of foam in porous media.” 2004.

- [108] T. C. Ransohoff, P. A. Gauglitz, and C. J. Radke, “Snap-off of gas bubbles in smoothly constricted noncircular capillaries,” *AIChE J.*, vol. 33, no. 5, pp. 753–765, May 1987.
- [109] B. Morin, Y. Liu, V. Alvarado, and J. Oakey, “A microfluidic flow focusing platform to screen the evolution of crude oil-brine interfacial elasticity,” *Lab Chip*, vol. 16, no. 16, pp. 3074–3081, 2016.
- [110] G. Roof, “Snap-Off of Oil Droplets in Water-Wet Pores,” *Soc Pet. Eng J*, vol. 10, no. 1, pp. 85–90, 1970.
- [111] A. R. Kavscek and C. J. Radke, “Fundamentals of Foam Transport in Porous Media,” in *Foams: Fundamentals and Applications in the Petroleum Industry*, L. L. Schramm, Ed. 1994, pp. 115–163.
- [112] Q. P. Nguyen, A. V. Alexandrov, P. L. Zitha, and P. K. Currie, “Experimental and Modeling Studies on Foam in Porous Media: A Review,” in *SPE International Symposium on Formation Damage Control*, 2000.
- [113] F. Friedmann, W. H. Chen, and P. A. Gauglitz, “Experimental and simulation study of high-temperature foam displacement in porous media,” *SPE Reserv. Eng. (Society Pet. Eng.)*, vol. 6, no. 1, pp. 37–45, Feb. 1991.
- [114] E. Rio, W. Drenckhan, A. Salonen, and D. Langevin, “Unusually stable liquid foams,” *Adv. Colloid Interface Sci.*, vol. 205, pp. 74–86, Mar. 2014.
- [115] A. L. Fameau and A. Salonen, “Effect of particles and aggregated structures on the foam stability and aging,” *Comptes Rendus Physique*, vol. 15, no. 8–9. Elsevier Masson SAS, pp. 748–760, 2014.
- [116] Z. Briceño-Ahumada, W. Drenckhan, and D. Langevin, “Coalescence in Draining Foams Made of Very Small Bubbles,” *Phys. Rev. Lett.*, vol. 116, no. 12, p. 128302, Mar. 2016.
- [117] A. V. Nguyen and H. J. Schulze, “Colloidal science of flotation,” *Colloid. Sci. Flot.*, 2004.

- [118] E. D. Manev and A. V. Nguyen, “Critical thickness of microscopic thin liquid films,” *Advances in Colloid and Interface Science*, vol. 114–115. Elsevier, pp. 133–146, 30-Jun-2005.
- [119] V. V. Yaminsky, S. Ohnishi, E. A. Vogler, and R. G. Horn, “Stability of aqueous films between bubbles. Part 1. the effect of speed on bubble coalescence in purified water and simple electrolyte solutions,” *Langmuir*, vol. 26, no. 11, pp. 8061–8074, Jun. 2010.
- [120] R. G. Horn, L. A. Del Castillo, and S. Ohnishi, “Coalescence map for bubbles in surfactant-free aqueous electrolyte solutions,” *Adv. Colloid Interface Sci.*, vol. 168, no. 1–2, pp. 85–92, Oct. 2011.
- [121] S. Hilgenfeldt, S. A. Koehler, and H. A. Stone, “Dynamics of Coarsening Foams: Accelerated and Self-Limiting Drainage,” *Phys. Rev. Lett.*, vol. 86, no. 20, pp. 4704–4707, May 2001.
- [122] P. M. Kruglyakov, S. I. Karakashev, A. V. Nguyen, and N. G. Vilкова, “Foam drainage,” *Current Opinion in Colloid and Interface Science*, vol. 13, no. 3. pp. 163–170, Jun-2008.
- [123] N. Vandewalle, J. F. Lentz, S. Dorbolo, and F. Brisbois, “Avalanches of popping bubbles in collapsing foams,” *Phys. Rev. Lett.*, vol. 86, no. 1, pp. 179–182, Jan. 2001.
- [124] P.-G. De Gennes, “The Physics of Foams,” *Phys. Today*, vol. 54, no. 3, p. 54, 2001.
- [125] M. Khajepour *et al.*, “Nanoparticles as Foam Stabilizer for Steam-Foam Process,” 2016.
- [126] D. Golomb, E. Barry, D. Ryan, P. Swett, and H. Duan, “Macroemulsions of liquid and supercritical CO₂-in-water and water-in-liquid CO₂ stabilized by fine particles,” in *Industrial and Engineering Chemistry Research*, 2006, vol. 45, no. 8, pp. 2728–2733.

- [127] Z. A. AlYousef, M. A. Almobarky, and D. S. Schechter, “The effect of nanoparticle aggregation on surfactant foam stability,” *Journal of Colloid and Interface Science*, vol. 511. pp. 365–373, 2018.
- [128] R. Singh and K. K. Mohanty, “Synergy between Nanoparticles and Surfactants in Stabilizing Foams for Oil Recovery,” 2014.
- [129] B. P. Binks, “Particles as surfactants - Similarities and differences,” *Curr. Opin. Colloid Interface Sci.*, vol. 7, no. 1–2, pp. 21–41, Mar. 2002.
- [130] Q. Sun, Z. Li, S. Li, L. Jiang, J. Wang, and P. Wang, “Utilization of Surfactant-Stabilized Foam for Enhanced Oil Recovery by Adding Nanoparticles,” 2014.
- [131] S. Kumar and A. Mandal, “Investigation on stabilization of CO₂ foam by ionic and nonionic surfactants in presence of different additives for application in enhanced oil recovery,” *Applied Surface Science*, vol. 420. pp. 9–20, 2017.
- [132] T. S. Horozov, “Foams and foam films stabilised by solid particles,” *Current Opinion in Colloid and Interface Science*, vol. 13, no. 3. pp. 134–140, Jun-2008.
- [133] R. Atkin, V. S. J. Craig, E. J. Wanless, and S. Biggs, “Mechanism of cationic surfactant adsorption at the solid-aqueous interface,” *Advances in Colloid and Interface Science*, vol. 103, no. 3. Elsevier, pp. 219–304, 30-May-2003.
- [134] S. Alzobaidi, M. Lotfollahi, I. Kim, K. P. Johnston, and D. A. DiCarlo, “Carbon Dioxide-in-Brine Foams at High Temperatures and Extreme Salinities Stabilized with Silica Nanoparticles,” *Energy and Fuels*, vol. 31, no. 10, pp. 10680–10690, Oct. 2017.
- [135] N. Yekeen, A. K. Idris, M. A. Manan, A. M. Samin, A. R. Risal, and T. X. Kun, “Bulk and bubble-scale experimental studies of influence of nanoparticles on foam stability,” *Chinese J. Chem. Eng.*, vol. 25, no. 3, pp. 347–357, Mar. 2017.
- [136] Z. Xue *et al.*, “Ultradry Carbon Dioxide-in-Water Foams with Viscoelastic

- Aqueous Phases,” *Langmuir*, vol. 32, no. 1, pp. 28–37, Jan. 2016.
- [137] T. N. Hunter, R. J. Pugh, G. V. Franks, and G. J. Jameson, “The role of particles in stabilising foams and emulsions,” *Advances in Colloid and Interface Science*, vol. 137, no. 2. pp. 57–81, 18-Mar-2008.
- [138] G. Kaptay, “On the equation of the maximum capillary pressure induced by solid particles to stabilize emulsions and foams and on the emulsion stability diagrams,” *Colloids Surfaces A Physicochem. Eng. Asp.*, vol. 282–283, pp. 387–401, Jul. 2006.
- [139] E. Dickinson, R. Ettelaie, T. Kostakis, and B. S. Murray, “Factors controlling the formation and stability of air bubbles stabilized by partially hydrophobic silica nanoparticles,” *Langmuir*, vol. 20, no. 20, pp. 8517–8525, Sep. 2004.
- [140] T. Kostakis, R. Ettelaie, and B. S. Murray, “Effect of high salt concentrations on the stabilization of bubbles by silica particles,” *Langmuir*, vol. 22, no. 3, pp. 1273–1280, Jan. 2006.
- [141] R. M. Enick, D. Olsen, J. Ammer, and W. Schuller, “Mobility and conformance control for CO₂ EOR via thickeners, foams, and gels - A literature review of 40 years of research and pilot tests,” in *SPE - DOE Improved Oil Recovery Symposium Proceedings*, 2012, vol. 2, pp. 910–921.
- [142] R. Singh and K. K. Mohanty, “Nanoparticle-stabilized foams for high-temperature, high-salinity oil reservoirs,” *Proc. - SPE Annu. Tech. Conf. Exhib.*, 2017.
- [143] J. Yu, D. Mo, N. Liu, and R. Lee, “The application of nanoparticle-stabilized CO₂ foam for oil recovery,” *Proc. - SPE Int. Symp. Oilf. Chem.*, vol. 1, no. April, pp. 341–349, 2013.
- [144] D. A. Espinoza, F. M. Caldelas, K. P. Johnston, S. L. Bryant, and C. Huh, “Nanoparticle-Stabilized Supercritical CO₂ Foams for Potential Mobility Control Applications,” in *SPE Improved Oil Recovery Symposium*, 2010.

- [145] A. Worthen *et al.*, “Multi-scale evaluation of nanoparticle-stabilized CO₂-in-water foams: From the benchtop to the field,” in *Proceedings - SPE Annual Technical Conference and Exhibition*, 2015, vol. 2015-January, pp. 4956–4968.
- [146] J. Yu, C. An, D. Mo, N. Liu, and R. Lee, “Foam mobility control for nanoparticle-stabilized CO₂ foam,” in *SPE - DOE Improved Oil Recovery Symposium Proceedings*, 2012, vol. 1, pp. 298–310.
- [147] A. A. Eftekhari, R. Krastev, and R. Farajzadeh, “Foam Stabilized by Fly Ash Nanoparticles for Enhancing Oil Recovery,” *Ind. Eng. Chem. Res.*, vol. 54, no. 50, pp. 12482–12491, Dec. 2015.
- [148] J. San, S. Wang, J. Yu, N. Liu, and R. Lee, “Nanoparticle-stabilized carbon dioxide foam used in enhanced oil recovery: Effect of different ions and temperatures,” *SPE J.*, vol. 22, no. 5, pp. 1416–1423, 2017.
- [149] N. Yekeen, M. A. Manan, A. K. Idris, A. M. Samin, and A. R. Risal, “Experimental investigation of minimization in surfactant adsorption and improvement in surfactant-foam stability in presence of silicon dioxide and aluminum oxide nanoparticles,” *Journal of Petroleum Science and Engineering*, vol. 159, pp. 115–134, 2017.
- [150] B. P. Binks, M. Kirkland, and J. A. Rodrigues, “Origin of stabilisation of aqueous foams in nanoparticle-surfactant mixtures,” *Soft Matter*, vol. 4, no. 12, pp. 2373–2382, 2008.
- [151] W. Yang, T. Wang, Z. Fan, Q. Miao, Z. Deng, and Y. Zhu, “Foams Stabilized by in Situ-Modified Nanoparticles and Anionic Surfactants for Enhanced Oil Recovery,” *Energy and Fuels*, vol. 31, no. 5, pp. 4721–4730, 2017.
- [152] N. Yekeen *et al.*, “A comprehensive review of experimental studies of nanoparticles-stabilized foam for enhanced oil recovery,” *J. Pet. Sci. Eng.*, vol. 164, no. December 2017, pp. 43–74, 2018.
- [153] J. L. Dickson, B. P. Binks, and K. P. Johnston, “Stabilization of carbon dioxide-in-water emulsions with silica nanoparticles,” *Langmuir*, vol. 20, no.

19, pp. 7976–7983, Sep. 2004.

- [154] N. D. Denkov, “Mechanisms of foam destruction by oil-based antifoams,” *Langmuir*, vol. 20, no. 22, pp. 9463–9505, Oct. 2004.
- [155] C. Dai *et al.*, “Spontaneous Imbibition Investigation of Self-Dispersing Silica Nanofluids for Enhanced Oil Recovery in Low-Permeability Cores,” *Energy and Fuels*, vol. 31, no. 3, pp. 2663–2668, Mar. 2017.
- [156] Y. Wu *et al.*, “Reducing surfactant adsorption on rock by silica nanoparticles for enhanced oil recovery,” *J. Pet. Sci. Eng.*, vol. 153, no. April, pp. 283–287, 2017.
- [157] B. A. Suleimanov, F. S. Ismailov, and E. F. Veliyev, “Nanofluid for enhanced oil recovery,” *J. Pet. Sci. Eng.*, vol. 78, no. 2, pp. 431–437, Aug. 2011.
- [158] U. T. Gonzenbach, A. R. Studart, E. Tervoort, and L. J. Gauckler, “Ultrastable Particle-Stabilized Foams,” *Angew. Chemie Int. Ed.*, vol. 45, no. 21, pp. 3526–3530, May 2006.
- [159] F. Q. Tang, Z. Xiao, J. A. Tang, and L. Jiang, “The effect of SiO₂ particles upon stabilization of foam,” *J. Colloid Interface Sci.*, vol. 131, no. 2, pp. 498–502, 1989.
- [160] F. Carn, A. Colin, O. Pitois, M. Vignes-Adler, and R. Backov, “Foam drainage in the presence of nanoparticle-surfactant mixtures,” *Langmuir*, vol. 25, no. 14, pp. 7847–7856, Jul. 2009.
- [161] I. Kim, A. Taghavy, D. DiCarlo, and C. Huh, “Aggregation of silica nanoparticles and its impact on particle mobility under high-salinity conditions,” *J. Pet. Sci. Eng.*, vol. 133, pp. 376–383, 2015.
- [162] M. A. Manan, S. Farad, A. Piroozian, and M. J. A. Esmail, “Effects of Nanoparticle Types on Carbon Dioxide Foam Flooding in Enhanced Oil Recovery,” *Pet. Sci. Technol.*, vol. 33, no. 12, pp. 1286–1294, Jun. 2015.
- [163] G. C. Frye and J. C. Berg, “Antifoam action by solid particles,” *J. Colloid*

- Interface Sci.*, vol. 127, no. 1, pp. 222–238, Jan. 1989.
- [164] Z. Li, Z. Liu, B. Li, S. Li, Q. Sun, and S. Wang, “Aqueous foams stabilized with particles and surfactants,” in *Society of Petroleum Engineers - SPE Saudi Arabia Section Technical Symposium and Exhibition 2012*, 2012.
- [165] N. Hu, Y. Li, Z. Wu, K. Lu, D. Huang, and W. Liu, “Foams stabilization by silica nanoparticle with cationic and anionic surfactants in column flotation: Effects of particle size,” *Journal of the Taiwan Institute of Chemical Engineers*, vol. 88, pp. 62–69, 2018.
- [166] R. Deleurence, C. Parneix, and C. Monteux, “Mixtures of latex particles and the surfactant of opposite charge used as interface stabilizers-influence of particle contact angle, zeta potential, flocculation and shear energy,” *Soft Matter*, vol. 10, no. 36, pp. 7088–7095, Sep. 2014.
- [167] A. Stocco, E. Rio, B. P. Binks, and D. Langevin, “Aqueous foams stabilized solely by particles,” in *Soft Matter*, 2011, vol. 7, no. 4, pp. 1260–1267.
- [168] A. E. Bayat, K. Rajaei, and R. Junin, “Assessing the effects of nanoparticle type and concentration on the stability of CO₂ foams and the performance in enhanced oil recovery,” *Colloids Surfaces A Physicochem. Eng. Asp.*, vol. 511, pp. 222–231, Dec. 2016.
- [169] U. T. Gonzenbach, A. R. Studart, E. Tervoort, and L. J. Gauckler, “Stabilization of foams with inorganic colloidal particles,” *Langmuir*, vol. 22, no. 26, pp. 10983–10988, Dec. 2006.
- [170] R. Singh, A. Gupta, K. K. Mohanty, C. Huh, D. Lee, and H. Cho, “Fly ash nanoparticle-stabilized CO₂-in-water foams for gas mobility control applications (SPE 175057),” in *Proceedings - SPE Annual Technical Conference and Exhibition*, 2015.
- [171] I. Ahmad, “The Potential of Fly Ash as a Foam Stabilizing Additive”, Master Thesis, Universiti Teknologi Petronas, 2016.

- [172] F. Guo, J. He, P. A. Johnson, and S. A. Aryana, "Stabilization of CO₂ foam using by-product fly ash and recyclable iron oxide nanoparticles to improve carbon utilization in EOR processes," *Sustain. Energy Fuels*, vol. 1, no. 4, pp. 814–822, 2017.
- [173] A. S. Hanamertani, R. M. Pilus, N. A. Manan, and M. I. A. Mutalib, "The use of ionic liquids as additive to stabilize surfactant foam for mobility control application," *J. Pet. Sci. Eng.*, vol. 167, pp. 192–201, Aug. 2018.
- [174] T. Sharma, G. Suresh Kumar, and J. S. Sangwai, "Enhanced oil recovery using oil-in-water (o/w) emulsion stabilized by nanoparticle, surfactant and polymer in the presence of NaCl," *Geosystem Eng.*, vol. 17, no. 3, pp. 195–205, May 2014.
- [175] A. S. Hanamertani, R. M. Pilus, A. K. Idris, S. Irawan, and I. M. Tan, "Ionic liquids as a potential additive for reducing surfactant adsorption onto crushed Berea sandstone," *J. Pet. Sci. Eng.*, pp. 480–490, Mar. 2018.
- [176] I. Ahamad, M. Awang, and M. Mumtaz, "Potential of Fly Ash as a Foam Stabilizing Additive," in *ICIPEG 2016*, Springer Singapore, 2017, pp. 157–165.
- [177] A. Dindi, D. V. Quang, L. F. Vega, E. Nashef, and M. R. M. Abu-Zahra, "Applications of fly ash for CO₂ capture, utilization, and storage," *Journal of CO₂ Utilization*, vol. 29. Elsevier Ltd, pp. 82–102, 01-Jan-2019.
- [178] G. M. Phong, R. M. Pilus, A. Mustaffa, L. Thangavel, and N. M. Mohamed, "Relationship between fly ash nanoparticle-stabilized-foam and oil production in core displacement and simulation studies," *Fuel*, vol. 266, 2020.
- [179] Q. Sun, N. Zhang, Z. Li, and Y. Wang, "Nanoparticle-Stabilized Foam for Mobility Control in Enhanced Oil Recovery," *Energy Technol.*, vol. 4, no. 9, pp. 1084–1096, 2016.
- [180] M. J. Edgell, D. R. Baer, and J. E. Castle, "Biased referencing experiments for the XPS analysis of non-conducting materials," *Appl. Surf. Sci.*, vol. 26, no. 2,

- pp. 129–149, Aug. 1986.
- [181] J. I. Goldstein *et al.*, “Introduction,” in *Scanning Electron Microscopy and X-ray Microanalysis*, Springer US, 2003, pp. 1–20.
- [182] R. Singh and K. K. Mohanty, “Foams with wettability-altering capabilities for oil-wet carbonates: A synergistic approach,” in *Proceedings - SPE Annual Technical Conference and Exhibition*, 2015, vol. 2015-January, pp. 4372–4394.
- [183] N. Hadian Nasr, S. M. Mahmood, and H. Hematpur, “A rigorous approach to analyze bulk and coreflood foam screening tests,” *J. Pet. Explor. Prod. Technol.*, vol. 9, no. 2, pp. 809–822, Jun. 2019.
- [184] A. S. Hanamertani, R. M. Pilus, N. A. Manan, S. Ahmed, and M. Awang, “Ionic Liquid Application in Surfactant Foam Stabilization for Gas Mobility Control,” *Energy and Fuels*, vol. 32, no. 6, pp. 6545–6556, 2018.
- [185] M. G. Rezk, J. Foroozesh, D. Zivar, and M. Mumtaz, “CO₂ storage potential during CO₂ enhanced oil recovery in sandstone reservoirs,” *J. Nat. Gas Sci. Eng.*, pp. 233–243, Jun. 2019.
- [186] S. R. M. Shafian *et al.*, “Enhancing the efficiency of immiscible Water Alternating Gas (WAG) injection in a matured, high temperature and high CO₂ solution gas reservoir - A laboratory study,” *Soc. Pet. Eng. - SPE Enhanc. Oil Recover. Conf. EORC 2013 Deliv. Promise NOW!*, pp. 892–905, 2013.
- [187] R. Farajzadeh, M. Lotfollahi, A. A. Eftekhari, W. R. Rossen, and G. J. H. Hirasaki, “Effect of permeability on implicit-texture foam model parameters and the limiting capillary pressure,” *Energy and Fuels*, vol. 29, no. 5, pp. 3011–3018, 2015.
- [188] M. Lotfollahi, A. Varavei, M. Delshad, R. Farajzadeh, and G. A. Pope, “A four-phase flow model to simulate chemical EOR with gas (SPE 173322),” in *Society of Petroleum Engineers - SPE Reservoir Simulation Symposium 2015*, 2015, vol. 3, pp. 2190–2222.

- [189] J. Groenenboom, S. S. Berhad, N. I. Kechut, and A. Mar-Or, “Foam-assisted WAG: Injection strategies to optimize performance (SPE 186991),” *Soc. Pet. Eng. - SPE/IATMI Asia Pacific Oil Gas Conf. Exhib. 2017*, 2017.
- [190] A. Ahmed, I. M. Saaid, A. A. Ahmed, R. M. Pilus, and M. K. Baig, “Evaluating the potential of surface-modified silica nanoparticles using internal olefin sulfonate for enhanced oil recovery,” *Pet. Sci.*, pp. 1–12, Dec. 2019.
- [191] C. Gilbert, “Synthesis and characterisation of iron nanoparticles by extraction from iron rich waste material for the remediation of acid mine drainage,” University of Western Cape, 2003.
- [192] D. A. Kramer, “Magnesium Compounds,” in *Kirk-Othmer Encyclopedia of Chemical Technology*, Hoboken, NJ, USA: John Wiley & Sons, Inc., 2001.
- [193] B. Ealet, M. H. Elyakhloufi, E. Gillet, and M. Ricci, “Electronic and crystallographic structure of γ -alumina thin films,” *Thin Solid Films*, vol. 250, no. 1–2, pp. 92–100, Oct. 1994.
- [194] J. L. G. Fierro, J. M. Palacios, and F. Tomas, “Characterization of catalyst and catchment gauzes used in medium- and low-pressure ammonia oxidation plants,” *J. Mater. Sci.*, vol. 27, no. 3, pp. 685–691, 1992.
- [195] S. L. T. Andersson and R. F. Howe, “X-ray photoelectron study of metal clusters in zeolites,” *J. Phys. Chem.*, vol. 93, no. 12, pp. 4913–4920, 1989.
- [196] C. D. Wagner *et al.*, “AUGER AND PHOTOELECTRON LINE ENERGY RELATIONSHIPS IN ALUMINUM-OXYGEN AND SILICON-OXYGEN COMPOUNDS.,” *J. Vac. Sci. Technol.*, vol. 21, no. 4, pp. 933–944, Nov. 1982.
- [197] S. L. Stipp and M. F. Hochella, “Structure and bonding environments at the calcite surface as observed with X-ray photoelectron spectroscopy (XPS) and low energy electron diffraction (LEED),” *Geochim. Cosmochim. Acta*, vol. 55, no. 6, pp. 1723–1736, Jun. 1991.
- [198] N. H. Turner, J. S. Murday, and D. E. Ramaker, “Quantitative Determination of

- Surface Composition of Sulfur Bearing Anion Mixtures by Auger Electron Spectroscopy,” *Anal. Chem.*, vol. 52, no. 1, pp. 84–92, Jan. 1980.
- [199] S. C. Wee, N. A. Md Akhir, and A. L. Rozman, “Investigation of Nanoparticles Dispersion in Sodium Hydroxide (NaOH) Solvent,” *MATEC Web Conf.*, vol. 87, 2016.
- [200] W. He and J. Nan, “Study on the impact of particle size distribution on turbidity in water,” *Desalin. Water Treat.*, vol. 41, no. 1–3, pp. 26–34, Mar. 2012.
- [201] A. Esfandyari Bayat, R. Junin, S. Shamshirband, and W. Tong Chong, “Transport and retention of engineered Al₂O₃, TiO₂, and SiO₂ nanoparticles through various sedimentary rocks,” *Sci. Rep.*, vol. 5, Sep. 2015.
- [202] A. Ahmed, I. M. Saaid, A. H. Tunio, R. M. Pilus, M. Mumtaz, and I. Ahmad, “Investigation of Dispersion Stability and IFT Reduction Using Surface Modified Nanoparticle: Enhanced Oil Recovery.” 2017.
- [203] C. R. Miranda, L. S. De Lara, and B. C. Tonetto, “Stability and mobility of functionalized silica nanoparticles for enhanced oil recovery applications,” in *Society of Petroleum Engineers - SPE International Oilfield Nanotechnology Conference 2012*, 2012, pp. 311–321.
- [204] M. T. G. Janssen, R. M. Pilus, and P. L. J. Zitha, “A Comparative Study of Gas Flooding and Foam-Assisted Chemical Flooding in Bentheimer Sandstones,” *Transp. Porous Media*, vol. 131, no. 1, pp. 101–134, Jan. 2020.
- [205] M. Janssen, A. Mutawa, R. Pilus, and P. Zitha, “Evaluation of foam-assisted surfactant flooding at reservoir conditions,” in *Society of Petroleum Engineers - SPE Europec, 81st EAGE Conference and Exhibition 2019*, 2019.
- [206] S. C. Ayirala and D. N. Rao, “Multiphase flow and wettability effects of surfactants in porous media,” in *Colloids and Surfaces A: Physicochemical and Engineering Aspects*, 2004, vol. 241, no. 1–3, pp. 313–322.

- [207] M. H. U. Bhuiyan, R. Saidur, M. A. Amalina, R. M. Mostafizur, and A. K. M. S. Islam, "Effect of nanoparticles concentration and their sizes on surface tension of nanofluids," in *Procedia Engineering*, 2015, vol. 105, pp. 431–437.
- [208] Z. Abbas, C. Labbez, S. Nordholm, and E. Ahlberg, "Size-dependent surface charging of nanoparticles," *J. Phys. Chem. C*, vol. 112, no. 15, pp. 5715–5723, Apr. 2008.
- [209] M. A. Brown *et al.*, "Effect of surface charge density on the affinity of oxide nanoparticles for the vapor-water interface," *Langmuir*, vol. 29, no. 16, pp. 5023–5029, Apr. 2013.
- [210] M. Luo, Y. Song, and L. L. Dai, "Heterogeneous or competitive self-assembly of surfactants and nanoparticles at liquid-liquid interfaces," in *Molecular Simulation*, 2009, vol. 35, no. 10–11, pp. 773–784.
- [211] M. Zargartalebi, R. Kharrat, and N. Barati, "Enhancement of surfactant flooding performance by the use of silica nanoparticles," *Fuel*, vol. 143, pp. 21–27, 2015.
- [212] F. Ravera, E. Santini, G. Loglio, M. Ferrari, and L. Liggieri, "Effect of nanoparticles on the interfacial properties of liquid/liquid and liquid/air surface layers," *J. Phys. Chem. B*, vol. 110, no. 39, pp. 19543–19551, Oct. 2006.
- [213] S. Ahualli, G. R. Iglesias, W. Wachter, M. Dulle, D. Minami, and O. Glatter, "Adsorption of anionic and cationic surfactants on anionic colloids: Supercharging and destabilization," *Langmuir*, vol. 27, no. 15, pp. 9182–9192, Aug. 2011.
- [214] A. M. S. Ragab and A. E. Hannora, "A comparative investigation of nano particle effects for improved oil recovery - experimental work," in *Society of Petroleum Engineers - SPE Kuwait Oil and Gas Show and Conference*, 2015.
- [215] O. A. Alomair, K. M. Matar, and Y. H. Alsaheed, "Nanofluids application for heavy oil recovery," in *Society of Petroleum Engineers - SPE Asia Pacific Oil and Gas Conference and Exhibition, APOGCE 2014 - Changing the Game:*

- Opportunities, Challenges and Solutions*, 2014, vol. 2, pp. 1346–1363.
- [216] A. Esfandyari Bayat, R. Junin, A. Samsuri, A. Piroozian, and M. Hokmabadi, “Impact of metal oxide nanoparticles on enhanced oil recovery from limestone media at several temperatures,” *Energy and Fuels*, vol. 28, no. 10, pp. 6255–6266, Oct. 2014.
- [217] A. Maestro, E. Rio, W. Drenckhan, D. Langevin, and A. Salonen, “Foams stabilised by mixtures of nanoparticles and oppositely charged surfactants: Relationship between bubble shrinkage and foam coarsening,” *Soft Matter*, vol. 10, no. 36, pp. 6975–6983, Sep. 2014.
- [218] I. Kim, A. J. Worthen, K. P. Johnston, D. A. DiCarlo, and C. Huh, “Size-dependent properties of silica nanoparticles for Pickering stabilization of emulsions and foams,” *J. Nanoparticle Res.*, vol. 18, no. 4, Apr. 2016.
- [219] N. Yekeen, A. K. Idris, M. A. Manan, A. M. Samin, A. R. Risal, and T. X. Kun, “Bulk and bubble-scale experimental studies of influence of nanoparticles on foam stability,” *Chinese Journal of Chemical Engineering*, vol. 25, no. 3, pp. 347–357, 2017.
- [220] F. Q. Tang, Z. Xiao, J. A. Tang, and L. Jiang, “The effect of SiO₂ particles upon stabilization of foam,” *J. Colloid Interface Sci.*, vol. 131, no. 2, pp. 498–502, 1989.
- [221] E. M. Hotze, T. Phenrat, and G. V. Lowry, “Nanoparticle aggregation: Challenges to understanding transport and reactivity in the environment,” *J. Environ. Qual.*, vol. 39, no. 6, pp. 1909–1924, Nov. 2010.
- [222] S. W. Bian, I. A. Mudunkotuwa, T. Rupasinghe, and V. H. Grassian, “Aggregation and dissolution of 4 nm ZnO nanoparticles in aqueous environments: Influence of pH, ionic strength, size, and adsorption of humic acid,” *Langmuir*, vol. 27, no. 10, pp. 6059–6068, Jun. 2011.
- [223] A. E. Bayat, K. Rajaei, and R. Junin, “Assessing the effects of nanoparticle type and concentration on the stability of CO₂ foams and the performance in

enhanced oil recovery,” *Colloids and Surfaces A: Physicochemical and Engineering Aspects*, vol. 511. pp. 222–231, 2016.

- [224] L. G. Phillips, S. T. Yang, and J. E. Kinsella, “Neutral Salt Effects on Stability of Whey Protein Isolate Foams,” *J. Food Sci.*, vol. 56, no. 2, pp. 588–589, Mar. 1991.
- [225] R. Aveyard, B. P. Binks, P. D. I. Fletcher, T. G. Peck, and C. E. Rutherford, “Aspects of aqueous foam stability in the presence of hydrocarbon oils and solid particles,” *Adv. Colloid Interface Sci.*, vol. 48, no. C, pp. 93–120, Apr. 1994.
- [226] T. B. Chea, N. A. M. Akhir, and A. K. Idris, “Investigation on the effect of types of nanoparticles and temperature on nanoparticles-foam stability,” *Proc. Int. Conf. Ind. Eng. Oper. Manag.*, vol. 2018-March, no. 2017, pp. 365–372, 2018.
- [227] J. P. Heller, C. L. Lien, and M. S. Kuntamukkula, “Foamlike Dispersions for Mobility Control in CO₂ Floods (SPE 11233),” *Soc. Pet. Eng. J.*, vol. 25, no. 4, pp. 603–613, 1985.
- [228] J. Gong *et al.*, “Laboratory Investigation of Liquid Injectivity in Surfactant-Alternating-Gas Foam Enhanced Oil Recovery,” *Transp. Porous Media*, no. August 2018, pp. 26–28, 2019.
- [229] A. A. A. Hussain, S. Vincent-Bonnieu, R. Z. Kamarul Bahrim, R. M. Pilus, and W. R. Rossen, “Impact of Crude Oil on Pre-Generated Foam in Porous Media,” *J. Pet. Sci. Eng.*, p. 106628, Nov. 2019.
- [230] R. Singh and K. K. Mohanty, “Synergy between nanoparticles and surfactants in stabilizing foams for oil recovery,” *Energy and Fuels*, vol. 29, no. 2, pp. 467–479, Feb. 2015.
- [231] M. J. Murphy, *Experimental Analysis of Electrostatic and Hydrodynamic Forces Affecting Nanoparticle Retention in Porous Media*. Master Thesis, University of Texas at Austin, 2012.

- [232] G. C. Wang and M. Spe-Aime, "A Laboratory Study of CO₂ Foam Properties and Displacement Mechanism," in *SPE Enhanced Oil Recovery Symposium*, 15-18 April, Tulsa, Oklahoma, 1984.
- [233] M. Simjoo, Y. Dong, A. Andrianov, M. Talanana, and P. L. J. Zitha, "Novel insight into foam mobility control," *SPE J.*, vol. 18, no. 3, pp. 416–427, 2013.
- [234] F. Hakiki, D. A. Maharsi, and T. Marhaendrajana, "Surfactant-polymer coreflood simulation and uncertainty analysis derived from laboratory study," *J. Eng. Technol. Sci.*, vol. 47, no. 6, pp. 706–725, Dec. 2015.
- [235] A. F. Belhaj, K. A. Elraies, M. S. Alnarabiji, J. A. B. M. Shuhli, S. M. Mahmood, and L. W. Ern, "Experimental Investigation of Surfactant Partitioning in Pre-CMC and Post-CMC Regimes for Enhanced Oil Recovery Application," *Energies*, vol. 12, no. 12, p. 2319, Jun. 2019.
- [236] L. Sun, B. Wang, W. Pu, H. Yang, and M. Shi, "The effect of foam stability on foam flooding recovery," *Pet. Sci. Technol.*, vol. 33, no. 1, pp. 15–22, Jan. 2015.